

REPORT DOCUMENTATION PAGE				Form Approved OMB No. 0704-0188	
Public reporting burden for this collection of information is estimated to average 1 hour per response, including the time for reviewing instructions, searching existing data sources, gathering and maintaining the data needed, and completing and reviewing the collection of information. Send comments regarding this burden estimate or any other aspect of this collection of information, including suggestions for reducing the burden, to Department of Defense, Washington Headquarters Services, Directorate for Information Operations and Reports (0704-0188), 1215 Jefferson Davis Highway, Suite 1204, Arlington, VA 22202-4302. Respondents should be aware that notwithstanding any other provision of law, no person shall be subject to any penalty for failing to comply with a collection of information if it does not display a currently valid OMB control number. PLEASE DO NOT RETURN YOUR FORM TO THE ABOVE ADDRESS.					
1. REPORT DATE (DD-MM-YYYY)		2. REPORT TYPE Final Report		3. DATES COVERED (From – To) 11 July 2003 - 11-Jul-05	
4. TITLE AND SUBTITLE Ultracold Atoms in Optical Lattices			5a. CONTRACT NUMBER FA8655-03-1-3039		
			5b. GRANT NUMBER		
			5c. PROGRAM ELEMENT NUMBER		
6. AUTHOR(S) Dr. Immanuel Felix Bloch			5d. PROJECT NUMBER		
			5d. TASK NUMBER		
			5e. WORK UNIT NUMBER		
7. PERFORMING ORGANIZATION NAME(S) AND ADDRESS(ES) Ludwig-Maximilian University of Munich Schellingstr. 4/III Munich 80799 Germany				8. PERFORMING ORGANIZATION REPORT NUMBER N/A	
9. SPONSORING/MONITORING AGENCY NAME(S) AND ADDRESS(ES) EOARD PSC 802 BOX 14 FPO 09499-0014				10. SPONSOR/MONITOR'S ACRONYM(S)	
				11. SPONSOR/MONITOR'S REPORT NUMBER(S) SPC 03-3039	
12. DISTRIBUTION/AVAILABILITY STATEMENT Approved for public release; distribution is unlimited.					
13. SUPPLEMENTARY NOTES					
14. ABSTRACT This report results from a contract tasking Ludwig-Maximilian University of Munich as follows: The grantee will investigate controlled collisions between atoms in optical lattices, production of strongly correlated quantum system with tunable interactions, low dimensional degenerate quantum systems, and rotating Bose-Einstein condensates in optical lattices -- observing the fractional Quantum Hall effect with bosons.					
15. SUBJECT TERMS EOARD, Quantum Bits, Bose-Einsten Condensate, Quantum Entanglement, Quantum Computing, Quantum Coherence					
16. SECURITY CLASSIFICATION OF:			17. LIMITATION OF ABSTRACT UL	18, NUMBER OF PAGES 63	19a. NAME OF RESPONSIBLE PERSON PAUL LOSIEWICZ, Ph. D.
a. REPORT UNCLAS	b. ABSTRACT UNCLAS	c. THIS PAGE UNCLAS			19b. TELEPHONE NUMBER <i>(Include area code)</i> +44 20 7514 4474

Final Report

Contract FA8655-03-1-3039

Title: “Ultracold atoms in optical lattices”

Total Funding Period 1 Aug 2003-31 Dec 2005

Prof. Immanuel Bloch

Johannes Gutenberg-University of Mainz, &
Ludwig-Maximilians-University, Munich, Germany

Website: www.physik.uni-mainz.de/quantum

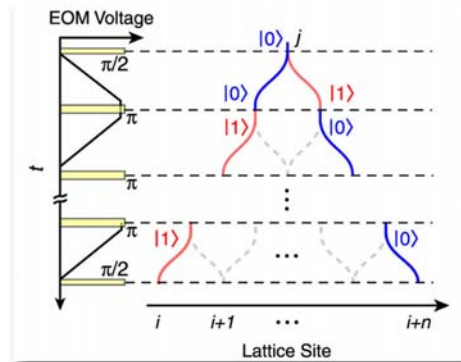
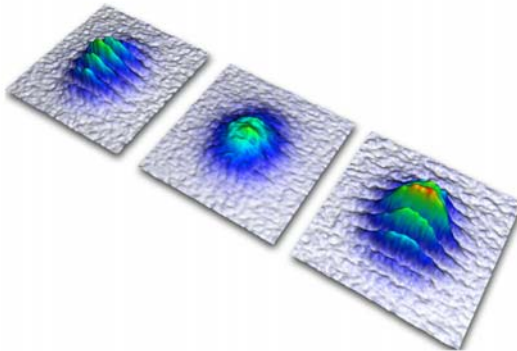
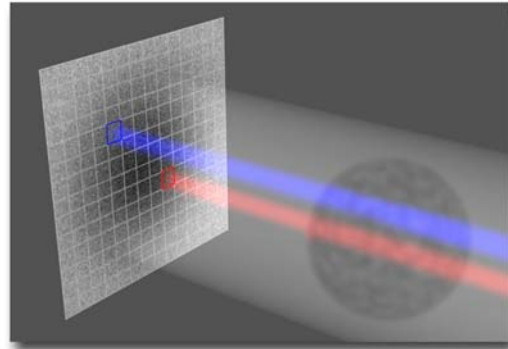
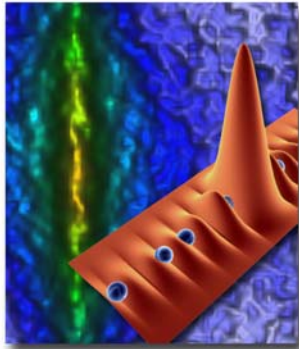


Table of Contents

TABLE OF CONTENTS	2
SUMMARY & OUTLINE	3
RESEARCH RESULTS	4
Quantum gate arrays with neutral atoms in optical lattices	4
Fully controlled molecule formation – chemical reaction at the quantum limit	6
Spatial quantum noise interferometry in expanding Ultracold atom clouds	7
Visibility of the Interference Pattern of a Mott Insulator – Fidelity of a Neutral Atom Quantum Gate Register	10
Coherent Spin Changing Collisions with Neutral Atoms in Optical Lattices	11
Measurement of the Atom Number Statistics in the SF-MI transition using Coherent Spin-Changing Collisions	13
Motional Qubit Manipulation – Mott Insulators in Excited States	14
CONCLUSION AND OUTLOOK	18
PUBLICATIONS OBTAINED DURING THE FUNDING PERIOD	19
REFERENCES	21
DECLARATIONS, DISCLAIMERS AND ACKNOWLEDGMENTS	24

Summary & Outline

This report summarizes the work and results obtained under contract FA8655-03-1-3039, titled “*Ultracold Atoms in Optical Lattices*”. The research focused on trapping ultracold neutral atoms in artificial periodic potentials made out of light – so called optical lattices. Such ultracold atoms in optical lattices form a completely novel and highly promising research field and find e.g. diverse applications as simulators for complex quantum many body systems, as e.g. initially conceived by Richard P. Feynman [1, 2]. Connected to this, they also show promising applications for quantum information processing. For example, by employing the superfluid to Mott insulator transition [3-5], a large quantum register of up to 100000 atoms can be initialized, where single atoms are located at each lattice site. Work in this contract has been directed towards analyzing the fidelity of such quantum registers and towards the realization of massively parallel quantum gates based on ultracold collisions between the atoms [6]. Novel entanglement techniques for ultracold atoms have also been developed that are based on spin changing collisions and could enable the generation of large scale & robust entanglement, with low decoherence rates. In recent years it has become clear that such a large scale entanglement can be seen as a fundamental resource for quantum computations [7, 8], so that generating and characterizing, as well as testing the robustness of such entanglement, is of fundamental importance in this respect.

During the contract period our research group relocated from the Ludwig-Maximilians-University in Munich to the Johannes Gutenberg-University in Mainz, Germany (close to Frankfurt) and the experiments had to be setup again in completely new laboratories. Although a delay in setting up the experiments again had to be expected, the group completed the reconstructions in a very fast period, such that almost no decrease in the research and publication activities could be noticed during this period.

The following pages summarize the research results obtained during the grant period and conclude with some novel results obtained in the last funding quarter, as well as with an outlook for future perspectives in this novel research field.

Research topics & results covered during this grant

- Realization of Neutral Atom Quantum Gates
- Realization of Novel Many Body Quantum States – the Tonks-Girardeau Gas
- Controlled Molecule Formation in Optical Lattices – Quantum Chemistry at the Quantum Limit
- Realization of Quantum Noise Correlation Techniques for Detecting and Characterizing Many-Body Quantum States in Optical Lattices
- Realization of Coherent Spin Changing Collisions for the Production of Entangled States
- Characterization of the Number Squeezing Fidelity of a Mott Insulator Neutral Atom Quantum Register
- Towards Single Qubit Manipulations – Mott insulators in excited states

The publications (among them **3 in Nature** and **6 in Physical Review Letters**) that were obtained during the funding period are summarized at the end of this report and reprints of selected publications have been attached to this file.

Research results

Quantum gate arrays with neutral atoms in optical lattices

By using ultracold atoms in a Mott insulating phase of an optical lattice we have been able to initialize a large register of quantum bits (qubits). In order to perform quantum gates within such a quantum memory, it is however necessary to induce interactions between neighboring atoms in a controlled way. For this we have realized a quantum conveyer belt, which has allowed us to transport single atoms over a controlled number of lattice sites depending on their internal state (see Figure 1).

The quantum conveyer belt has been realized by using an optical standing wave configuration, in which the polarization of the laser beams was controlled via electro-optical modulators. By rotating the polarization of one of the counter-propagating laser beams, the atoms can be moved over a defined number of lattice sites. In the experiment a coherent transport of the atoms over a distance of up to 7 lattice sites has been demonstrated [Mandel03a].

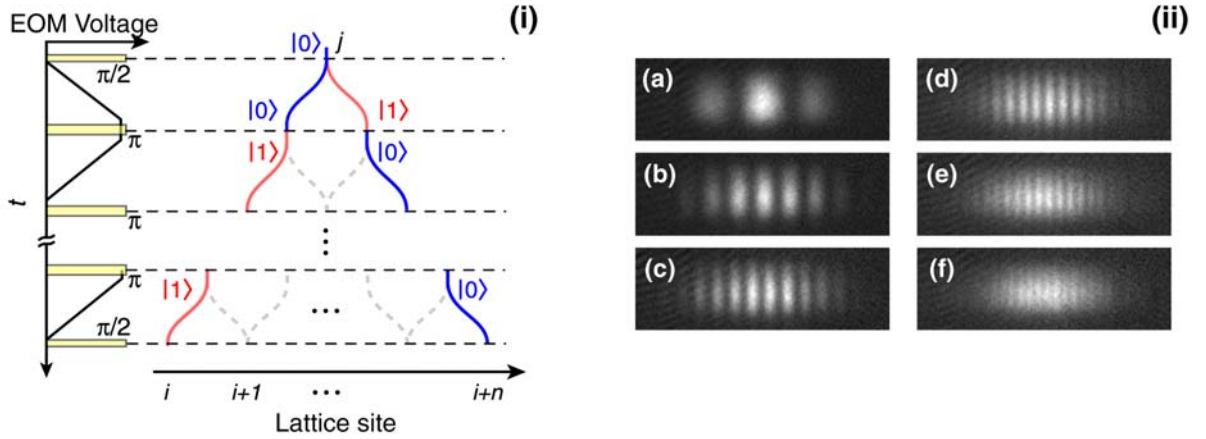


Figure 1 (i) Schematic sequence used for the quantum conveyer belt. A single atom on lattice site j can be transported over an arbitrary number of lattice sites depending on its spin state (marked as blue and red curves). (ii) This has allowed us to split the wave function of the atom in a coherent way, such that a single atom simultaneously moves to the left and to the right. The coherence of the split wave-packets has been demonstrated in an interference experiment. For larger distances between the split wave-functions, the period of the interference pattern decreases.

In one of our latest experiments we have used such a quantum conveyer belt together with coherent collisional interactions between the atoms in order to realize a massively parallel quantum gate array. Starting point for the experiment is again a Mott insulating state, with single atoms on each lattice site. The atoms are first prepared in logic state $|0\rangle$ and then coherent microwave radiation is used to place them in a superposition of the two quantum logic states $|0\rangle$ and $|1\rangle$. Now the quantum conveyer belt is activated, such that an atom in state $|1\rangle$ ($|0\rangle$) is moved to the neighboring lattice site to the left (right). There the atom interacts with the neighboring atom through coherent collisions and the quantum many body wave-function acquires a phase shift ϕ . This collisional phase shift can be completely controlled through the hold time of the atoms at a common lattice site (see Figure 2a). After such a coherent interaction the atoms are returned to their original lattice site.

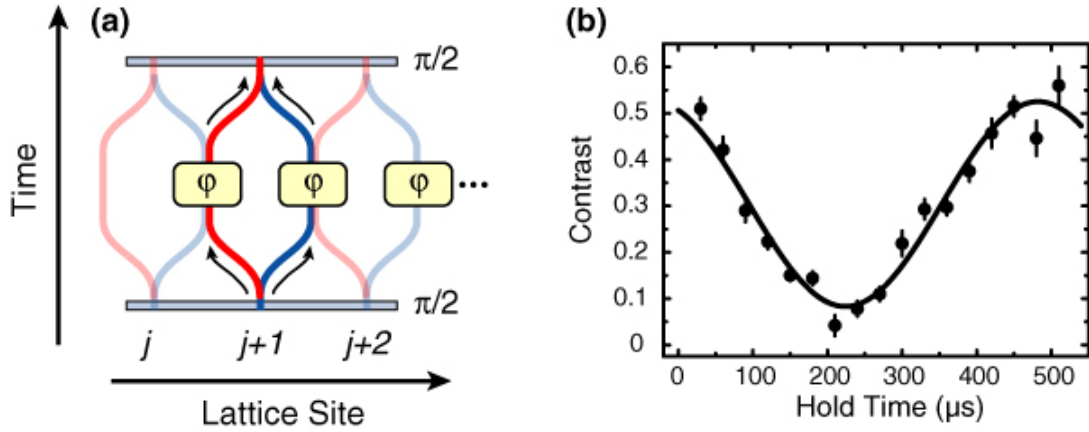


Figure 2 (a) Schematic sequence of the collisional quantum gate array. Neighboring atoms are brought into controlled contact and interact with each other through a coherent collisional interaction. This controlled collision is spin dependent and realizes a massively parallel quantum gate array. (b) When the quantum gate array is applied to the atoms in the lattice, the system undergoes entanglement oscillations that are visible in the contrast of a Ramsey type experiment [Mandel03b].

The action of such a massively parallel quantum gate array leads to highly entangled multi-particle states, so called “cluster states” [Mandel03b]. Such cluster states have been shown to be highly useful for a novel type of quantum computer, which has been devised by Dr. Hans Briegel at the University of Munich. In such a “one-way” quantum computer, the initial cluster state acts as a resource for the computation power of the quantum computer and an arbitrary algorithm can be implemented on such an entangled cluster through single particle operations only. In future research we would like to create such cluster states in two-dimensions and learn how to characterize the massive entanglement present in such a cluster. Furthermore, if we will be able to address single atoms in the cluster one could test the unique model of the proposed quantum computer. The main advantage of the lattice system lies in the natural large size of the system, which is so far unrivalled by any other physical system. Also the neutral atoms are very well decoupled from the environment such that decoherence is minimized.

Realization of a new low-dimensional quantum phase - the “Tonks-Girardeau” gas

In another line of research, we have been interested in using ultracold quantum gases in optical lattices as model systems for challenging quantum phases of condensed matter physics. Here the strongly correlated quantum states, where the interactions between the particles dominate the behaviour of the quantum system, pose great challenges to experiment and theory. The Tonks-Girardeau gas, proposed about 40 years ago [9], is especially remarkable in this respect. In such a gas the intriguing properties of low-dimensional Bose-systems combine with those of a strongly correlated state yielding an astonishing quantum behaviour [10, 11]. One of the most profound aspects of this quantum behaviour is the fact that bosonic particles acquire fermionic properties. We have been able

to prepare such a Tonks-Girardeau gas in an optical lattice and with the help of colleagues from theoretical physics identify this novel quantum phase. An array of 1D bosonic quantum gases has first been prepared in a two-dimensional optical lattice potential. The addition of a third lattice along the long axis of the quantum gases has allowed us to enter the Tonks-Girardeau regime by increasing the effective mass and thereby enhancing the role of interactions. We have measured the momentum distribution and compared it with the theoretical prediction based on a fermionization approach, observing a remarkable agreement. The work has been published in *Nature* [Widera04b].

Fully controlled molecule formation – chemical reaction at the quantum limit

Two atoms placed in the ground state of a single lattice site form an ideal starting point for molecule formation. In one of the most recent experiments, we have been able to show that two such ground state atoms can be coherently coupled to a molecular state using an optical two-photon transition. The fascinating new aspect hereby has been that we have not only been able to control the internal state in which the molecule is formed, but also its motional quantum state can be fully addressed (see Figure 3 and Figure 4) [Rom04a]. This forms a chemical reaction in which all quantum degrees of freedom of the molecule are now under the complete control. If such a unique control can be extended to more complex objects, one could envisage building molecules one-by-one and completely controlling the quantum states in this formation process.

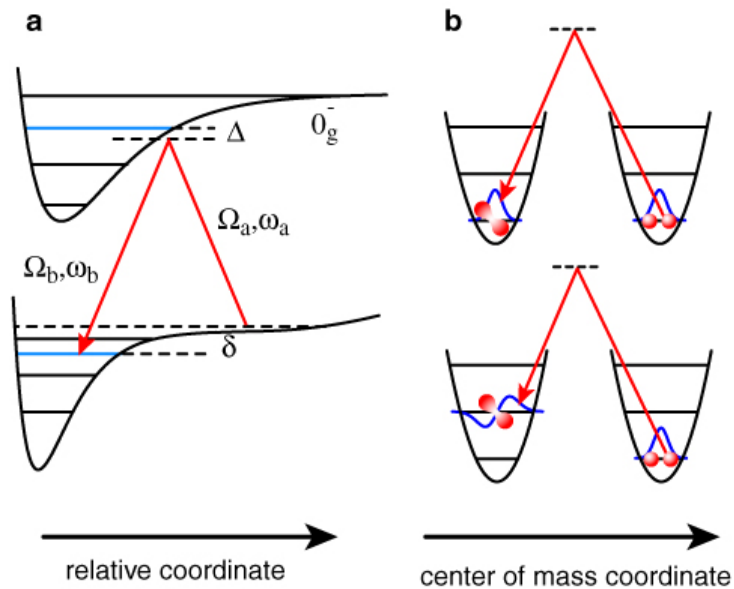


Figure 3 (a) Using a two-photon process, one can convert two free atoms into a molecule in a defined ro-vibrational quantum state. **(b)** Moreover, with atoms in an optical lattice, one can also control the external quantum degree of freedom in the molecule formation process. Thereby all quantum degrees of freedom of the molecule are under the complete control of the experimentalist and an ultimate chemical reaction at the quantum limit has been realized.

The coupling of two atomic atoms to a molecular state, however, also has relevance to quantum information processing. With such a coherent coupling it should in fact be possible to alter the collisional properties of the atoms, similar to how this is done with Feshbach resonances. This would then allow us to significantly speed up the collisional quantum gates.

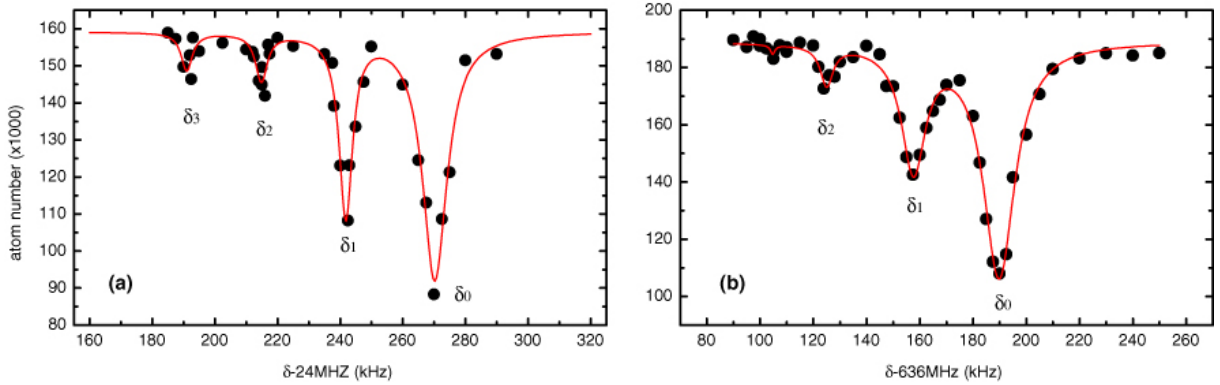


Figure 4 (a,b) Experimental results demonstrating that we are able to address the internal and motional quantum degree of freedom of the molecules. The highest resonance frequency corresponds to molecules formed in the motional ground state, whereas the sidebands at lower frequency correspond to excited motional quantum states.

Spatial quantum noise interferometry in expanding Ultracold atom clouds

For now almost 9 years, absorption imaging of released ultracold quantum gases has been a standard detection method for revealing information on the macroscopic quantum state of the atoms in the trapping potential. For strongly correlated quantum states in optical lattices, however, the average signal in the momentum distribution that one usually observes, e.g. for a Mott insulating state of matter, is a featureless Gaussian wave packet. From this Gaussian wave packet one cannot deduce anything about the strongly correlated quantum states in the lattice potential apart from the fact that phase coherence has been lost. Recently, however, the widespread interest in strongly correlated quantum gases in optical lattices, has lead to the prediction of fascinating new quantum phases for ultracold atoms, e.g. with anti-ferromagnetic structure, spin waves or charge density waves. So far it has not been clear how one could detect those states. Recently a theoretical proposal by Altman *et al.* [12] (Harvard University) has shown that noise correlation interferometry could be a powerful tool to directly visualize such quantum states. Based on first successful experiments in our group in Mainz, where we have indeed observed such noise correlations, we are planning to explore the full potential of this powerful method for ultracold atoms in optical lattices. In spin-mixtures of ^{87}Rb , we plan to engineer antiferromagnetic phases and spin waves that will be directly detected with this method. Noise correlation in expanding ultracold atom clouds can in fact be seen as a powerful way to read out the quantum states of an optical lattice based quantum simulator.

So far the detection of interesting quantum states in optical lattices has mostly relied on absorption imaging of expanding gas clouds. While in the regime of a Bose-Einstein condensate with long range phase coherence, one observes a matter wave interference pattern, the absorption images in a Mott insulator state however do not reveal much structure as the average signal is just an expanding Gaussian wave packet (from the localized wave packets on each lattice site). In fact, nothing can be learnt from the average signal regarding the strongly correlated quantum state apart from that phase coherence is absent. Recently, however, Altman *et al.* have proposed to use noise correlations in expanding atom clouds as a novel detection scheme for strongly correlated quantum systems in optical lattices. The basic effect relies on fundamental Hanbury Brown-Twiss correlations in the fluctuation signal of an atomic cloud. For bosons e.g. a bunching effect of the fluctuations is predicted to occur at special momenta of the expanding cloud, which directly reflect the ordering of the atoms in the lattice.

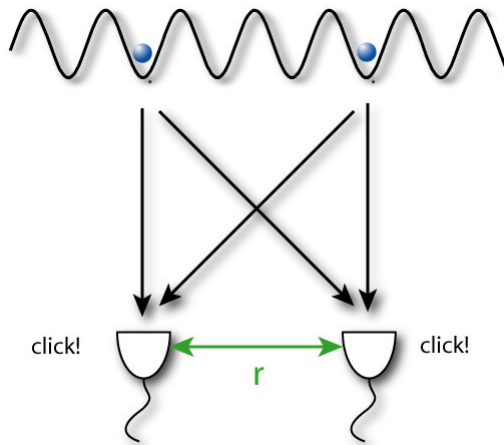


Figure 5 Hanbury Brown-Twiss correlations in expanding quantum gases from an optical lattice. For Bosonic particles that are detected at distances r (e.g. on a CCD camera), an enhanced detection probability exists due to the two indistinguishable paths the particles can take to the detector. This leads to enhanced fluctuations at special detection distances r , depending on the ordering of the atoms in the lattice. Detection of the noise correlation can therefore yield novel information on the quantum phases in an optical lattice.

In a recent experiment, we have been able to observe first signals on such Hanbury Brown-Twiss correlations in the quantum noise of an expanding atom cloud from a Mott insulating state of matter (see Figure 6). The weak correlation signal on a level of only 10^{-4} level has been detected proving this to be a powerful and versatile way for detecting novel quantum phase in optical lattice. Further quantitative analysis of the correlation signals has so far been hindered by the low performance CCD imaging systems that we are using. A major funding request in this proposal is therefore dedicated towards a sophisticated CCD camera system that would allow us to establish noise correlation interferometry as a powerful and very quantitative new detection method for ultracold atoms.

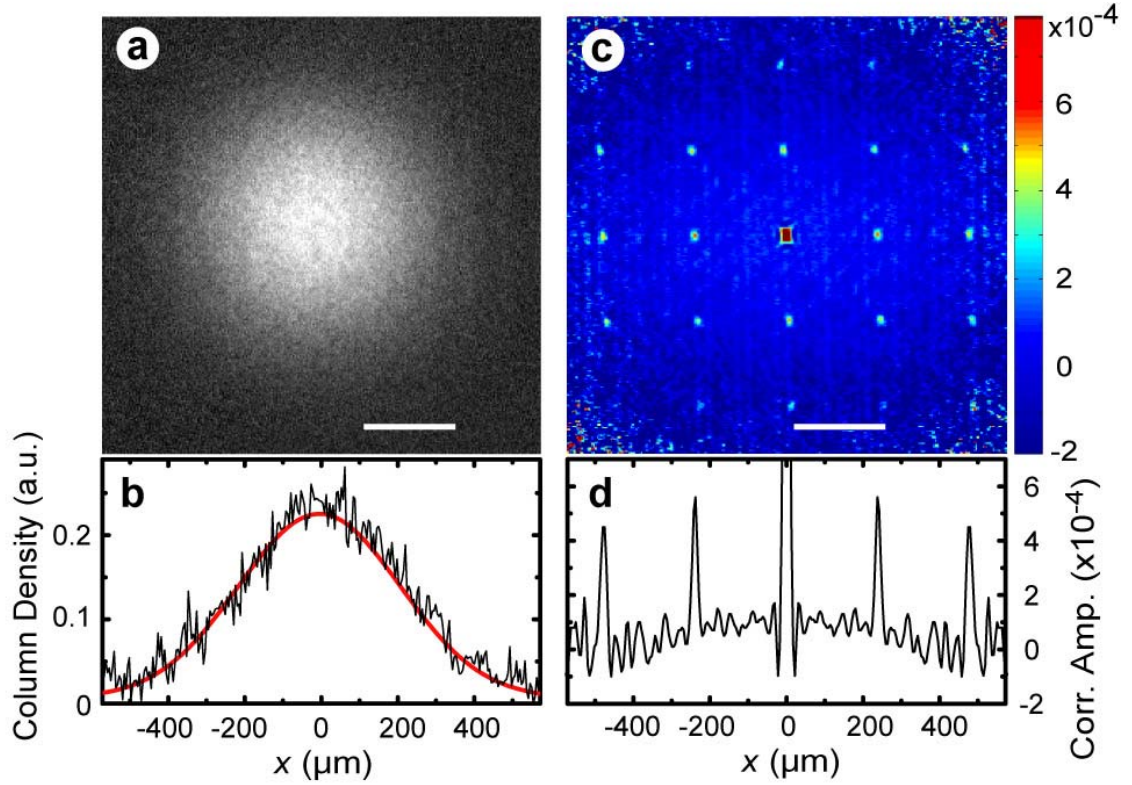


Figure 6 Single shot absorption image including quantum fluctuations and associated spatial correlation function. **a** 2D Column density distribution of a Mott insulating atomic cloud containing 6×10^5 atoms, released from a 3D optical lattice potential with a lattice depth of $50 E_r$. The white bars indicate the reciprocal lattice scale l defined in eq. (2). **b** Horizontal cut (black line) through the centre of the image in **a** and Gaussian fit (red line) to the average over 43 independent images each one similar to **a**. **c** Spatial noise correlation function obtained by analyzing the same set of images, which shows a regular pattern revealing the lattice order of the particles in the trap. **d** Horizontal profile through centre of pattern, containing the peaks separated by integer multiples of l . The width of the individual peaks is determined by the optical resolution of our imaging system. (from S. Fölling *et al.* [Fölling05a])

Creation and Detection of Spinwave and Antiferromagnetic phases in Spin Mixtures

Some of the most interesting and intriguing phases that can be detected with noise correlation interferometry are antiferromagnetic phases and spin waves in optical lattices. We plan to create such spin-waves and antiferromagnetic states by employing the spin-dependent transport and controlled collisions that were first demonstrated in our group [13, 14] and initially proposed by [6, 15, 16]. In ref. [16] it was in fact explicitly suggested to employ the controlled collisions, which essentially allow for a controllable Ising interaction, to create spin waves and spin excitations in lattice systems. For some time now it has however not been clear how such states could be detected in the experiments. However, the novel idea of detecting noise correlations opens a whole new path for detecting many quantum states, including spin waves in optical lattice potentials. We plan

to use our knowledge on the spin-dependent transport [13] and on controlled collisions [14] to excite spin-waves by a repeated application of the collisional operation in a 3D lattice. Furthermore our first results on the noise-correlation interferometry show that such states can indeed be detected (see Figure 7).

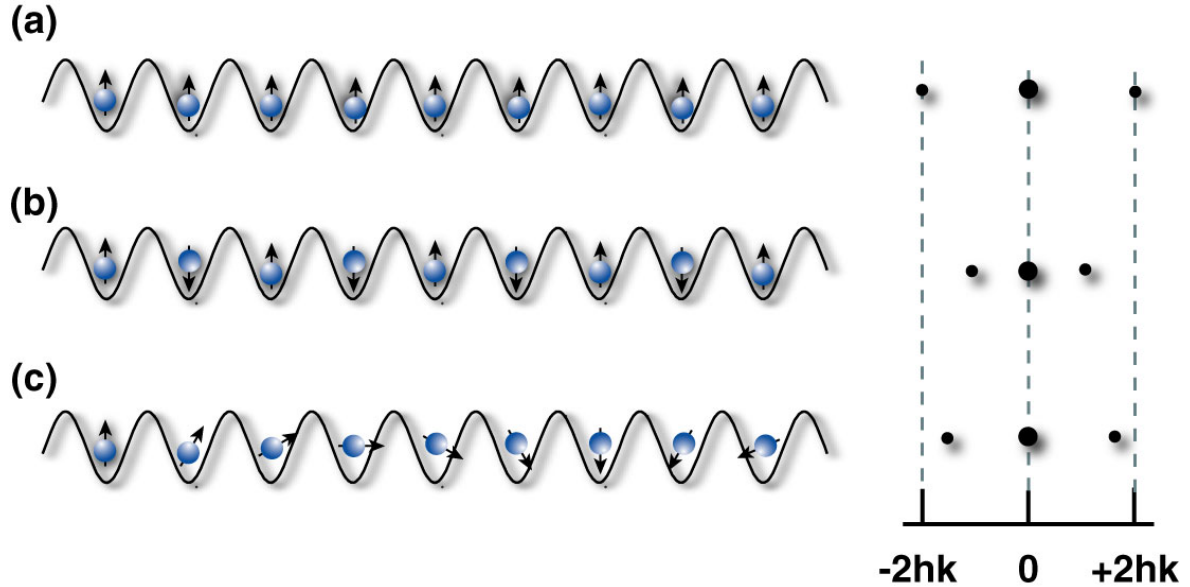


Figure 7 Different strongly correlated many body quantum states (a) Mott insulator, (b) Anti-Ferromagnet and (c) Spin wave with quasimomentum q lead to unique correlation signals, when a spin dependent detection is employed. The graphs on the right hand side schematically display the expected HBT correlation signals in the noise of the expanding atom clouds.

Visibility of the Interference Pattern of a Mott Insulator – Fidelity of a Neutral Atom Quantum Gate Register

A fundamental aspect of ultracold bosonic gases is their phase coherence. The existence of long-range phase coherence, inherent to the description of a Bose-Einstein condensate in terms of a coherent matter wave, was experimentally demonstrated in interferometric [17, 18] or spectroscopic [19] experiments. More recently, attention has been paid to fundamental mechanisms that may degrade or even destroy long-range coherence, for example thermal phase fluctuations in elongated condensates [10, 20], or the superfluid to Mott insulator (MI) transition undergone in optical lattices [3-5].

For a Bose-Einstein condensate released from an optical lattice, the density distribution after expansion shows a sharp interference pattern. In a perfect Mott Insulator, where atomic interactions pin the density to precisely an integer number of atoms per site, phase coherence is completely lost and no interference pattern is expected. The transition between these two limiting cases happens continuously as the lattice depth is increased. In the superfluid phase, a partial loss of long range coherence due to an increased quantum depletion has been observed for lattice depths below the MI transition [21-23]. Conversely, in the insulating phase, numerical simulations [24, 25] predict a residual interference,

although *long-range* coherence and superfluidity have vanished. We observe that the interference pattern persists in the MI phase, and that its visibility decays rather slowly with increasing lattice depth. We explain this behavior as a manifestation of short-range coherence in the insulating phase, fundamentally due to a coherent admixture of particle/hole pairs to the ground state for large but finite lattice depths.

$$|\Psi\rangle_{MI} = |\Psi_0\rangle_{MI} + \frac{J}{U} \sum_{\langle i,j \rangle} \hat{a}_i^\dagger \hat{a}_j |\Psi_0\rangle_{MI}$$

In addition, we also observe reproducible “kinks” in the visibility at well-defined lattice depths. We interpret them as signature of density redistribution in the shell structure of a MI in an inhomogeneous potential, when regions with larger-than-unity filling form.

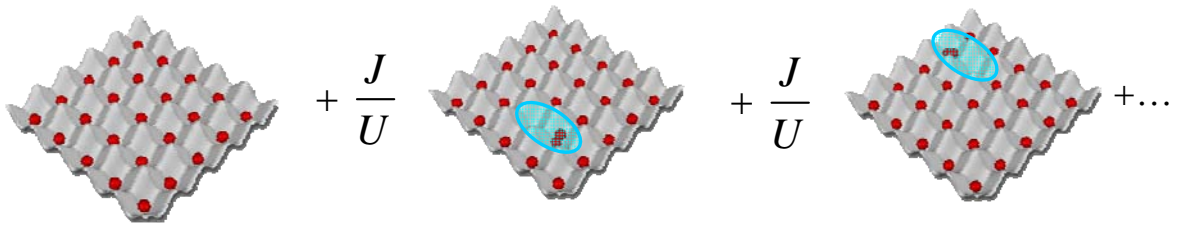


Figure 8 A Mott insulating ground state at finite lattice depths, always possesses particle-hole excitations, even at zero temperatures. Such particle hole excitations are detrimental for quantum information purposes. For deep lattices they can however be compressed, to become negligible. In this work, we have shown, how the time-of-flight interference pattern of atoms released from the lattice potential can be used to identify and characterize such particle-hole defects [26].

The experimental results furthermore show that particle-hole excitations can be sufficiently suppressed for deep lattices, which is important for quantum information applications. In general it is crucial to keep track of the particle-hole pairs, when characterizing the fidelity of the Mott insulating state as a quantum register. Our results show that the visibility of the interference pattern together with other novel measurement and characterization techniques provide this possibility.

Coherent Spin Changing Collisions with Neutral Atoms in Optical Lattices

In a collisional event between two atoms in the vibrational ground state of each lattice site the spin of the individual atoms (m_1, m_2) during the collisional process can be changed into (m_3, m_4) (see Figure 9). This occurs due to an interference in the different scattering channels present in the hyperfine manifold of an Alkali atom and forms the basis for spinor dynamics in BEC systems [27, 28].

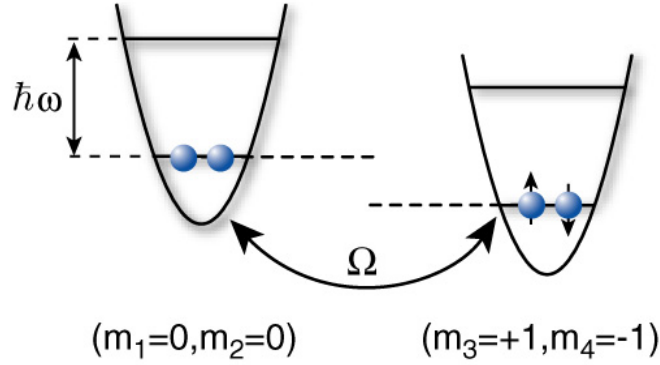


Figure 9 Two-atoms in the vibrational ground state of a single lattice site can undergo a spin changing collisions, in which the spin state of the individual atoms is changed, however, the total magnetization is conserved. Such coherent spin changing collisions can be described as coherent coupling between the initial and final state, leading to Rabi-type oscillations between the two two-particle states.

Here, however, both atoms occupy only a single ground state wave function and the spatial motion of the atom is frozen out and cannot give rise to decoherence. This has allowed us to observe high contrast Rabi-Oscillations between two-particle states of equal magnetization. An atom pair on a single lattice site with magnetic quantum number $|m_1 = 0, m_2 = 0\rangle$ was shown to be coherently coupled to the triplet spin pair $|m_1 = +1, m_2 = -1\rangle$, a Bell state on each lattice site [29]. Such type of Bell states have been shown to possess very long lived coherence times [30], making them very suitable for the generation of robust multi-particle entanglement. We plan to investigate the fundamental process for atoms in the $F=1$ hyperfine manifold of ^{87}Rb , for which no loss process due to hyperfine changing collisions exists. Recently we have demonstrated high contrast Rabi floppings between the two-particle states $|m_F = 0, m_F = 0\rangle \leftrightarrow 1/\sqrt{2}(|m_F = +1, m_F = -1\rangle + |m_F = -1, m_F = +1\rangle)$, purely induced by spin-changing collision processes. Already in first experiments a high visibility of these coherent spin changing collisions, close to 80% was observed, demonstrating the coherent nature of the coupling process and the low decoherence processes present.

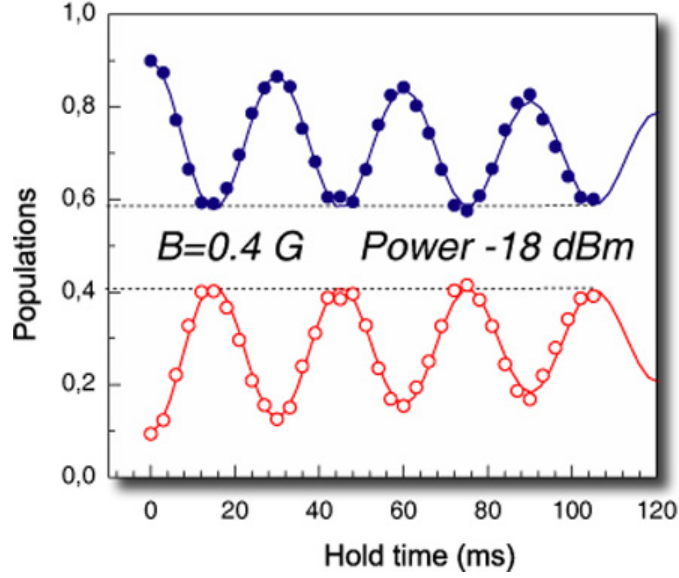


Figure 10 Coherent collisional spin dynamics. The blue datapoints display the fraction of total atoms in spin state $|0,0\rangle$ and the hollow red datapoints display the fraction of total atoms in a Bell state $|+1,-1\rangle$. The process has been shifted into resonance by using a “AC-Zeeman” effect, which allows a control of the two-body process through highly controllable microwave fields alone [31].

One drawback of such Bell pairs on each lattice is that individual atoms cannot be addressed separately. A next goal will be to convert such Bell pairs into addressable Bell pairs, useful for quantum information.

Measurement of the Atom Number Statistics in the SF-MI transition using Coherent Spin-Changing Collisions

One of the most fundamental signatures of the Mott insulator transition undergone by ultracold atomic gases in optical lattices [3-5] is a drastic change in atom number statistics. In a very shallow lattice, ultracold bosons tend to form a Bose-Einstein condensate. In this case, a measurement of the probability for finding n atoms at a given lattice site would reveal a characteristic Poisson distribution with large on-site fluctuations. However, for deeper and deeper lattices, the influence of repulsive interactions, which disfavor such fluctuations, becomes increasingly dominant. This results in the emergence of number-squeezed states with a sub-Poissonian atom number distribution [21]. Above a critical lattice depth, the ultracold gas enters the MI regime, where the number fluctuations are increasingly suppressed. In experiments so far, number-squeezed states due to strong correlations were detected through the observation of increased phase fluctuations - the canonically conjugate variable to number fluctuations [4, 21], or of an increased timescale for phase diffusion in a collapse-and-revival experiment [32].

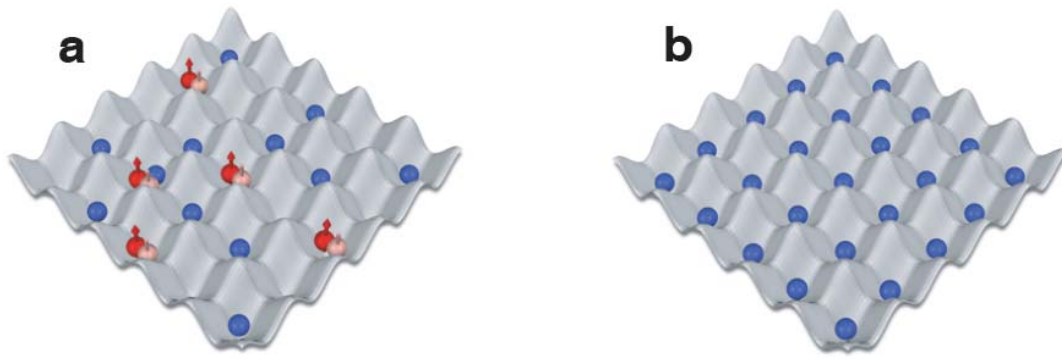


Figure 11 Illustration of the number statistics measurement. Spin changing collisions turn atom pairs initially in the Zeeman substate $m = 0$ (blue) to pairs in $m = \pm 1$ states (red and grey). For one atom per site on average, whether this occurs depends drastically on the many-body correlations. For a MI state (a), only isolated atoms are found and no $m = \pm 1$ pairs are created. On the contrary, for a Bose-Einstein condensate (b), large on-site fluctuations create a finite number of sites with 2 or 3 atoms, where ± 1 pairs can be created.

In a very recent experiment (see [33]), we have directly observed the continuous suppression of number fluctuations when the ultracold sample evolves from the superfluid (SF) regime to deep in the Mott insulator (MI) regime. The idea behind our measurement is illustrated in Figure 11. After producing an ultracold gas in an optical lattice, we suddenly increase the lattice intensity, suppressing tunneling and freezing the number distribution. A probe sensitive only to the presence of atom pairs at a given lattice site is finally applied. Close to unity filling, a non-zero probe signal is obtained only if initially large on-site fluctuations produce a non-zero fraction of sites with two atoms. While we observe this behavior for very shallow lattices, i.e. in the SF regime, the probe signal is progressively suppressed when approaching the Mott transition, and goes to zero for very deep lattices, indicating the emergence of number-squeezed states and finally of a MI with almost vanishing fluctuations.

Motional Qubit Manipulation – Mott Insulators in Excited States

The manipulation of ultracold atoms in optical lattices has so far been restricted to atoms in the motional ground state of each lattice site. In our most recent work, we have investigated the possibilities of preparing atoms in excited motional states at each lattice sites (see Figure 12). Such single atom controllability can become important for novel quantum gate schemes based on motional degrees of freedom [34], and allows the creation of novel quantum spin systems, where the role of the spin orientation is mapped onto a vibrational excitation along one of two lattice axes. The novel possibilities of many body physics in excited bands of the lattice, was first laid out by Isaacson and Girvin from Yale

university [35]. Here a particle can be made to selectively tunnel in a specific direction of the periodic potential by exciting it to the first excited band along this direction. For such a situation a strong enhancement of the tunnel coupling between the lattice sites exists, allowing the particle to move almost freely along such a direction (see Fig. 9).

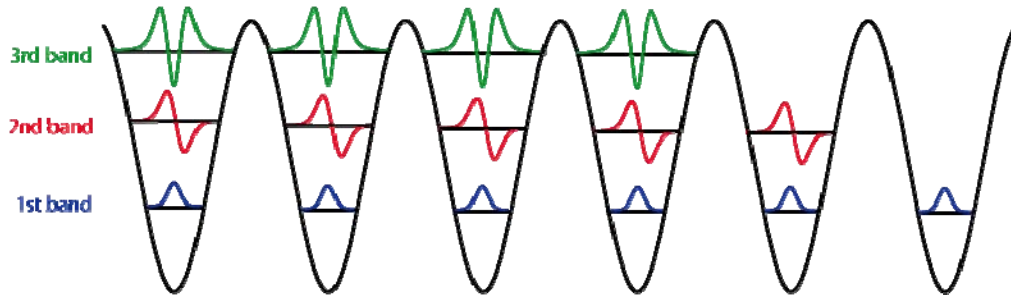


Figure 12 Motional quantum states of neutral atoms in optical lattices. Each of the potential wells of the optical lattice can be approximated by a harmonic oscillator potential, in which atoms can be excited to different motional states. Tunnel coupling between the different motional states leads to the formation of energy bands, with tunnel coupling in higher bands becoming increasingly stronger.

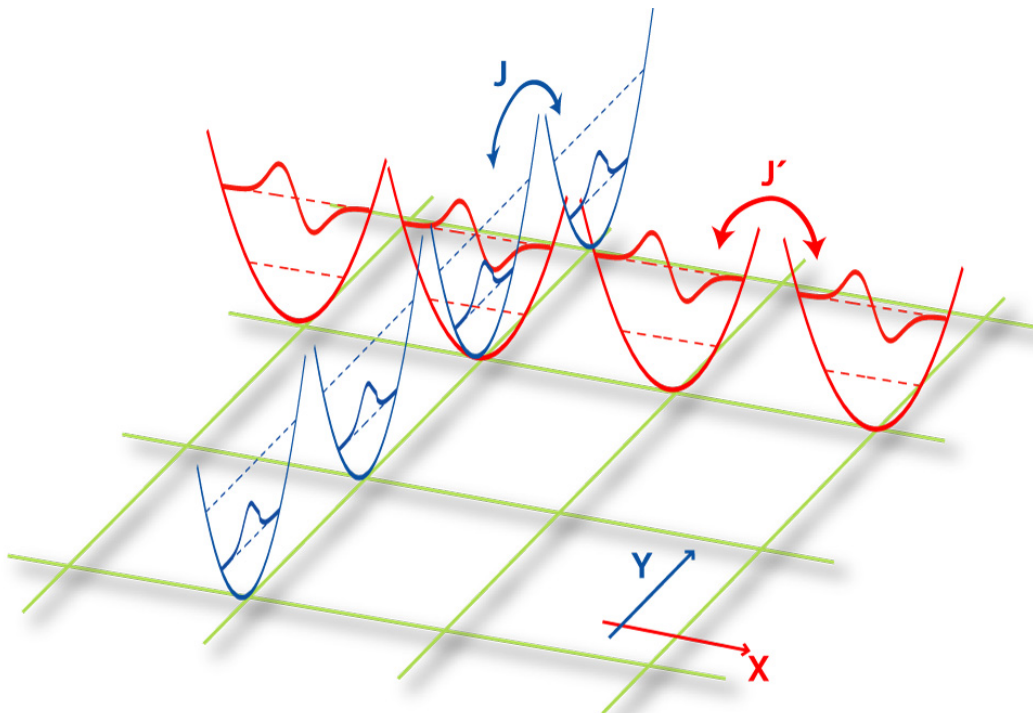


Figure 13 Coupled 1D many body systems can be created via particles that have been selectively excited to the first excited vibrational state along one lattice axis. Such an arrangement allows the simulation of spin Hamiltonians, where the spin degree of freedom is replaced by the vibrational excitation degree of freedom (see [35])

In order to excite atoms into specific motional excited states, we have begun to use stimulated Raman transitions using counterpropagating laser beams, whose difference frequency is controlled by an acousto optical modulator. By tuning the difference frequency of the Raman lasers to a frequency separation of motional states, a coherent

Rabi flopping between those states can be induced (see Figure 15). By turning off the Laser coupling at a specific point in time of such a Rabi oscillation, we can transfer the population between different motional states or create superposition states. Examples of selectively exciting different motional states of the atoms in the lattice can be seen in Figure 16.

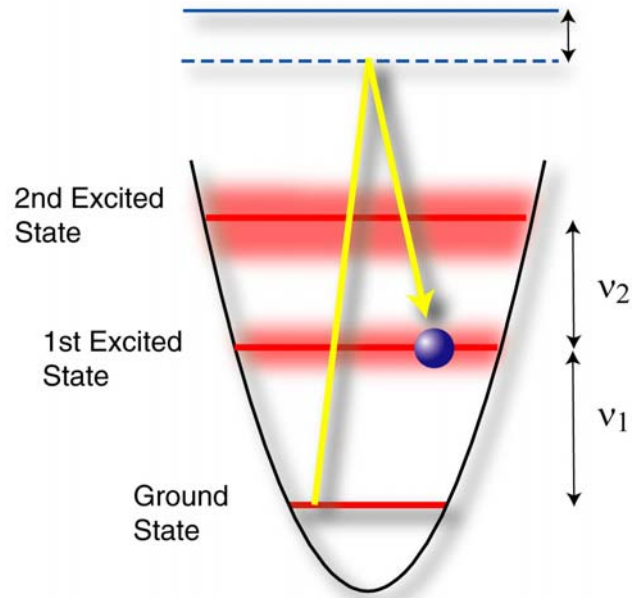


Figure 14 Raman excitation scheme to populate different motional quantum states in an optical potential well. Counterpropagating laser beams are used to drive stimulated Raman transitions. When the difference frequency of the two lasers is tuned to the vibrational separation of the quantum states, atoms can be resonantly and coherently coupled to different motional states.

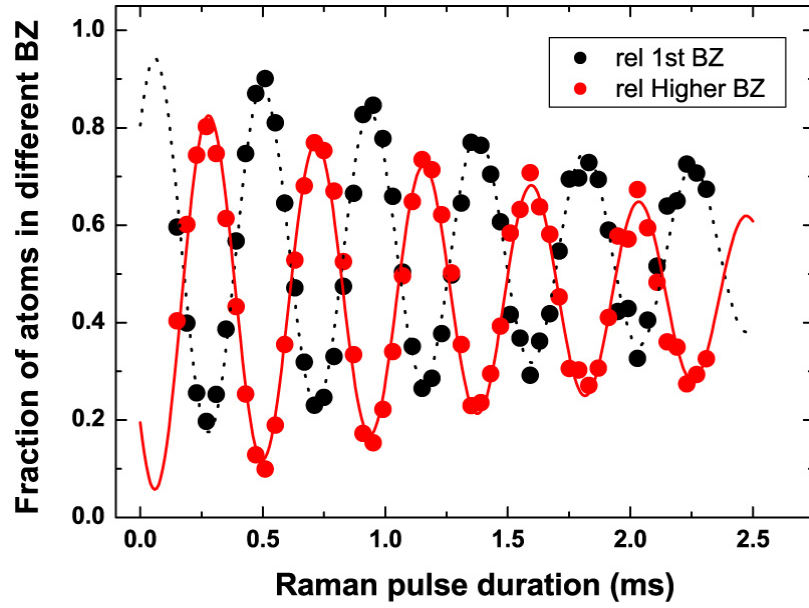


Figure 15 Coherent Rabi flopping between atoms in the motional ground and 1st excited state. High transfer efficiencies of more than 80% have been achieved.

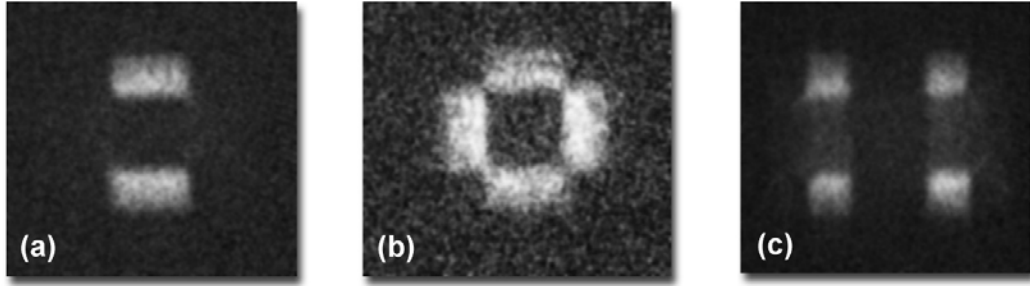


Figure 16 Atoms prepared in different motional quantum states. The excited state populations are detected by using an adiabatic mapping technique of the excited quantum state populations onto the Brillouin zones of the lattice (see refs. [36, 37]). Atoms have been excited to vibrational quantum states (a) ($n_x=0, n_y=1, n_z=0$), (b) ($n_x=1, n_y=0, n_z=0$) and ($n_x=0, n_y=1, n_z=0$), and (c) ($n_x=1, n_y=1, n_z=0$).

Conclusion and Outlook

The work demonstrated during this grant period shows some of the fascinating potential of using ultracold atoms in optical lattices as quantum simulators for many body systems, as well as their potential for applications in quantum information processing. The inherent parallelism and the high degree of controllability make them unique and highly promising for future research. It is very likely that within the next few years we are going to see fundamental problems of condensed matter physics, such as high-T_c superconductivity, being solved by neutral atom quantum simulators [38]. The addition of fermions in optical lattices is a next natural step and is also currently carried out in a second experiment in our group. A major advancement of the field would be the spatial addressability of single atoms at individual lattice sites. We are currently conceiving a next generation experiment, which will allow such an ultrahigh spatial resolution that will take the experimental controllability of ultracold atoms in optical lattices to a next level. Such single atom manipulation capabilities will be crucial for reading and writing quantum information into the system, to detect and reveal fundamental quantum correlations and to probe large scale entanglement with neutral atoms in optical lattices. Next to local atom manipulation possibilities, the search for robust entanglement is an important requirement for quantum information processing. With spin changing collisions, as explored during this contract, a novel way of producing robust and long lived entanglement has been discovered. In a next step it will become important to connect the entangled states produced in this way such as to create large scale and robust entangled states. Initial efforts to explore such possibilities are currently being set up in our laboratory.

Neutral atoms in optical lattices are maturing as novel “synthetic quantum materials” and will profoundly enhance our understanding of complex quantum matter in the future. They have already now brought research at the forefront of condensed matter science together with research at the forefront of quantum optics and atomic physics and have led to important collaborations and interdisciplinary research across different research fields. In this way, ultracold atoms in optical lattices have begun to become important catalysts for solving some of the most outstanding problems in quantum many body systems, with a very promising future ahead and direct consequences for material science research.

Publications obtained during the funding period

2003

[Mandel03a] Mandel, O., M. Greiner, A. Widera, T. Rom, T.W. Hänsch and I. Bloch, *Coherent transport of neutral atoms in spin-dependent optical lattice potentials*, **Physical Review Letters**, 91, 010407, (2003).

[Mandel03b] Mandel, O., M. Greiner, A. Widera, T. Rom, T.W. Hänsch and I. Bloch, *Controlled collisions for multi-particle entanglement of optically trapped atoms*, **Nature**, 425, p. 937, (2003)

[Bloch03] Bloch, I., M. Greiner, O. Mandel and T. W. Hänsch *Coherent cold collisions with neutral atoms in optical lattices*. **Phil. Trans. R. Soc. Lond. A**, 361, 1409 (2003).

2004

[Widera04a] Widera, A., O. Mandel, M. Greiner, S. Kreim, T.W. Hänsch and I. Bloch, *Entanglement interferometry for precision measurement of atomic scattering properties*, **Physical Review Letters**, 92, 160406 (2004).

[Widera04b] Paredes, B., V. Murg, I. Cirac, G. Shlyapnikov, A. Widera, O. Mandel, S. Fölling, M. Greiner, T.W. Hänsch and I. Bloch, *Tonks-Girardeau gas in an optical lattice* **Nature**, 429, 277 (2004).

[Rom04a] Rom, T., T. Best, O. Mandel, A. Widera, M. Greiner, T. W. Hänsch and I. Bloch *State selective production of molecules in optical lattices*. **Physical Review Letters**, 93, 073002 (2004).

2005-2006

[Fölling05a] Fölling, S., F. Gebier, A. Widera, O. Mandel, T. Gericke and I. Bloch *Spatial quantum noise interferometry in expanding ultracold atom clouds*, **Nature**, 434, 481 (2005).

[Gerbier05a] Gerbier, F., A. Widera, S. Fölling, O. Mandel, T. Gericke and I. Bloch *Phase coherence of an atomic Mott insulator*, **Physical Review Letters**, 95, 050404 (2005).

[Gerbier0b] Gerbier, F., A. Widera, S. Fölling, O. Mandel, T. Gericke and I. Bloch *Interference pattern and visibility of a Mott insulator*, **Physical Review A**, 72, 053606 (2005).

[Bloch05b] I. Bloch, *Exploring Quantum Matter with Ultracold Atoms in Optical Lattices*, **Journal of Physics B**, 38, S629 (2005).

[Widera05] Widera, A., F. Gerbier, S. Fölling, O. Mandel, T. Gericke and I. Bloch
Coherent collisional spin dynamics in optical lattices,
Physical Review Letters, 95, 190405 (2005).

[Gerbier06] Gerbier, F., S. Fölling, A. Widera, O. Mandel and I. Bloch
Probing Number squeezing of Ultracold Atoms across the Superfluid-Mott Insulator Transition
Physical Review Letters, 96, 090401 (2006)

Publications related to the general audience or review articles

[Bloch04a] Bloch, I.
Quantum gases in optical lattices,
Physics World, 17, 25 (2004).

[Bloch05a] Bloch, I.
Ultracold quantum gases in optical lattices.
Nature Physics, 1, 23 (2005).

[Bloch05c] M. Greiner and I. Bloch
Exploring Quantum Matter with Ultracold Atoms in Optical Lattices
Adv. At. Mol. Phys. 52, 1-47 (2005).

References

1. R.P. Feynman, "Quantum mechanical computers". *Opt. News* 11, 11 (1985)
2. R.P. Feynman, "Quantum mechanical computers". *Found. Phys.* 16, 507 (1986)
3. D. Jaksch, C. Bruder, J.I. Cirac, C.W. Gardiner, and P. Zoller, "Cold Bosonic Atoms in Optical Lattices". *Phys. Rev. Lett.* 81, 3108 (1998)
4. M. Greiner, O. Mandel, T. Esslinger, T.W. Hänsch, and I. Bloch, "Quantum phase transition from a superfluid to a Mott insulator in a gas of ultracold atoms". *Nature* 415, 39 (2002)
5. T. Stöferle, H. Moritz, C. Schori, M. Köhl, and T. Esslinger, "Transition from a strongly interacting 1D superfluid to a Mott insulator". *Phys. Rev. Lett.* 92, 130403 (2004)
6. D. Jaksch, H.J. Briegel, J.I. Cirac, C.W. Gardiner, and P. Zoller, "Entanglement of atoms via cold controlled collisions". *Phys. Rev. Lett.* 82, 1975 (1999)
7. H.J. Briegel and R. Raussendorf, "Persistent entanglement in arrays of interacting particles". *Phys. Rev. Lett.* 86, 910 (2001)
8. R. Raussendorf and H.J. Briegel, "A one-way quantum computer". *Phys. Rev. Lett.* 86, 5188 (2001)
9. M. Girardeau, "Relationship between Systems of Impenetrable Bosons and Fermions in One Dimension". *J. Math. Phys.* 1, 516 (1960)
10. D.S. Petrov, G.V. Shlyapnikov, and J.T.M. Walraven, "Regimes of Quantum Degeneracy in Trapped 1D Gases". *Phys. Rev. Lett.* 85, 3745 (2000)
11. V. Dunjko, V. Lorent, and M. Olshanii, "Bosons in Cigar-Shaped Traps: Thomas-Fermi Regime, Tonks-Girardeau Regime, and In Between". *Phys. Rev. Lett.* 86, 5413 (2001)
12. E. Altman, E. Demler, and M. Lukin, "Probing many-body states of ultracold atoms via noise correlations". *Phys. Rev. A* 70, (2004)
13. O. Mandel, M. Greiner, A. Widera, T. Rom, T.W. Hänsch, and I. Bloch, "Coherent transport of neutral atoms in spin-dependent optical lattice potentials". *Phys. Rev. Lett.* 91, 010407 (2003)
14. O. Mandel, M. Greiner, A. Widera, T. Rom, T.W. Hänsch, and I. Bloch, "Controlled Collisions for Multiparticle Entanglement of Optically Trapped Atoms". *Nature* 425, 937 (2003)
15. G. Brennen, C.M. Caves, P.S. Jessen, and I.H. Deutsch, "Quantum logic gates in optical lattices". *Phys. Rev. Lett.* 82, 1060 (1999)
16. A. Sorensen and K. Molmer, "Spin-spin interaction and spin squeezing in optical lattices". *Phys. Rev. Lett.* 83, 2274 (1999)
17. M.R. Andrews, C.G. Townsend, H.-J. Miesner, D.S. Durfee, D.M. Kurn, and K. W., "Observation of Interference Between Two Bose Condensates". *Science* 275, 637 (1997)
18. I. Bloch, T.W. Hänsch, and T. Esslinger, "Measurement of the spatial coherence of a trapped Bose gas at the phase transition". *Nature* 403, 166 (2000)
19. J. Stenger, S. Inouye, A.P. Chikkatur, D.M. Stamper-Kurn, D.E. Pritchard, and K. W., "Bragg Spectroscopy of a Bose-Einstein Condensate". *Phys. Rev. Lett.* 82, 4569 (1999)

20. S. Richard, F. Gerbier, J.H. Thywissen, M. Hugbart, P. Bouyer, and A. Aspect, "Momentum Spectroscopy of 1D Phase Fluctuations in Bose-Einstein Condensates". *Phys. Rev. Lett.* 91, 010405 (2003)
21. C. Orzel, A.K. Tuchman, M.L. Fenselau, M. Yasuda, and M.A. Kasevich, "Squeezed states in a Bose-Einstein condensate". *Science* 291, 2386 (2001)
22. Z. Hadzibabic, S. Stock, B. Battelier, V. Bretin, and J. Dalibard, "Interference of an array of independent Bose-Einstein condensates". *Phys. Rev. Lett.* 93, 180403 (2004)
23. C. Schori, T. Stöferle, H. Moritz, M. Köhl, and T. Esslinger, "Excitations of a Superfluid in a Three-Dimensional Optical Lattice". *Phys. Rev. Lett.* 93, 240402 (2004)
24. V.A. Kashurnikov, N.V. Prokof'ev, and B. Svistunov, "Revealing the superfluid-Mott insulator transition in an optical lattice". *Phys. Rev. A* 66, 031601(R) (2002)
25. R. Roth and K. Burnett, "Superfluidity and Interference Pattern of Ultracold Bosons in Optical Lattices". *Phys. Rev. A* 67, 031602 (2003)
26. F. Gerbier, A. Widera, S. Fölling, O. Mandel, T. Gericke, and I. Bloch, "Phase coherence of an atomic Mott insulator". *Phys. Rev. Lett.* 95, 050404 (2005)
27. H. Schmaljohann, M. Erhard, J. Kronjäger, M. Kottke, S. van Staa, L. Cacciapuoti, J.J. Arlt, K. Bongs, and K. Sengstock, "Dynamics of F=2 Spinor Bose-Einstein Condensates". *Phys. Rev. Lett.* 92, 040402 (2004)
28. M.-S. Chang, C.D. Hamley, M.D. Barrett, J.A. Sauer, K.M. Fortier, W. Zhang, L. You, and M.S. Chapman, "Observation of Spinor Dynamics in Optically Trapped 87Rb Bose-Einstein Condensates". *Phys. Rev. Lett.* 92, 140403 (2004)
29. A. Widera, F. Gerbier, S. Fölling, T. Gericke, O. Mandel, and I. Bloch, "Coherent collisional spin dynamics in optical lattices". *Phys. Rev. Lett.* 95, 190405 (2005)
30. C.F. Roos, G.P.T. Lancaster, R. M., H. Häffner, W. Hänsel, S. Gulde, C. Becher, J. Eschner, F. Schmidt-Kaler, and R. Blatt, "Bell States of Atoms with Ultralong Lifetimes and their Tomographics State Analysis". *Phys. Rev. Lett.* 92, 220402 (2004)
31. F. Gerbier, A. Widera, S. Fölling, O. Mandel, and I. Bloch, "Resonant control of spin dynamics in ultracold quantum gases via microwave dressing". *Phys. Rev. A*. to be submitted (2005)
32. M. Greiner, O. Mandel, T.W. Hänsch, and I. Bloch, "Collapse and revival of the matter wave field of a Bose-Einstein condensate". *Nature* 419, 51 (2002)
33. F. Gerbier, S. Fölling, A. Widera, O. Mandel, and I. Bloch, "Probing the number statistics of ultracold atoms across the superfluid-Mott insulator transition". *Phys. Rev. Lett.* 96, 090401 (2006)
34. T. Calarco, U. Dörner, P.S. Julienne, C.S. Williams, and P. Zoller, "Quantum computations with atoms in optical lattices: Marker qubits and molecular interactions". *Phys. Rev. A* 70, 012306 (2004)
35. A. Isaacson and S. Girvin, "Multiflavor bosonic Hubbard models in the first excited Bloch band of an optical lattice". *Phys. Rev. A* 72, 053604 (2005)
36. M. Greiner, I. Bloch, O. Mandel, T.W. Hänsch, and T. Esslinger, "Exploring phase coherence in a 2D lattice of Bose-Einstein condensates". *Phys. Rev. Lett.* 87, 160405 (2001)
37. I. Bloch and M. Greiner, *Exploring Quantum Matter with Ultracold Atoms in Optical Lattices*, in *Adv. At. Mol. Phys.*, P.R. Berman and C.C. Lin, Editors. 2005, Elsevier: Amsterdam. p. 1.

38. **W. Hofstetter, J.I. Cirac, P. Zoller, E. Demler, and M.D. Lukin, "High-Temperature Superfluidity of Fermionic Atoms in Optical Lattices". Phys. Rev. Lett. 89, 220407 (2002)**

Delarations, Disclaimers and Acknowledgments

Acknowledgement of Support: This material is based upon work supported by the European Office of Aerospace Research and Development, Air Force Office of Scientific Research, Air Force Laboratory, under contract FA8655-03-1-3039.

Disclaimer: Any opinions, findings and conclusions or recommendations expressed in this material are those of the authors and do not necessarily reflect the views of the European Office of Aerospace Research and Development, Air Force Office of Scientific Research, Air Force Laboratory.

The Contractor, Professor Immanuel Bloch, hereby declares that, to the best of his knowledge and belief, the technical data delivered herewith under Contract No. FA8655-03-1-3039 is complete, accurate, and complies with all requirements of the contract.

DATE: ____March 24, 2006____

Name and Title of Authorized Official:



Prof. Dr. Immanuel Bloch_____

I certify that there were no subject inventions to declare as defined in FAR 52.227-13, during the performance of this contract.

DATE: ____March 24, 2006____

Name and Title of Authorized Official:



Publication Reprints

Coherent Transport of Neutral Atoms in Spin-Dependent Optical Lattice Potentials

Olaf Mandel, Markus Greiner, Artur Widera, Tim Rom, Theodor W. Hänsch, and Immanuel Bloch*

Ludwig-Maximilians-Universität, Schellingstrasse 4/III, 80799 Munich, Germany

Max-Planck-Institut für Quantenoptik, 85748 Garching, Germany

(Received 13 January 2003; published 3 July 2003)

We demonstrate the controlled coherent transport and splitting of atomic wave packets in spin-dependent optical lattice potentials. Such experiments open intriguing possibilities for quantum state engineering of many body states. After first preparing localized atomic wave functions in an optical lattice through a Mott insulating phase, we place each atom in a superposition of two internal spin states. Then state selective optical potentials are used to split the wave function of a single atom and transport the corresponding wave packets in two opposite directions. Coherence between the wave packets of an atom delocalized over up to seven lattice sites is demonstrated.

DOI: 10.1103/PhysRevLett.91.010407

PACS numbers: 03.75.Lm, 03.75.Mn, 05.30.Jp, 05.60.Gg

Over the past few years Bose-Einstein condensates (BEC's) in optical lattices have opened fascinating new experimental possibilities in condensed matter physics, atomic physics, quantum optics, and quantum information processing. Already now the study of Josephson junction-like effects [1,2], the formation of strongly correlated quantum phases [3–5], and the observation of the collapse and revival of the matter wave field of a BEC [6] have shown some of these diverse applications. In an optical lattice, neutral atoms can be trapped in the intensity maxima (or minima) of a standing wave light field due to the optical dipole force [7,8]. So far the optical potentials used have been mostly independent of the internal ground state of the atom. However, it has been suggested that by using spin-dependent periodic potentials one could bring atoms on different lattice sites into contact and thereby realize fundamental quantum gates [9–12], create large scale entanglement [13,14], excite spin waves [15,16], study quantum random walks [17], or form a universal quantum simulator to simulate fundamental complex condensed matter physics Hamiltonians [18]. Here we report on the realization of a coherent spin-dependent transport of neutral atoms in optical lattices [19,20]. We show how the wave packet of an atom that is initially localized to a single lattice site can be split and delocalized in a controlled and coherent way over a defined number of lattice sites.

In order to realize a spin-dependent transport for neutral atoms in optical lattices, a standing wave configuration formed by two counterpropagating laser beams with linear polarization vectors enclosing an angle θ has been proposed [9,13]. Such a standing wave light field can be decomposed into a superposition of a σ^+ and σ^- polarized standing wave laser field, giving rise to lattice potentials $V_+(x, \theta) = V_{\max} \cos^2(kx + \theta/2)$ and $V_-(x, \theta) = V_{\max} \cos^2(kx - \theta/2)$. Here k is the wave vector of the laser light used for the standing wave and V_{\max} is the potential depth of the lattice. By changing the polarization angle θ one can thereby control the separation between the two

potentials $\Delta x = \theta/180^\circ \cdot \lambda_x/2$. When increasing θ , both potentials shift in opposite directions and overlap again when $\theta = n \cdot 180^\circ$, with n being an integer. For a spin-dependent transfer two internal spin states of the atom should be used, where one spin state dominantly experiences the $V_+(x, \theta)$ potential and the other spin state mainly experiences the $V_-(x, \theta)$ dipole force potential. Such a situation can be realized in rubidium by tuning the wavelength of the optical lattice laser to a value of $\lambda_x = 785$ nm between the fine structure splitting of the rubidium $D1$ and $D2$ transitions. Then the dipole potential experienced by an atom in, e.g., the $|1\rangle \equiv |F=2, m_F=-2\rangle$ state is given by $V_1(x, \theta) = V_-(x, \theta)$ and that for an atom in the $|0\rangle \equiv |F=1, m_F=-1\rangle$ state is given by $V_0(x, \theta) = 3/4 V_+(x, \theta) + 1/4 V_-(x, \theta)$. If an atom is now first placed in a coherent superposition of both internal states $1/\sqrt{2}(|0\rangle + i|1\rangle)$ and the polarization angle θ is continuously increased, the spatial wave packet of the atom is split with both components moving in opposite directions.

As in our previous experiments, Bose-Einstein condensates of up to 3×10^5 atoms are created in the $|F=1, m_F=-1\rangle$ hyperfine state in a harmonic magnetic trap with almost isotropic oscillation frequencies of $\omega = 2\pi \times 16$ Hz. A three dimensional lattice potential is then superimposed on the Bose-Einstein condensate and the intensity raised in order to drive the system into a Mott insulating phase [5]. The atoms are thereby localized to individual lattice sites with no long range phase coherence. Tunneling between neighboring lattice sites is suppressed and irrelevant for the observed dynamics of the experiment. Two of the three orthogonal standing wave light fields forming the lattice potential are operated at a wavelength of $\lambda_{y,z} = 840$ nm. For the third standing wave field along the horizontal x direction a laser at a wavelength of $\lambda_x = 785$ nm is used. Along this axis a quarter wave plate and an electro-optical modulator (EOM) allow us to dynamically rotate the polarization vector of the retroreflected laser beam through an angle θ

by applying an appropriate voltage to the EOM (see Fig. 1). Initially the polarization angle θ is set to a lin || lin polarization configuration. After reaching the Mott insulating phase we completely turn off the harmonic magnetic trapping potential but maintain a 1 G homogeneous magnetic field along the x direction in order to preserve the spin polarization of the atoms. This homogeneous field is actively stabilized to an accuracy of ≈ 1 mG. Shortly before moving the atoms along this standing wave direction we adiabatically turn off the lattice potentials along the y and z directions. This is done in order to reduce the interaction energy, which strongly depends on the confinement of the atoms at a single lattice site. We can thereby study the transport process itself at a single-particle level, without having to take into account the phase shifts in the many body state that result from a coherent collisional interaction between atoms.

By using microwave radiation around 6.8 GHz we are able to drive Rabi oscillations between the $|0\rangle$ and the $|1\rangle$ state with resonant Rabi frequencies of $\Omega = 2\pi \times 40$ kHz, such that, e.g., a π pulse can be achieved in a time of 12.5 μ s. The microwave field therefore allows us to place the atom into an arbitrary superposition of the two internal states $|0\rangle$ or $|1\rangle$.

During the shifting process of the atoms it is crucial to avoid unwanted vibrational excitations, especially if the shifting process would be repeated frequently. We therefore analyze the time scale for such a movement process in the following way. First the atom is placed either in state $|0\rangle$ or state $|1\rangle$ by using microwave pulses in a standing wave lin || lin polarization configuration. Then we rotate the polarization to an angle $\theta = 180^\circ$ in a linear ramp within a time τ , such that again a lin || lin polarization configuration is achieved. However, during this process the atoms will have moved by a distance $\pm \lambda_x/4$ depending on their internal state. In order to determine whether any higher lying vibrational states have been populated, we adiabatically turn off the lattice potential within a time of 500 μ s. The population of the energy bands is then mapped onto the population of the corresponding Brillouin zones [21,22]. By counting the num-

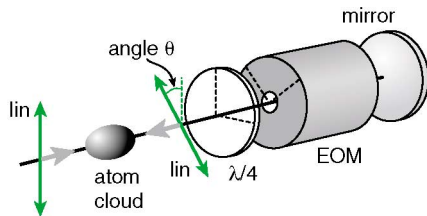


FIG. 1 (color online). Schematic experimental setup. A one dimensional optical standing wave laser field is formed by two counterpropagating laser beams with linear polarizations. The polarization angle of the returning laser beam can be adjusted through an electro-optical modulator. The dashed lines indicate the principal axes of the wave plate and the EOM.

ber of atoms outside of the first Brillouin zone of the system relative to the total number of atoms we are able to determine the fraction of vibrationally excited atoms after the shifting of the lattice potential (see Fig. 2). For a perfectly linear ramp with infinite acceleration at the beginning and ending of the ramp one would expect the fraction of atoms in the first vibrational state to be given by $|c_1(\tau)|^2 = 2v^2/(a_0\omega)^2 \sin^2(\omega\tau/2)$, where $v = \lambda_x/(4\tau)$ is the shift velocity, a_0 is the size of the ground state harmonic oscillator wave function, and ω is the vibrational frequency on each lattice site.

We have measured the vibrational frequencies on a lattice site for different polarization angles θ by slightly modulating the lattice position and observing a resonant transfer of atoms to the first excited vibrational state. For atoms in the $|1\rangle$ state the vibrational frequencies remain constant for different polarization angles θ as the lattice potential depth $V_1(x, \theta)$ remains constant. However, for atoms in the $|0\rangle$ state the lattice potential depth $V_0(x, \theta)$ decreases to 50% in a lin \perp lin configuration. In order to reduce this effect we tilt the EOM by 3° and thereby decrease the strength of the σ^- standing wave but increase the strength of the σ^+ standing wave in such a polarization configuration. Then both trapping frequencies for the $|0\rangle$ and the $|1\rangle$ state decrease to approximately 85% in a lin \perp lin configuration relative to their initial value of $\omega = 2\pi \times 45$ kHz in a lin || lin standing wave configuration. For such trapping frequencies of ≈ 45 kHz during the transport process, the excitation probability should remain below 5% for shifting times longer than $\approx 2\pi/\omega_x$, taking into account the finite bandwidth of our

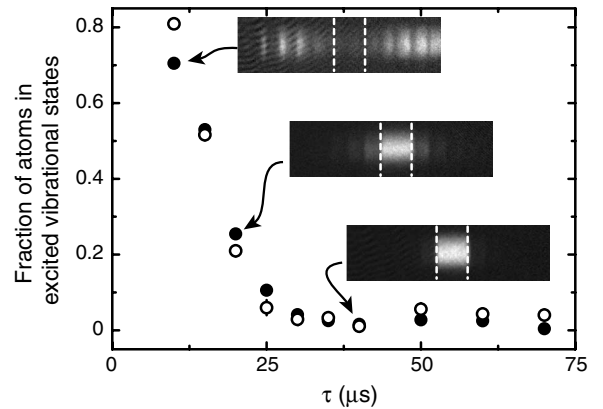


FIG. 2. Fraction of atoms in excited vibrational states after moving the lattice potential in a time τ over a distance of $\lambda_x/4$. Filled (hollow) circles denote atoms in the $|1\rangle$ ($|0\rangle$) state. The images show the population of the Brillouin zones when the lattice potential was adiabatically ramped down after the shifting process. These absorption images correspond to the $|1\rangle$ state and were taken after a time of flight period of 14 ms. The white dashed lines in the images denote the borders of the first Brillouin zone. Atoms within this Brillouin zone correspond to atoms in the vibrational ground state on each lattice site.

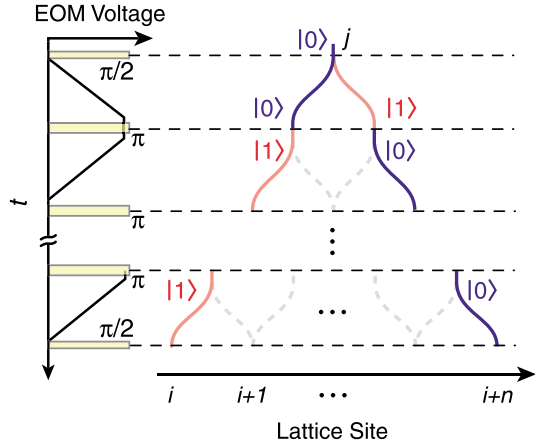


FIG. 3 (color online). General interferometer sequence used to delocalize an atom over an arbitrary number of lattice sites. Initially an atom is localized to the j th lattice site. The graph on the left indicates the EOM voltage and the sequence of $\pi/2$ and π microwave pulses that are applied over time (see text).

high voltage amplifier. This finite bandwidth smooths the edges of our linear voltage ramp and thereby efficiently suppresses the oscillatory structure in the calculated excitation probability (see Fig. 2).

In order to verify the coherence of the spin-dependent transport we use the interferometer sequence of Fig. 3. Let us first consider the case of a single atom being initially localized to the j th lattice site. First, the atom is placed in a coherent superposition of the two internal states $|0\rangle_j$ and $|1\rangle_j$ with a $\pi/2$ microwave pulse (here the index denotes the position in the lattice). Then the polarization angle θ is rotated to 180° , such that the spatial wave packet of an atom in the $|0\rangle$ and the $|1\rangle$ state are transported in opposite directions. The final state after such a movement process is then given by $1/\sqrt{2}(|0\rangle_j + i\exp(i\beta)|1\rangle_{j+1})$, where the wave function of an atom has been delocalized over the j th and the $(j+1)$ th lattice site. The phase β between the two wave packets depends on the accumulated kinetic and potential energy phases in the transport process and in general will be nonzero. In order to reveal the coherence between the two wave packets, we apply a final $\pi/2$ microwave pulse that erases the which way information encoded in the hyperfine states. We then release the atoms from the confining potential by suddenly turning off the standing wave optical potential and observe the momentum distribution of the trapped atoms in the $|1\rangle$ state with absorption imaging after a time of flight period. As a result of the above sequence, the spatial wave packet of an atom in the $|0\rangle$ ($|1\rangle$) state is delocalized over two lattice sites resulting in a double slit momentum distribution $w(p) \propto \exp[-p^2/(\hbar/\sigma_x)^2] \cdot \cos^2(p\delta x_0/2\hbar + \beta/2)$ [see Fig. 4(a)], where δx_0 denotes the separation between the two wave packets and σ_x is the spatial extension of the Gaussian ground state wave function on each lattice site. In order to increase the separation be-

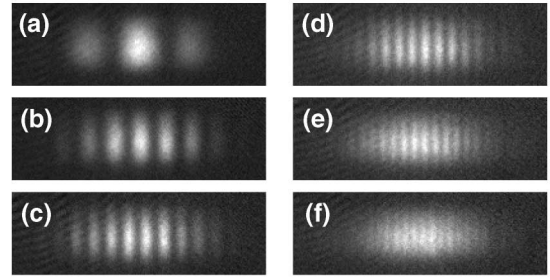


FIG. 4. Observed interference patterns in state $|1\rangle$ after initially localized atoms have been delocalized over (a) two, (b) three, (c) four, (d) five, (e) six, and (f) seven lattice sites using the interferometer sequence of Fig. 3. The time of flight period before taking the images was 14 ms and the horizontal size of each image is $880 \mu\text{m}$. The shift time for this experiment was $50 \mu\text{s}$.

tween the two wave packets further, one could increase the polarization angle θ to further integer multiples of 180° . In practice, such an approach is, however, limited by the finite maximum voltage that can be applied to the EOM. In order to circumvent this limitation we apply a microwave π pulse after the polarization has been rotated to $\theta = +180^\circ$, thereby swapping the role of the two hyperfine states. By then returning the polarization vector to $\theta = 0^\circ$, we do not bring the two wave packets of an atom back to their original site but rather further increase the separation between the wave packets (see Fig. 3). The interlaced π pulse provides a further advantage of canceling inhomogeneous phase shifts acquired in the single-particle phase β in a spin-echo-like sequence. With increasing separation between the two wave packets the fringe spacing of the interference pattern further decreases (see Fig. 4). We have been able to observe such interference patterns for two wave packets delocalized over up to seven lattice sites [see Fig. 4(f)]. When

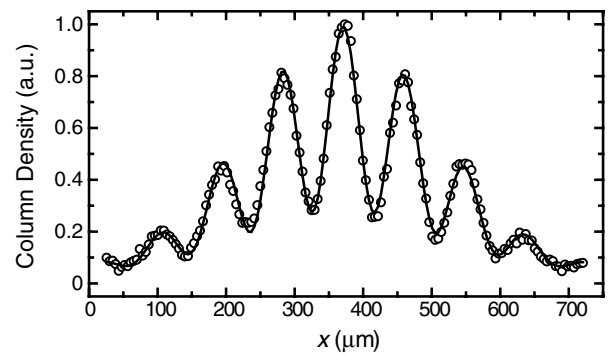


FIG. 5. Profile of the interference pattern obtained after delocalizing atoms over three lattice sites with a $\pi/2$ - π - $\pi/2$ microwave pulse sequence. The solid line is a fit to the interference pattern with a sinusoidal modulation, a finite visibility ($\approx 60\%$), and a Gaussian envelope. The time of flight period was 15 ms.

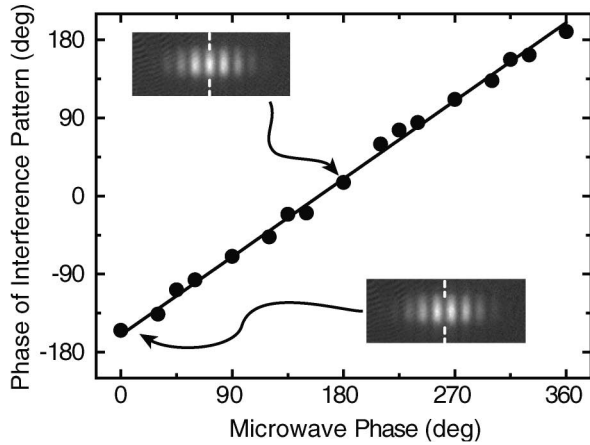


FIG. 6. Phase of the interference pattern vs the phase α of the final microwave $\pi/2$ pulse in a $\pi/2$ - π - $\pi/2$ delocalization sequence (see Fig. 3). The absorption images show the measured interference pattern for $\alpha = 0^\circ$ and $\alpha = 180^\circ$ after a time of flight period of 15 ms. The solid line is a linear fit to the data with unity slope and a variable offset. The dashed lines in the images correspond to the center of the envelope of the interference pattern.

moving the atoms over up to three lattice sites, the visibility of the interference pattern remains rather high with up to 60% (see Fig. 5). These high contrast interference patterns directly prove the coherence of the transport process and also show that the single-particle phase β acquired for each atom is almost constant throughout the cloud of atoms in our system. If the movement process is repeated more often, inhomogeneously acquired phase shifts over the cloud of atoms significantly decrease the visibility.

For many further applications of the coherent spin-dependent transport it will also be crucial that the single-particle phase β is not only constant throughout the cloud of atoms within a single run of the experiment but is also reproducible between different sets of experiments. We have verified this by varying the phase α of the final microwave $\pi/2$ pulse in a sequence where an atom is delocalized over three lattice sites. In Fig. 6 we plot the experimentally measured phase of the interference pattern vs the phase α of the final microwave pulse obtained in different runs of the experiment. We find a high correlation between the detected phase of the interference pattern vs the phase of the applied microwave pulse which proves that indeed the single-particle phase is constant between different experiments and can be canceled via the phase of the final microwave pulse.

In conclusion we have demonstrated the coherent spin-dependent transport of neutral atoms in optical lattices, thereby showing an essential level of coherent control for many future applications. The method demonstrated here, e.g., provides a simple way to continuously tune the interspecies interactions by controlling the overlap of

the two ground state wave functions for the two spin states. Furthermore, if such a transport is carried out in a three dimensional lattice, where the on-site interaction energy between atoms is large, one could induce interactions between almost any two atoms on different lattice sites in a controlled way. Such controlled interactions of Ising or Heisenberg type could then be used to simulate the behavior of quantum magnets [15], to realize quantum gates between different atoms [9–12], or to generate highly entangled cluster states [10,13] that could form the basis of a one-way quantum computer [11].

We thank Ignacio Cirac and Hans Briegel for stimulating discussions, Alexander Altmeyer for help during the initial phase of the experiment, and Anton Scheich for assistance with the electronics. We also acknowledge financial support from the AFOSR and from the Bayerische Forschungsförderung.

*Electronic addresses: imb@mpq.mpg.de; <http://www.mpq.mpg.de/~haensch/bec>

- [1] B. P. Anderson and M. A. Kasevich, *Science* **282**, 1686 (1998).
- [2] F. S. Cataliotti *et al.*, *Science* **293**, 843 (2001).
- [3] D. Jaksch *et al.*, *Phys. Rev. Lett.* **81**, 3108 (1998).
- [4] C. Orzel *et al.*, *Science* **291**, 2386 (2001).
- [5] M. Greiner *et al.*, *Nature (London)* **415**, 39 (2002).
- [6] M. Greiner *et al.*, *Nature (London)* **419**, 51 (2002).
- [7] P. S. Jessen and I. H. Deutsch, *Adv. At. Mol. Opt. Phys.* **37**, 95 (1996).
- [8] R. Grimm, M. Weidemüller, and Y. B. Ovchinnikov, *Adv. At. Mol. Opt. Phys.* **42**, 95 (2000).
- [9] G. K. Brennen *et al.*, *Phys. Rev. Lett.* **82**, 1060 (1999).
- [10] H.-J. Briegel *et al.*, *J. Mod. Opt.* **47**, 415 (2000).
- [11] R. Raussendorf and H.-J. Briegel, *Phys. Rev. Lett.* **86**, 5188 (2001).
- [12] G. K. Brennen, I. H. Deutsch, and C. J. Williams, *Phys. Rev. A* **65**, 022313 (2002).
- [13] D. Jaksch *et al.*, *Phys. Rev. Lett.* **82**, 1975 (1999).
- [14] H.-J. Briegel and R. Raussendorf, *Phys. Rev. Lett.* **86**, 910 (2001).
- [15] A. Sørensen and K. Mølmer, *Phys. Rev. Lett.* **83**, 2274 (1999).
- [16] Spin waves have recently been observed in H. J. Lewandowski *et al.*, *Phys. Rev. Lett.* **88**, 070403 (2002); J. M. McGuirk *et al.*, *Phys. Rev. Lett.* **89**, 090402 (2002).
- [17] W. Dür *et al.*, *Phys. Rev. A* **66**, 052319 (2002).
- [18] E. Jané *et al.*, *quant-ph/0207011*
- [19] Spin-dependent transport of neutral atoms has also been observed at National Institute of Standards and Technology. William Phillips (private communication).
- [20] In a fixed polarization configuration, spin-dependent tunneling between two lattice sites has been observed in D. L. Haycock *et al.*, *Phys. Rev. Lett.* **85**, 3365 (2000).
- [21] A. Kastberg *et al.*, *Phys. Rev. Lett.* **74**, 1542 (1995).
- [22] M. Greiner *et al.*, *Phys. Rev. Lett.* **87**, 160405 (2001).

of 3.2×10^{12} cm for a prograde orbit of $J/(GM_{\text{BH}}/c) = 0.52$; the last stable retrograde orbit for that spin parameter has a period of 38 min at a radius of 4×10^{12} cm). Lense-Thirring precession and viscous (magnetic) torques will gradually force the accreting gas into the black hole's equatorial plane²⁹. Recent numerical simulations indicate that a (prograde) disk analysis is appropriate to first order even for the hot accretion flow at the Galactic Centre²⁷. □

Received 13 July; accepted 23 September 2003; doi:10.1038/nature02065.

- Schödel, R. *et al.* A star in a 15.2 year orbit around the supermassive black hole at the centre of the Milky Way. *Nature* **419**, 694–696 (2002).
- Ghez, A. M. *et al.* The first measurement of spectral lines in a short-period star bound to the Galaxy's central black hole: A paradox of youth. *Astrophys. J.* **586**, L127–L131 (2003).
- Eisenhauer, F. *et al.* A geometric determination of the distance to the Galactic Center. *Astrophys. J. Lett.* (in the press); preprint at (<http://arXiv.org/astro-ph/0306220>) (2003).
- Doeleman, S. S. *et al.* Structure of SgrA* at 86 GHz using VLBI closure quantities. *Astron. J.* **121**, 2610–2617 (2001).
- Backer, D. C. & Sramek, R. A. Proper motion of the compact, nonthermal radio source in the Galactic Center, SgrA*. *Astrophys. J.* **524**, 805–815 (1999).
- Baganoff, F. K. *et al.* Chandra X-ray spectroscopic imaging of SgrA* and the central parsec of the Galaxy. *Astrophys. J.* **591**, 891–915 (2003).
- Hornstein, S. D. *et al.* Limits on the short-term variability of SgrA* in the near-IR. *Astrophys. J.* **577**, L9–L13 (2002).
- Melia, F. & Falcke, H. The supermassive black hole at the Galactic Center. *Annu. Rev. Astron. Astrophys.* **39**, 309–352 (2001).
- Lenzen, R., Hofmann, R., Bizenberger, P. & Tüsche, A. CONICA: The high-resolution near-infrared camera for the ESO VLT. *Proc. SPIE 3354* (IR Astronomical Instrumentation), 606–614 (1998).
- Rousset, G. *et al.* Design of the Nasmyth adaptive optics system (NAOS) of the VLT. *Proc. SPIE 3353* (Adaptive Optics Technology), 508–516 (1998).
- Benlloch, S., Wilms, J., Edelson, R., Raoqob, T. & Staubert, T. Quasi-periodic oscillation in Seyfert galaxies: Significance levels. The case of Mrk 766. *Astrophys. J.* **562**, L121–L124 (2001).
- Ghez, A. M. *et al.* Variable infrared emission from the supermassive black hole at the center of the Milky Way. *Astrophys. J. Lett.* (submitted); preprint at (<http://arXiv.org/astro-ph/0309076>) (2003).
- Baganoff, F. K. Multi-wavelength monitoring of SgrA* during Chandra observations of multiple X-ray flares. *High Energy Astrophysics Division (HEAD) AAS Abstr.* 3.02, 35 (2003).
- Alexander, T. & Sternberg, A. Near-IR microlensing of stars by the supermassive black hole in the Galactic Center. *Astrophys. J.* **520**, 137–148 (1999).
- Yuan, F., Markoff, S. & Falcke, H. A jet-ADAF model for SgrA*. *Astron. Astrophys.* **854**, 854–863 (2002).
- Liu, S. & Melia, F. New constraints on the nature of the radio emission in SgrA*. *Astrophys. J.* **561**, L77–L80 (2001).
- Yuan, F., Quataert, E. & Narayan, R. Nonthermal electrons in radiatively inefficient flow models of SgrA*. *Astrophys. J.* (submitted); preprint at (<http://arXiv.org/astro-ph/0304125>) (2003).
- Markoff, S., Falcke, H., Yuan, F. & Biermann, P. L. The nature of the 10ksec X-ray flare in SgrA*. *Astron. Astrophys.* **379**, L13–L16 (2001).
- Baganoff, F. K. *et al.* Rapid X-ray flaring from the direction of the supermassive black hole at the Galactic Centre. *Nature* **413**, 45–48 (2001).
- Porquet, D. *et al.* XMM-Newton observation of the brightest X-ray flare detected so far from SgrA*. *Astron. Astrophys.* **407**, L17–L20 (2003).
- Zhao, J.-H. *et al.* Variability of SgrA*: Flares at 1 mm. *Astrophys. J.* **586**, L29–L32 (2003).
- Miyazaki, A., Tstsumi, T. & Tsuboi, M. Flares of SgrA* at short submm wavelengths. *Astron. Nachr.* **324**, 3–9 (2003).
- Nayakshin, S., Cuadra, J. & Sunyaev, R. X-ray flares from SgrA*: Star-disk interactions? *Astron. Astrophys.* (in the press); preprint at (<http://arXiv.org/astro-ph/0304126>) (2003).
- Hollywood, J. M. & Melia, F. General relativistic effects on the infrared spectrum of thin accretion disks in active galactic nuclei: Application to SgrA*. *Astrophys. J. Suppl.* **112**, 423–455 (1997).
- Bardeen, J. M., Press, W. M. & Teukolsky, S. A. Rotating black holes: Locally non-rotating frames, energy extraction and scalar synchrotron radiation. *Astrophys. J.* **178**, 347–369 (1972).
- Melia, F., Bromley, C., Liu, S. & Walker, C. K. Measuring the black hole spin in SgrA*. *Astrophys. J.* **554**, L37–L40 (2001).
- De Villiers, J.-P., Hawley, J. F. & Krolik, J. H. Magnetically driven accretion flows in the Kerr metric I: Models and overall structure. *Astrophys. J.* (submitted); preprint at (<http://arXiv.org/astro-ph/0307260>) (2003).
- Nowak, M. A., Wagoner, R. V., Begelman, M. C. & Lehr, D. E. The 67 Hz feature in the black hole candidate GRS1915 + 105 as a possible diskoseismic mode. *Astrophys. J.* **477**, L91–L94 (1997).
- Bardeen, J. M. & Petterson, J. A. The Lense-Thirring effect and accretion disks around Kerr black holes. *Astrophys. J.* **105**, L65–L67 (1975).

Acknowledgements This Letter is based on observations at the VLT of the European Observatory (ESO) in Chile. We thank the teams who developed and constructed the near-infrared camera CONICA and the AO system NAOS, and especially their principal investigators, R. Lenzen, R. Hofmann and G. Rousset. We thank H. Falcke and S. Markoff for access to their database of the SgrA* SED, as well as discussions of emission processes. We are grateful to D. Porquet and P. Predehl for discussions of their XMM data, S. Nayakshin, M. Rees, R. Sunyaev and especially E. Quataert for discussions of accretion disk physics, and A. Sternberg for suggestions on the paper.

Competing interests statement The authors declare that they have no competing financial interests.

Correspondence and requests for materials should be addressed to R.G. (genzel@mpe-garching.mpg.de).

Controlled collisions for multi-particle entanglement of optically trapped atoms

Olaf Mandel, Markus Greiner, Artur Widera, Tim Rom, Theodor W. Hänsch & Immanuel Bloch

Sektion Physik, Ludwig-Maximilians-Universität, Schellingstrasse 4/III, D-80799 Munich, Germany, and the Max-Planck-Institut für Quantenoptik, D-85748 Garching, Germany

Entanglement lies at the heart of quantum mechanics, and in recent years has been identified as an essential resource for quantum information processing and computation^{1–4}. The experimentally challenging production of highly entangled multi-particle states is therefore important for investigating both fundamental physics and practical applications. Here we report the creation of highly entangled states of neutral atoms trapped in the periodic potential of an optical lattice. Controlled collisions between individual neighbouring atoms are used to realize an array of quantum gates, with massively parallel operation. We observe a coherent entangling–disentangling evolution in the many-body system, depending on the phase shift acquired during the collision between neighbouring atoms. Such dynamics are indicative of highly entangled many-body states; moreover, these are formed in a single operational step, independent of the size of the system^{5,6}.

Bose–Einstein condensates have been loaded into the periodic dipole force potential of a standing-wave laser field—a so-called optical lattice. In these systems, it has been possible to probe fundamental many-body quantum mechanics in an unprecedented way, with experiments ranging from Josephson junction tunnel arrays^{7,8} to the observation of a Mott insulating state of quantum gases^{9,10}. Important applications of atoms in a Mott insulating state in quantum information processing were envisaged early on. The Mott state itself, with one atom per lattice site, could act as a huge quantum memory, in which information would be stored in atoms at different lattice sites. Going beyond these ideas, it has been suggested that controlled interactions between atoms on neighbouring lattice sites could be used to realize a massively parallel array of neutral-atom quantum gates^{5,11–14}, with which a large multi-particle system could be highly entangled⁶ in a single operational step. Furthermore, the repeated application of the quantum gate array could form the basis for a universal quantum simulator along the original ideas of Feynman for a quantum computer as a simulator of quantum dynamics^{15–17}.

The basic requirement for such control over the quantum state of a many-body system, including its entanglement, is the precise microscopic control of the interactions between atoms on different lattice sites. To illustrate this, let us consider the case of two neighbouring atoms, initially in state $|\Psi\rangle = |0\rangle_j |0\rangle_{j+1}$ placed on the j th and $(j+1)$ th lattice site of the periodic potential in the spin-state $|0\rangle$. First, both atoms are brought into a superposition of two internal states $|0\rangle$ and $|1\rangle$, using a $\pi/2$ pulse such that $|\Psi\rangle = (|0\rangle_j + |1\rangle_j)(|0\rangle_{j+1} + |1\rangle_{j+1})/2$. Then, a spin-dependent transport¹⁸ splits the spatial wave packet of each atom such that the wave packet of the atom in state $|0\rangle$ moves to the left, whereas the wave packet of the atom in state $|1\rangle$ moves to the right. The two wave packets are separated by a distance $\Delta x = \lambda/2$, such that now $|\Psi\rangle = (|0\rangle_j |0\rangle_{j+1} + |0\rangle_j |1\rangle_{j+2} + |1\rangle_{j+1} |0\rangle_{j+1} + |1\rangle_{j+1} |1\rangle_{j+2})/2$, where in the notation atoms in state $|0\rangle$ have retained their original lattice site index and λ is the wavelength of the laser forming the optical periodic potential. The collisional interaction between the atoms^{5,12,19} over a time t_{hold} will lead to a distinct phase shift $\varphi = U_{01} t_{\text{hold}}/\hbar$, when

both atoms occupy the same lattice site $j + 1$ resulting in: $|\Psi\rangle = (|0\rangle_j|0\rangle_{j+1} + |0\rangle_j|1\rangle_{j+2} + e^{-i\varphi}|1\rangle_{j+1}|0\rangle_{j+1} + |1\rangle_{j+1}|1\rangle_{j+2})/2$. Here U_{01} is the onsite-interaction matrix element that characterizes the interaction energy when an atom in state $|0\rangle$ and an atom in state $|1\rangle$ are placed at the same lattice site and \hbar is Planck's constant divided by 2π . Alternatively, a dipole-dipole interaction has been proposed¹¹ for generating a state-dependent phase shift φ . The final many-body state after bringing the atoms back to their original site and applying a last $\pi/2$ pulse can be expressed as $|\Psi\rangle = \frac{1+e^{-i\varphi}}{2}|1\rangle_j|1\rangle_{j+1} + \frac{1-e^{-i\varphi}}{2}|\text{BELL}\rangle$. Here $|\text{BELL}\rangle$ denotes the Bell-like state corresponding to $(|0\rangle_j|0\rangle_{j+1} - |1\rangle_{j+1}) + |1\rangle_j(|0\rangle_{j+1} + |1\rangle_{j+1})/2$.

This scheme can be generalized when more than two particles are placed next to each other, starting from a Mott insulating state of matter^{9,10}. In such a Mott insulating state, atoms are localized to lattice sites, with a fixed number of atoms per site. For three particles for example, one can show that if $\varphi = (2n + 1)\pi$ (with n being an integer), so-called maximally entangled Greenberger-Horne-Zeilinger (GHZ) states²⁰ are realized. For a string of $N > 3$ atoms, where each atom interacts with its left- and right-hand neighbour (see Fig. 1), the entire string of atoms can be entangled to form so-called cluster states in a single operational step^{5,6}. The controlled interactions described above can be viewed as being equivalent to an ensemble of quantum gates acting in parallel^{3,5}.

The experimental set-up used to load Bose-Einstein condensates into the three-dimensional optical lattice potential (see Methods section) is similar to our previous work^{10,19}. Briefly, we start with a quasi-pure Bose-Einstein condensate of 10^5 ^{87}Rb atoms in the $|F = 1, m_F = -1\rangle$ state in a harmonic magnetic trapping potential with isotropic trapping frequencies of $\omega = 2\pi \times 14$ Hz. Here F and m_F denote the total angular momentum and the magnetic quantum number of the atom's hyperfine state. The three-dimensional periodic potential of an optical lattice is then ramped up over a period of 80 ms to a potential depth of $25E_r$, such that the Bose-Einstein condensate is converted into a Mott insulating state. Here

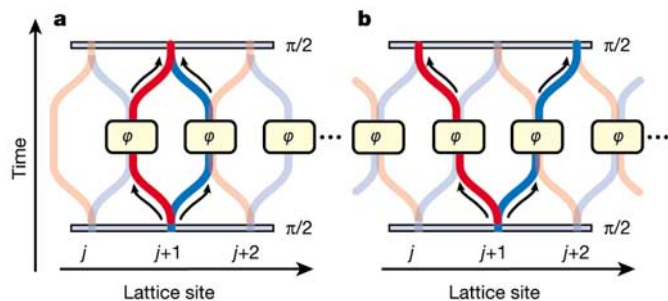


Figure 1 Schematic multiple quantum gate sequences based on controlled interactions. **a**, A chain of neutral atoms on different lattice sites is first placed in a coherent superposition of two spin-states $|0\rangle$ (red) and $|1\rangle$ (blue) with a $\pi/2$ microwave pulse. Then a spin-dependent transport is used to split the spatial wave packet of an atom, and move these two components along two opposite directions depending on their spin-state. The wave packets are separated by a lattice period such that each atom is brought into contact with its neighbouring atom. Owing to the collisional interaction between the atoms, a phase shift φ is acquired during a time t_{hold} that the atoms are held on a common lattice site depending on the spin-state of the atoms. After such a controlled collisional interaction, the wave packets of the individual atoms are returned to their original site and a final microwave $\pi/2$ pulse is applied to all atoms. This multiple quantum gate sequence can be equivalently described as a controllable quantum Ising interaction^{6,12}. **b**, In a slight modification of such a sequence, the atoms are not returned to their original lattice site $j + 1$ but rather delocalized further over the j th and $(j + 2)$ th lattice site after the controlled collisional interaction. The small arrows indicate the different paths that a single atom will follow during the multiple quantum gate sequence. Both sequences can be viewed as multi-particle interferometers, where the many-body output state of the interferometer can in general not be expressed as a product state of single-particle wavefunctions.

E_r denotes the recoil energy $E_r = \hbar^2 k^2 / 2m$, with $k = 2\pi/\lambda$ being the wavevector of the laser light and m the mass of a single atom. For our experimental parameters of atom number and harmonic confinement, such a Mott insulator should consist mainly of a central core with $n = 1$ atoms per lattice site^{9,21,22}. The magnetic trapping potential is then rapidly switched off, but an actively stabilized magnetic offset field of 1 G along the transport direction is maintained to preserve the spin polarization of the atoms. With the optical standing wave along this direction, we are able to realize a spin-dependent transport of the atoms. After turning off the magnetic trapping field, we wait another 40 ms for the electronics to stabilize the magnetic offset field. Thereafter, 3.5 ms before the quantum gate sequence is initiated, we adiabatically increase the lattice depth along this axis to $34 E_r$ such that atoms remain in the vibrational ground state, are tightly confined and can be moved as fast as possible without excitations to higher vibrational states.

In the experiment, the two hyperfine states $|F = 1, m_F = -1\rangle \equiv |0\rangle$ and $|F = 2, m_F = -2\rangle \equiv |1\rangle$ form the logical basis of a single-atom qubit at each lattice site. These two states can be coupled

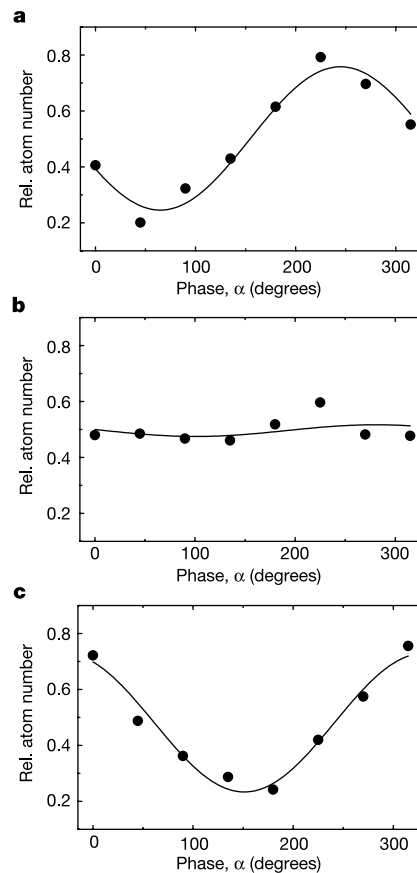


Figure 2 Experimentally measured Ramsey fringes for different hold times t_{hold} during which atoms undergo a controlled collisional interaction with their neighbouring atoms. The experimental sequence used is similar to the one in Fig. 1a, where atoms are returned to their original lattice site after the controlled interaction. The hold times t_{hold} are **a**, 30 μs , **b**, 210 μs and **c**, 450 μs . The relative number of atoms $N_{\text{rel}} = N_1/N_{\text{tot}}$ in the $|1\rangle$ state versus the phase α of the final microwave $\pi/2$ pulse is measured. A state-selective absorption imaging of the atom cloud is used to obtain N_1 after a time-of-flight period of 12 ms, and 110 μs thereafter the total atom number is measured to yield N_{tot} . The solid line indicates a fit of a sinusoidal function with variable amplitude and an offset to the data from which the visibility of the Ramsey fringe is extracted. The change in the phase of the Ramsey fringes for different hold times is mainly caused by the different exposure times of the two spin-states of an atom to differential light shifts of the optical lattice that are not perfectly cancelled in the spin-echo sequence.

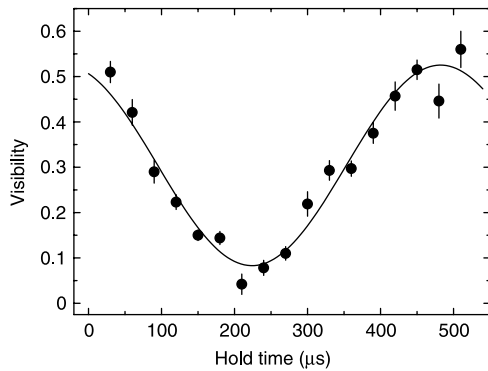


Figure 3 Visibility of Ramsey fringes versus hold times on neighbouring lattice sites for the experimental sequence similar to the one displayed in Fig. 1a. The solid line is a sinusoidal fit to the data including an offset and a finite amplitude. Such a sinusoidal behaviour of the visibility versus the collisional phase shift (determined by the hold time t_{hold}) is expected for a Mott insulating state with an occupancy of $n = 1$ atom per lattice site²³. The maximum observed visibility is limited to 55% by inhomogeneities and time-dependent fluctuations of the lattice potentials throughout the cloud of atoms that are not perfectly compensated by the applied spin-echo sequence (see text).

coherently using resonant microwave radiation around 6.8 GHz. A $\pi/2$ pulse allows us to place the atom in a coherent superposition of the two states within a time of 6 μs . After creating such a coherent superposition, we use a spin-dependent transfer to split and move the spatial wavefunction of the atom over half a lattice spacing in two opposite directions depending on its internal state (see Fig. 1). Such a movement process is carried out within a time of 40 μs in order to avoid any vibrational excitations¹⁸ (the probability for excitations into higher-lying vibrational states was measured to be less than 3%). Atoms on neighbouring sites then interact for a variable amount of time t_{hold} . After half of the hold time, a microwave π pulse is applied. This spin-echo type π pulse is mainly used to cancel unwanted single-particle phase shifts, due, for example, to inhomogeneities in the trapping potentials. It does not, however, affect the non-trivial and crucial collisional phase shift due to the interactions between the atoms. After such a controlled collision, the atoms are moved back to their original site. Then a final $\pi/2$ microwave pulse with variable phase α is applied, and the atom number in state $|1\rangle$ relative to the total atom number is recorded.

The Ramsey fringes obtained in this way are shown in Fig. 2 for some different hold times t_{hold} , and for a wider range of hold times their visibility is plotted in Fig. 3. For short hold times, where no significant collisional phase shift is acquired, a Ramsey fringe with a

visibility of approximately 50% is recorded. For longer hold times we notice a strong reduction in the visibility of the Ramsey fringe, with an almost vanishing visibility of approximately 5% for a hold time of 210 μs (Fig. 2b). This hold time corresponds to an acquired collisional phase shift of $\varphi = \pi$ for which we expect a minimum visibility if the system is becoming entangled.

For such an entangled state the probability for finding atoms in state $|1\rangle$ becomes independent of the phase α corresponding to a vanishing Ramsey fringe. This can be seen, for example, for the two-particle case: when the phase α of the last pulse is kept variable, the maximally entangled state for a collisional phase $\varphi = (2n + 1)\pi$ can be expressed as: $|\Psi(\varphi = \pi)\rangle = \frac{1}{\sqrt{2}}(|0\rangle|-\rangle + |1\rangle|+\rangle)$, where $|-\rangle, \alpha \equiv \frac{1}{\sqrt{2}}(c_-^-|0\rangle - c_-^-|1\rangle)$ and $|+\rangle, \alpha \equiv \frac{1}{\sqrt{2}}(c_+^+|0\rangle + c_+^+|1\rangle)$ with $c_{\pm}^{\pm} \equiv e^{\pm i\alpha}\cos\alpha$ and $c_{\pm}^{\mp} \equiv -(\pm i\sin\alpha - 1)$. Here the probability for finding an atom in either spin-state, for example, $P(|1\rangle)$, is independent of α and equal to 1/2: $P(|1\rangle) = \frac{1}{8}\{|c_+^+|^2 + |c_-^-|^2 + 2|c_+^+|^2\} = \frac{1}{2}$. This indicates that no single-particle operation can place all atoms in either spin-state when a maximally entangled state has been created. The disappearance of the Ramsey fringe has been shown to occur not only for a two-particle system, but is a general feature for an arbitrary N -particle array of atoms that have been highly entangled with the above experimental sequence^{3,23}. A vanishing Ramsey fringe can therefore in principle not distinguish between two-particle or multi-particle entanglement.

For longer hold times, the visibility of the Ramsey fringe increases again reaching a maximum of 55% for a hold time of 450 μs . Here the system becomes disentangled again, as the collisional phase shift is close to $\varphi = 2\pi$ and the Ramsey fringe is restored with maximum visibility.

The coherent ‘entanglement oscillations’ of the many-body system⁶ are recorded for longer hold times by using the multi-particle interferometer sequence of Fig. 1b, where the atoms are not brought back to their original site but are rather kept delocalized¹⁸. This allows us to observe the Ramsey fringe of the previous sequence as a spatial interference pattern in a single run of the experiment in analogy to a double-slit interference experiment, when a state-selective time-of-flight detection is used. Images of such an interference pattern can be seen in Fig. 4 for different hold times t_{hold} . The coherent evolution again indicates the entangling–disentangling dynamics that the system undergoes for different collisional phase shifts φ (see Fig. 5).

Although the observed coherent dynamics in the vanishing and re-emergence of the Ramsey fringe does not provide a rigorous proof of a highly entangled multi-particle state, it is very indicative of such a state. So far, we cannot employ single-atom measurement techniques to detect correlations between individual atoms in the cluster that would provide a quantitative measurement for the size

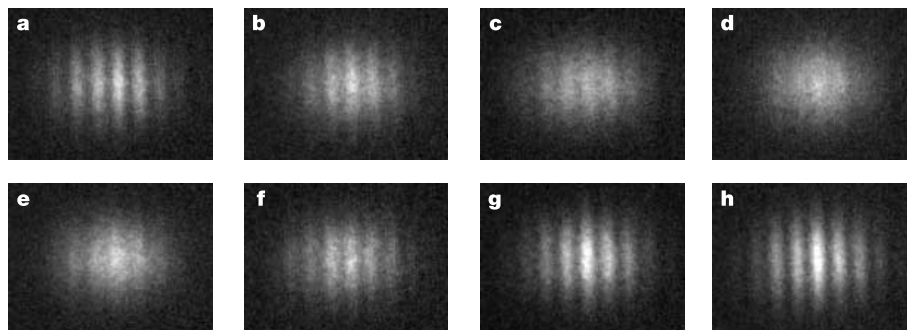


Figure 4 Spatial interference patterns recorded after applying the multiple quantum gate sequence of Fig. 1b for different collisional interaction times t_{hold} . The different hold times (μs) of 30 (a), 90 (b), 150 (c), 210 (d), 270 (e), 330 (f), 390 (g) and 450 (h) lead to different collisional phase shifts φ , ranging from $\varphi \approx 0$ (a) to just over $\varphi \approx 2\pi$ (h). The

vanishing and reappearance of the interference pattern is caused by the coherent entangling–disentangling dynamics in the many-body system due to the controlled collisions between neighbouring atoms. The state-selective absorption images were obtained after a time-of-flight period of 11 ms.

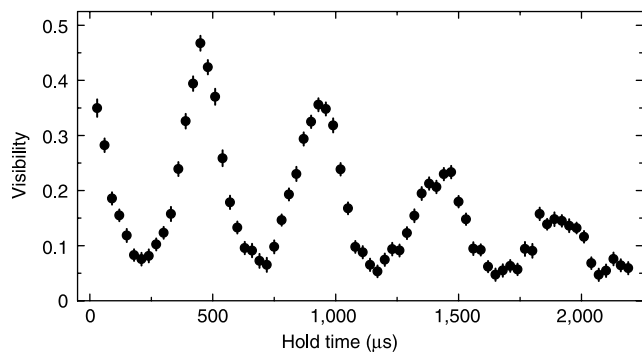


Figure 5 Visibility of the spatial interference patterns versus different collisional interaction times t_{hold} . We have been able to observe up to four entangling–disentangling cycles in the experiment. The reduced visibility for longer hold times is mainly caused by a dephasing over the trapped cloud of atoms due to inhomogeneities in the external potentials.

of the entangled many-body state. It is clear, however, that the minimum visibility observed in the Ramsey fringes is dependent on the quality of our initial Mott insulating state and the fidelity of the quantum gate operations. In an ideal experimental situation with perfect fidelity for the multi-particle quantum gates and a defect-free Mott insulating state, this visibility should vanish for a phase shift of $\varphi = (2n + 1)\pi$. For a finite fidelity of the quantum gates, caused, for example, by a 5% fractional error in the pulse areas of the microwave pulses, the minimum visibility would already increase to $\sim 2\%$. If defects are present in the initial quantum state of the Mott insulator—for example, vacant lattice sites—then the entangled cluster state will not extend beyond this vacancy and the visibility of the Ramsey fringe will become non-zero owing to isolated atoms in the lattice. We have noticed, for example, that the quality of the Mott insulating state deteriorates owing to its prolonged uncompensated exposure to the potential gradient of gravity after the magnetic trapping potential is turned off. In addition to an imperfect creation of the Mott state, such vacancies could be caused by the superfluid shell of atoms surrounding the Mott insulating core^{9,21,22} or spontaneous emission due to the laser light, which leads to excitations of approximately 5% of the atoms for our total experimental sequence times.

In our one-dimensional lattice shift the system is very susceptible to vacant lattice sites, as a defect will immediately limit the size of the cluster. However, the scheme can be extended to two or three dimensions by using two additional lattice shift operations along the remaining orthogonal lattice axes. As long as the filling factor of lattice sites exceeds the percolation threshold (31% for a three-dimensional simple cubic lattice system²⁴) a large entangled cluster should be formed, making massive entanglement of 100,000 atoms possible in only three operational steps. For some of the applications of such a highly entangled state it will, however, be crucial to locate the position of the defects in the lattice.

In the future, it will be interesting to explore schemes for quantum computing that are based only on single-particle operations and measurements on such a cluster state². Here the large amount of entanglement in a cluster state can be viewed as a resource for quantum computations. But now, even without the possibility of manipulating single atoms in the periodic potential, a quantum computer based on the controlled collisions demonstrated here could be able to simulate a wide class of complex hamiltonians of condensed-matter physics that are translationally invariant^{12,17}. □

Methods

Optical lattices

A three-dimensional array of microscopic potential wells is created by overlapping three orthogonal optical standing waves at the position of the Bose–Einstein condensate. In our

case the atoms are trapped in the intensity maxima of the standing-wave light field owing to the resulting dipole force^{25,26}. The laser beams for two of the periodic potentials are operated at a wavelength of $\lambda = 820$ nm with beam waists of approximately $210 \mu\text{m}$ at the position of the Bose–Einstein condensate. This gaussian laser beam profile leads to an additional isotropic harmonic confinement of the atoms with trapping frequencies of 40 Hz for lattice potential depths of $25E_r$. In this configuration, we populate almost 100,000 lattice sites with an average atom number per lattice site of up to 1 in the centre of the lattice. The lattice structure is of simple cubic type, with a lattice spacing of $\lambda/2$ and oscillation frequencies in each lattice potential well of approximately 30 kHz for a potential depth of $25 E_r$.

State-dependent lattice potentials

Along a third orthogonal direction a standing-wave potential at a wavelength of $\lambda_x = 785$ nm is used, formed by two counter-propagating laser beams with linear polarization vectors^{5,11,18}. The angle θ between these polarization vectors can be dynamically adjusted through an electro-optical modulator and additional polarization optics. Such a lin-angle-lin polarization configuration can be decomposed into a σ^+ and a σ^- polarized standing-wave laser field, giving rise to potentials $V_+(x, \theta) = V_0 \cos^2(k_x x + \theta/2)$ and $V_-(x, \theta) = V_0 \cos^2(k_x x - \theta/2)$. Here V_0 is the potential depth of the lattice. By changing the polarization angle θ one can control the separation $\Delta x = (\theta/\pi)(\lambda_x/2)$ between the two potentials. When increasing θ , both potentials shift in opposite directions and overlap again for $\theta = n\pi$. For our experimental conditions, the dipole potential experienced by atoms in the $|1\rangle$ state is given by $V_-(x, \theta)$ and for atoms in the $|0\rangle$ state, it is dominated by the $V_+(x, \theta)$ potential¹⁸. For these laser beams, a waist of $150 \mu\text{m}$ has been used, resulting in a maximum potential depth of $34E_r$ and corresponding maximum vibrational trapping frequencies of 39 kHz.

Received 3 June; accepted 12 August 2003; doi:10.1038/nature02008.

- Gottesman, D. & Chuang, I. L. Demonstrating the viability of universal quantum computation using teleportation and single-qubit operations. *Nature* **402**, 390–393 (1999).
- Raussendorf, R. & Briegel, H. J. A one-way quantum computer. *Phys. Rev. Lett.* **86**, 5188–5191 (2001).
- Briegel, H. J., Calarco, T., Jaksch, D., Cirac, J. I. & Zoller, P. Quantum computing with neutral atoms. *J. Mod. Opt.* **47**, 415–451 (2000).
- Terhal, B. M., Wolf, M. M. & Doherty, A. C. Quantum entanglement: A modern perspective. *Phys. Today* **56**, 46–52 (2003).
- Jaksch, D., Briegel, H. J., Cirac, J. I., Gardiner, C. W. & Zoller, P. Entanglement of atoms via cold controlled collisions. *Phys. Rev. Lett.* **82**, 1975–1978 (1999).
- Briegel, H. J. & Raussendorf, R. Persistent entanglement in arrays of interacting particles. *Phys. Rev. Lett.* **86**, 910–913 (2001).
- Anderson, B. P. & Kasevich, M. A. Macroscopic quantum interference from atomic tunnel arrays. *Science* **282**, 1686–1689 (1998).
- Cataliotti, F. S. *et al.* Josephson junction arrays with Bose–Einstein condensates. *Science* **293**, 843–846 (2001).
- Jaksch, D., Bruder, C., Cirac, J. I., Gardiner, C. W. & Zoller, P. Cold bosonic atoms in optical lattices. *Phys. Rev. Lett.* **81**, 3108–3111 (1998).
- Greiner, M., Mandel, O., Esslinger, T., Hansch, T. W. & Bloch, I. Quantum phase transition from a superfluid to a Mott insulator in a gas of ultracold atoms. *Nature* **415**, 39–44 (2002).
- Brennen, G., Caves, C. M., Jessen, P. S. & Deutsch, I. H. Quantum logic gates in optical lattices. *Phys. Rev. Lett.* **82**, 1060–1063 (1999).
- Sørensen, A. & Mølmer, K. Spin-spin interaction and spin squeezing in optical lattices. *Phys. Rev. Lett.* **83**, 2274–2277 (1999).
- Brennen, G., Song, D. & Williams, C. J. A quantum computer architecture using nonlocal interactions. *Phys. Rev. A* **67**, 050302 (2003).
- Pachos, J. K. & Knight, P. L. Quantum computation with a one-dimensional optical lattice. Preprint at (<http://xxx.lanl.gov/quant-ph/0301084>) (2003).
- Feynman, R. P. Quantum mechanical computers. *Opt. News* **11**, 11–20 (1985).
- Feynman, R. P. Quantum mechanical computers. *Found. Phys.* **16**, 507–531 (1986).
- Jané, E., Vidal, G., Dür, W., Zoller, P. & Cirac, J. I. Simulation of quantum dynamics with quantum optical systems. *Quant. Inform. Comput.* **3**, 15–37 (2003).
- Mandel, O. *et al.* Coherent transport of neutral atoms in spin-dependent optical lattice potentials. *Phys. Rev. Lett.* **91**, 010407 (2003).
- Greiner, M., Mandel, O., Hansch, T. W. & Bloch, I. Collapse and revival of the matter wave field of a Bose–Einstein condensate. *Nature* **419**, 51–54 (2002).
- Greenberger, D. M., Horne, M. A. & Zeilinger, A. in *Bell's Theorem, Quantum Theory, and Conceptions of the Universe* (ed. Kafatos, M.) 69–72 (Kluwer Academic, Dordrecht, 1989).
- Kashurnikov, V. A., Prokof'ev, N. V. & Svistunov, B. V. Revealing the superfluid–Mott–insulator transition in an optical lattice. *Phys. Rev. A* **66**, 031601 (2002).
- Batrouni, G. G. *et al.* Mott domains of bosons confined on optical lattices. *Phys. Rev. Lett.* **89**, 117203 (2002).
- Jaksch, D. Bose–Einstein condensation and applications. *Naturwissenschaftliche Fakultat*. PhD thesis, 97–197, Leopold-Franzens-Univ., Innsbruck (1999).
- Stauffer, D. & Aharony, A. *Introduction to Percolation Theory* (Taylor and Francis, London, 1991).
- Grimm, R., Weidemüller, M. & Ovchinnikov, Y. B. Optical dipole traps for neutral atoms. *Adv. At. Mol. Opt. Phys.* **42**, 95–170 (2000).
- Jessen, P. S. & Deutsch, I. H. Optical Lattices. *Adv. At. Mol. Opt. Phys.* **37**, 95–139 (1996).

Acknowledgements We thank H. Briegel and I. Cirac for discussions, and A. Altmeyer and T. Best for experimental assistance. This work was supported by the EU under the QUEST programme, the AFOSR and the Bayerische Forschungsförderung.

Competing interests statement The authors declare that they have no competing financial interests.

Correspondence and requests for materials should be addressed to I.B. (imb@mpq.mpg.de).

Entanglement Interferometry for Precision Measurement of Atomic Scattering Properties

Artur Widera,^{1,2,*} Olaf Mandel,^{1,2} Markus Greiner,³ Susanne Kreim,^{1,2}
Theodor W. Hänsch,^{1,2} and Immanuel Bloch^{1,2,4}

¹Ludwig-Maximilians-Universität, Schellingstrasse 4/III, 80799 Munich, Germany

²Max-Planck-Institut für Quantenoptik, 85748 Garching, Germany

³JILA, University of Colorado, Boulder, Colorado 80309-0440, USA

⁴Johannes-Gutenberg-Universität, Staudingerweg 7, 55128 Mainz, Germany

(Received 30 October 2003; published 23 April 2004)

We report on a matter wave interferometer realized with entangled pairs of trapped ⁸⁷Rb atoms. Each pair of atoms is confined at a single site of an optical lattice potential. The interferometer is realized by first creating a coherent spin superposition of the two atoms and then tuning the interstate scattering length via a Feshbach resonance. The selective change of the interstate scattering length leads to an entanglement dynamics of the two-particle state that can be detected in a Ramsey interference experiment. This entanglement dynamics is employed for a precision measurement of atomic interaction parameters. Furthermore, the interferometer allows us to separate lattice sites with one or two atoms in a nondestructive way.

DOI: 10.1103/PhysRevLett.92.160406

PACS numbers: 03.75.Gg, 03.75.Lm, 03.75.Mn, 34.50.-s

The controlled creation of entanglement is one of the most subtle and challenging tasks in modern quantum mechanics, with both wide reaching practical and fundamental implications. In neutral atom based systems, significant progress has been made during recent years in the generation of large spin-squeezed samples of atomic gases [1] or the controlled creation of Greenberger-Horne-Zeilinger (GHZ) states [2] in cavity QED systems [3]. In addition, it has been recognized early on that in binary spin superpositions of Bose-Einstein condensed quantum gases (with spin states $|0\rangle$ and $|1\rangle$) a large amount of entanglement could be created by controlling the difference in interaction strengths $\chi = 1/2(U_{00} + U_{11} - 2U_{01})$ between the particles in different spin states [4–8]. Here, U_{ij} denotes the interaction matrix element between atoms in spin states i and j . Such control can either be achieved by moving atoms on different sites in spin-dependent optical lattice potentials [5,8–11] or by tuning the scattering lengths, such that $\chi \neq 0$ [4,7,12]. In the latter case, the simple creation of a coherent spin superposition, e.g., by an initial $\pi/2$ pulse, followed by a subsequent evolution of the spin system, would automatically lead to highly spin-squeezed or entangled N -particle GHZ-like states. Here we demonstrate such entanglement dynamics with pairs of atoms trapped in the ground state of a potential well in an optical lattice. Such pairs form a unique and highly controllable model system to study interactions between two particles. By using a recently predicted interstate Feshbach resonance in ⁸⁷Rb [13], we are able to control χ and thus accelerate the ensuing entanglement evolution, so that it is observable in a Ramsey type experiment within our coherence time. We show that this dynamical evolution of the atom pairs into entangled and disentangled states can be used to obtain precise information on the scattering properties of the systems. The entangle-

ment interferometer makes it furthermore possible to separate singly occupied lattice sites from doubly occupied sites in a nondestructive way.

The Ramsey interferometer sequence used in the experiment consists of two $\pi/2$ pulses that couple the two states $|0\rangle \equiv |F=1, m_F=+1\rangle$ and $|1\rangle \equiv |F=2, m_F=-1\rangle$. Here, F and m_F denote the total angular momentum and its projection, respectively. The pulse separation is t_{hold} and the phase α of the last pulse can be varied. Between the two $\pi/2$ pulses, the interaction behavior χ of the atoms is modified by using a Feshbach resonance occurring between atoms in hyperfine states $|0\rangle$ and $|1\rangle$ [13,14]. In the case of a single isolated atom, initially in the state $\psi_1^i = |0\rangle$, the effect of a changing interaction behavior has no consequence for the particle since it does not interact with other particles. After applying the experimental sequence shown in Fig. 1, the final state reads $\psi_1^f = 1/2(b_+|0\rangle - b_-|1\rangle)$ with $b_{\pm} \equiv 1 \pm e^{\mp i\alpha}$. The probability of finding the atom in state $|1\rangle$ is simply given by $P_1^f(\alpha) = \frac{1}{2}(1 - \cos\alpha)$, which describes the usual Ramsey fringes without decoherence.

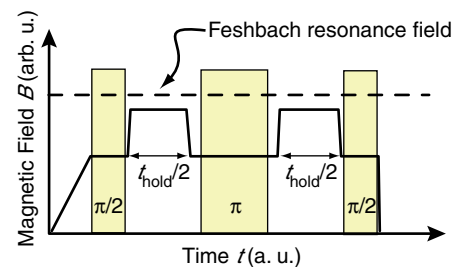


FIG. 1 (color online). Ramsey interferometer sequence (shaded bars). Ramsey fringes are obtained by varying the phase α of the last microwave $\pi/2$ pulse. The magnetic field can be ramped to different magnetic field values in order to change the interaction properties of the atoms.

In the case of two particles, the change of interaction parameters leads to an additional entangling-disentangling dynamics which is markedly different. Let us consider two bosonic atoms in the internal state $\psi_2^i = |0\rangle \otimes |0\rangle \equiv |00\rangle$. First, a $\pi/2$ pulse places the atoms in a coherent superposition of the two internal states $\psi_2 = \frac{1}{2}(|00\rangle - |01\rangle - |10\rangle + |11\rangle)$. After a time t , each two-particle state obtains a phase factor $e^{-i\phi_{ij}}$ due to interactions, where $\phi_{ij} = (U_{ij}/\hbar)t_{\text{hold}}$ is the collisional phase shift, with $U_{ij} = (4\pi\hbar^2 a_{ij})/m \times \int d^3x |\varphi_i|^2 |\varphi_j|^2$ being the on-site interaction matrix element. Here, a_{ij} represents the elastic scattering length between particles in states i and j , $\varphi_{i(j)}$ is the ground state wave function of an atom in spin state $i(j)$, and m the mass of a single atom. For $t = t_{\text{hold}}/2$, the two-particle state then evolves into $\psi_2 = \frac{1}{2}(e^{-i(\phi_{00}/2)}|00\rangle - e^{-i(\phi_{01}/2)}|01\rangle - e^{-i(\phi_{10}/2)}|10\rangle + e^{-i(\phi_{11}/2)}|11\rangle)$, where $\phi_{01} = \phi_{10}$. After a spin echo π pulse, a further interaction time $t_{\text{hold}}/2$ and a last $\pi/2$ pulse, the final state reads $\psi_2^f = \frac{1}{2}\{c_c^+|00\rangle - c_s(|01\rangle + |10\rangle) + c_c^-|11\rangle\}$, where $c_c^\pm \equiv e^{\mp i\alpha}(\cos\alpha \pm e^{-i\phi_\chi})$, $c_s \equiv i\sin\alpha$, and $\phi_\chi \equiv -(\phi_{00} + \phi_{11} - 2\phi_{01})/2$. The probability of finding an atom in state $|1\rangle$ can then be expressed by $P_2^f(\alpha, \phi_\chi) = \frac{1}{2}(1 - \cos\alpha \cos\phi_\chi)$, which is modulated in amplitude compared to the case of single atoms.

Four main cases illustrate the dynamics of the two-particle system. (i) For $\phi_\chi = 0$ the Ramsey fringe $P_2^f(\alpha, \phi_\chi = 0) = \frac{1}{2}(1 - \cos\alpha)$ is identical to the fringe of an isolated particle as shown above. (ii) If the interactions lead to a phase difference of $\phi_\chi = \pi/2$, the final state $\psi_2^f(\phi_\chi = \pi/2)$ is a maximally entangled Bell-like state. For such a state, the corresponding Ramsey fringe $P_2^f(\alpha, \phi_\chi = \pi/2) = \frac{1}{2}$ does not exhibit any modulation [11]. (iii) When the phase difference is increased to $\phi_\chi = \pi$, the system is disentangled again, and the corresponding Ramsey fringe $P_2^f(\alpha, \phi_\chi = \pi) = \frac{1}{2}(1 + \cos\alpha)$ is phase shifted by π with respect to the case of a single particle. It should be noted that for this interaction phase the state vectors of isolated atoms and atoms being part of an atom pair are orthogonal to each other. Therefore, by choosing a specific single particle phase, either isolated atoms or atom pairs can be transferred into the $|F = 2\rangle$ state and removed by a subsequent resonant laser pulse. The remaining atoms would form a pure lattice of either single atoms or atom pairs, which again can evolve to Bell-like pairs. For even larger phase differences, the system entangles and disentangles again, until for (iv) $\phi_\chi = 2\pi$ the system exhibits a Ramsey fringe which is in phase with the fringe of a single atom. In a system containing N_1 isolated single atoms and $N_2/2$ isolated pairs of atoms, the total fringe will be a weighted sum of the two distinct fringes and will have a visibility according to:

$$V(\chi) = V_0 e^{-(t/\tau_1)} \{(1 - n_2) + n_2 e^{-(t/\tau_2)} \cos\phi_\chi\}, \quad (1)$$

where we have included decoherence and two-body losses with time constants τ_1 and τ_2 , respectively, V_0 is a finite

initial visibility [15] and $n_i = N_i/(N_1 + N_2)$, $i = 1, 2$ with $n_1 + n_2 = 1$. Whereas the contribution of isolated atoms to the fringe visibility V remains unaffected under a change of χ , the total fringe signal shows a dynamics with the same periodicity as P_2^f . In the following, we consider the experimentally relevant case $N_1 > N_2$. For zero phase difference $\phi_\chi = 0$, we expect to measure a Ramsey fringe with high visibility V . The visibility decreases for increasing ϕ_χ and reaches a minimum for $\phi_\chi = \pi$ where the fringes from single atoms and from atom pairs are out of phase and partially compensate each other in the total signal. For larger interaction phase differences, the total visibility increases, until it shows a maximum for $\phi_\chi = 2\pi$, where the two Ramsey fringes are completely in phase again. It should be noted that the interaction time t_R after which $\phi_\chi = 2\pi$ depends on the difference in the interaction matrix elements U_{ij} , and for constant overlap of the wave functions on the elastic scattering length difference $\Delta a_{s,\chi} \equiv -\frac{1}{2}(a_{00} + a_{11} - 2a_{01})$.

The experimental setup is similar to our previous work [16,17]. We start with a BEC of up to 3×10^5 ^{87}Rb atoms trapped in the hyperfine ground state $|F = 1, m_F = -1\rangle$. We load the BEC into a pure two- or three-dimensional optical lattice potential formed by three mutually orthogonal standing waves of far detuned light. For the three-dimensional case, the system undergoes a Mott-insulator transition [16,18] with one and two atoms per site. The wavelengths used for the different standing waves are 829 nm (y and z axis) and 853 nm (x direction), with trapping frequencies at each lattice site of $\omega_x = 2\pi \times 33$, $\omega_y = 2\pi \times 43$, and $\omega_z = 2\pi \times 41$ kHz. In order to preserve spin polarization of the atoms in the optical trap, we maintain a 1 G magnetic offset field along the x direction. The atoms are prepared in the Feshbach resonance sensitive spin superposition by transferring the population from the $|F = 1, m_F = -1\rangle$ state into the $|0\rangle \equiv |F = 1, m_F = +1\rangle$ hyperfine level via a radio frequency (rf) Landau-Zener sweep. We then increase the magnetic field to 8.63 G. By applying a microwave field around 6.8 GHz and rf radiation around 6 MHz, we are able to coherently couple the two internal states $|0\rangle$ and $|1\rangle$ with a two-photon transition similar to [19].

In order to locate the position of the Feshbach resonance through enhanced atomic losses, we load the BEC into a two-dimensional (x and y axis) optical lattice potential. The atomic density is thereby strongly increased compared to a simple dipole trap, thus loss processes occur with higher probability. The magnetic field is subsequently increased to different values within 10 μs . After holding the atoms for 1 ms at a specific magnetic field, we switch off all trapping potentials and magnetic fields to measure the remaining total atom number in a time-of-flight (TOF) measurement (see Fig. 2). The magnetic field has been calibrated by measuring the frequency of the $|F = 1, m_F = -1\rangle \rightarrow |F = 2, m_F = -2\rangle$ microwave transition at different magnetic field values and employing the Breit-Rabi formula to determine the

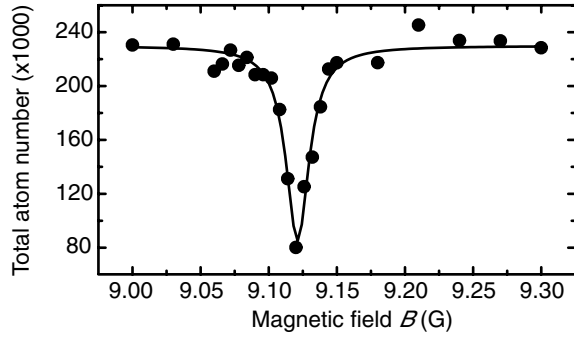


FIG. 2. Measurement of total atom number versus magnetic field in a 2D optical lattice. The solid line is a Lorentzian fit to the data with center at 9.121(9) G and a width of 20(5) mG. The hold time at the various magnetic field values is 1 ms.

actual field strength. Because of background magnetic field fluctuations, the magnetic field calibration has an uncertainty of 3 mG, noise of the magnetic field creating current source introduces an uncertainty of 2 mG and an additional systematic error of 4 mG is added by the optical trapping potential. The measured position of 9.121(9) G of the resonance agrees well with the predicted value of 9.123 G within our measurement uncertainty [20]. In order to determine the ratio of single to paired atoms in our three-dimensional lattice potential, we monitor the loss of atoms when we hold the atomic sample at the resonance magnetic field for a variable time (see Fig. 3).

Lattice sites which are occupied by more than one atom are depleted within 3 ms due to the increased two-body collision rates and the high density at single lattice sites. Isolated atoms, however, are protected from collisions and remain trapped. Assuming a negligible number of sites with three atoms, a fit with an exponential decay yields a time constant of 1.3(2) ms and a ratio $N_1/N_2 \approx 1.1$.

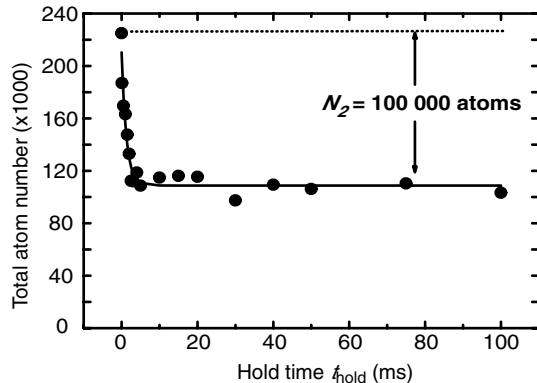


FIG. 3. Time resolved measurement of the total atom number at the measured Feshbach resonance in a 3D lattice potential. Sites with more than one atom are emptied within 3 ms, whereas sites with only one atom are protected from loss. The solid line is a fit to an exponential decay with offset, from which we find to have a ratio $N_1/N_2 \approx 1.1$.

In order to determine the elastic scattering properties, we apply the Ramsey interferometer sequence that has been described earlier (see Fig. 1). At each magnetic field value, we record the Ramsey fringe visibility for different interaction times t_{hold} (see, e.g., Fig. 4 for a field of $B = 9.081$ G).

The revival time t_R at which the visibility shows its maximum is determined by a fit using Eq. (1). This revival time depends on the difference in the interaction matrix element. A single revival of the fringe visibility could in principle also be caused by a complete loss of lattice sites with two atoms. We have, however, checked that even for the more pronounced losses at the Feshbach resonance the system exhibits dynamics due to interaction after the first revival. In this case, losses would shift the revival time by a few percent.

In order to extract information on the changes in the scattering length from the revival times, one can measure the on-site matrix element U_{00} through a collapse and revival experiment that we have demonstrated earlier [17]. For the same experimental parameters, we find $U_{00} = h/396(11) \mu\text{s}$. Using this information we can calculate $\chi/U_{00} = \Delta a_{s,\chi}/a_{00}$, which expresses the change in scattering length measured in units of the scattering length a_{00} . In order to map out the change in the elastic scattering length on the Feshbach resonance, $\Delta a_{s,\chi}/a_{00}$ has been measured for several magnetic fields and is shown in Fig. 5. Since the entanglement interferometer can only measure absolute values of $\Delta a_{s,\chi}/a_{00}$, we perform a usual time of flight measurement to obtain information on the sign of the scattering length differences. For this, we leave the Feshbach field switched on for the first 3 ms of the TOF [21]. During this time, the altered interaction energy is converted into kinetic energy, and the size of the atom cloud is measured. For magnetic fields

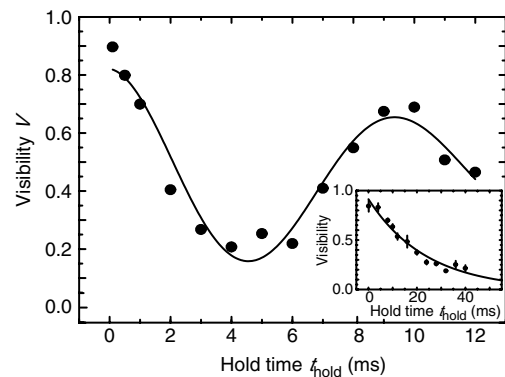


FIG. 4. Measured visibility dynamics due to entanglement in the system for a magnetic field value of 9.081 G. The solid line is a fit using Eq. (1) yielding a revival time $t_R = 2\pi t_{\text{hold}}/\phi_\chi = 9.5(2)$ ms, $V_0 = 0.82(4)$, $n_2 = 0.5$, $\tau_1 = 41(13)$ ms, and $\tau_2 = 20(5)$ ms. The inset is a measurement of the Ramsey sequence for a constant magnetic field $B = 8.63$ G, away from the Feshbach resonance, and the solid line is a fit describing an exponential decay of the fringe visibility.

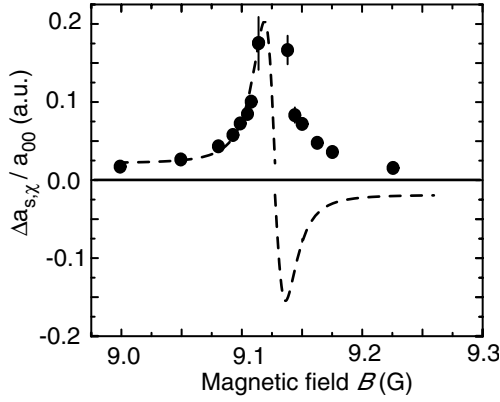


FIG. 5. Measured absolute value of the change of elastic scattering length for magnetic field values around the Feshbach resonance (dots). Both sides were fitted separately to a dispersive curve with a common center [9.128(9) G] and width [15(4) mG]. In order to illustrate the dispersive behavior of $\Delta a_{s,\chi}$ (dashed line), the fitted branch above the resonance is flipped to negative values according to the sign determined by the TOF measurement.

below the Feshbach resonance, we have found the cloud to be slightly larger (9% change in size) in the axial direction, whereas it is slightly smaller above the Feshbach resonance. From this, we conclude that the interspecies scattering length grows and shrinks below and above the Feshbach resonance field, respectively.

Since we ramp the magnetic field through the resonance in order to address the region above the resonance, atoms acquire a small collisional phase before the hold time starts. This is why we fit both branches of the scattering length change separately to a dispersive profile, with the constraint of a common center and width. The fit yields a center of 9.128(9) G and a width of 15(4) mG, in good agreement with our loss measurements. The two branches show an offset from $\Delta a_{s,\chi} = 0$, because even far away from the Feshbach resonance, the different scattering lengths a_{ij} do not compensate to $\chi = 0$. The difference in sign of the offsets below and above the resonance is artificial, since our measurement is insensitive to the sign of $\Delta a_{s,\chi}$, which has been obtained through the TOF measurement.

The interferometric method presented allows for high precision measurements of relative changes of the scattering lengths. In order to demonstrate this, we assume an error-free scattering length $a_{00} = 100.4 a_0$ [22], where a_0 is the Bohr radius. With this, we determine the change of elastic scattering length for $B = 9.081$ G to be $\Delta a_{s,\chi} = 4.2(1) a_0$.

In conclusion, we have presented a novel interferometric method to create and investigate entanglement dynamics in an array of spin superpositions of neutral atoms. The observed entanglement oscillations allow the precise determination of interaction properties between atoms in different spin states. We have demonstrated the

versatility of the interferometer by characterizing the elastic scattering properties of a recently predicted weak interstate Feshbach resonance in ^{87}Rb . We have found both the elastic and inelastic channel of the measured Feshbach resonance to be in good agreement with the theoretical prediction. The two-particle interferometer furthermore enables the direct creation of arrays of Bell states, together with the nondestructive separation of singly from doubly occupied sites.

We would like to thank Dieter Jaksch and Servaas Kokkelmans for useful discussions, Anton Scheich for support with the electronics, and Tim Rom and Thorsten Best for assistance with the experiment. We also acknowledge financial support from the Bayerische Forschungsförderung and AFOSR.

*Electronic address: widera@uni-mainz.de

- [1] B. Julsgaard, A. Kozhekin, and E. S. Polzik, *Nature (London)* **413**, 400 (2001).
- [2] D. M. Greenberger, M. A. Horne, A. Shimony, and A. Zeilinger, *Am. J. Phys.* **58**, 1131 (1990).
- [3] A. Rauschenbeutel *et al.*, *Science* **288**, 2024 (2000).
- [4] A. Sørensen, L.-M. Duan, J. I. Cirac, and P. Zoller, *Nature (London)* **409**, 63 (2001).
- [5] D. Jaksch, H.-J. Briegel, J. I. Cirac, C. W. Gardiner, and P. Zoller, *Phys. Rev. Lett.* **82**, 1975 (1999).
- [6] K. Helmerson and L. You, *Phys. Rev. Lett.* **87**, 170402 (2001).
- [7] L. You, *Phys. Rev. Lett.* **90**, 030402 (2003).
- [8] A. Sørensen and K. Mølmer, *Phys. Rev. Lett.* **83**, 2274 (1999).
- [9] G. K. Brennen, C. M. Caves, P. S. Jessen, and I. H. Deutsch, *Phys. Rev. Lett.* **82**, 1060 (1999).
- [10] O. Mandel *et al.*, *Phys. Rev. Lett.* **91**, 010407 (2003).
- [11] O. Mandel *et al.*, *Nature (London)* **425**, 937 (2003).
- [12] A. Micheli, D. Jaksch, J. I. Cirac, and P. Zoller, *Phys. Rev. A* **67**, 013607 (2003).
- [13] E. van Kempen, S. Kokkelmans, D. J. Heinzen, and B. J. Verhaar, *Phys. Rev. Lett.* **88**, 093201 (2002).
- [14] M. Erhard, H. Schmaljohann, J. Kronjäger, K. Bongs, and K. Sengstock, *cond-mat/0309318*.
- [15] Here the visibility is defined as $V = (P_{\text{max}}^{\text{tot}} - P_{\text{min}}^{\text{tot}}) / (P_{\text{max}}^{\text{tot}} + P_{\text{min}}^{\text{tot}})$.
- [16] M. Greiner *et al.*, *Nature (London)* **415**, 39 (2002).
- [17] M. Greiner *et al.*, *Nature (London)* **419**, 51 (2002).
- [18] D. Jaksch, C. Bruder, J. I. Cirac, C. W. Gardiner, and P. Zoller, *Phys. Rev. Lett.* **81**, 3108 (1998).
- [19] D. S. Hall, M. R. Matthews, J. R. Ensher, C. E. Wieman, and E. A. Cornell, *Phys. Rev. Lett.* **81**, 1539 (1998).
- [20] The interstate Feshbach resonance has recently also been detected through atom loss measurements by Erhard *et al.* [14]. There the resonance was found to be located at a magnetic field of 9.08(1) G.
- [21] S. Inouye, M. R. Andrews, J. Stenger, H.-J. Miesner, D. M. Stamper-Kurn, and W. Ketterle, *Nature (London)* **392**, 151 (1998).
- [22] S. Kokkelmans (private communication).

after cratering events and catastrophic disruptions. The newly created object's orbits will gradually evolve and perhaps be transported into one of the strong resonances that can pump the orbit's eccentricity to Earth-crossing values. Smaller objects will migrate faster under the influence of the Yarkovsky effect²¹, and once in a resonance the dynamical lifetime of objects of any size is of the order of only a few million years². However, cosmic ray exposure ages tell us that most OC meteorites are tens of millions of years old²². This indicates that even the smallest meteoroids spend a considerable amount of time migrating from their point of origin into the resonances, and the larger objects that eventually become NEOs probably require even more time. Thus, we expect that NEOs of S-complex provenance will display a size-dependent range of spectra ranging from Q (or OC) to S. This prediction is supported by numerous reports in the past decade indicating Q-like spectra and a size-dependent trend to OC-like spectra with decreasing size in the NEO population^{23–26}. However, space weathering in the main belt occurs faster than the lifetimes of NEOs, as suggested by meteoritic cosmic ray exposure ages²². Thus, observational evidence for a large number of OC-like spectra amongst the NEOs^{23–26} implies that regular re-surfacing of these objects keep them looking younger longer. □

Received 21 October 2003; accepted 7 April 2004; doi:10.1038/nature02578.

1. Vokrouhlický, D. & Farinella, P. Efficient delivery of meteorites to the Earth from a wide range of asteroid parent bodies. *Nature* **407**, 606–608 (2000).
2. Gladman, B. J. *et al.* Dynamical lifetimes of objects injected into asteroid belt resonances. *Science* **277**, 197–201 (1997).
3. Wisdom, J. Meteorites may follow a chaotic route to earth. *Nature* **315**, 731–733 (1985).
4. Adams, J. B. & McCord, T. B. Alteration of lunar optical properties: Age and composition effects. *Science* **171**, 567–571 (1971).
5. Moroz, L. V., Fisenko, A. V., Semjonova, L. F., Pieters, C. M. & Korotaeva, N. N. Optical effects of regolith processes on S-asteroids as simulated by laser shots on ordinary chondrite and other mafic materials. *Icarus* **122**, 366–382 (1996).
6. Sasaki, S., Nakamura, K., Hamabe, Y., Kurahashi, E. & Hiroi, T. Production of iron nanoparticles by laser irradiation in a simulation of lunar-like space weathering. *Nature* **410**, 555–557 (2001).
7. Chapman, C. R. S-type asteroids, ordinary chondrites, and space weathering: The evidence from Galileo's fly-bys of Gaspra and Ida. *Meteorit. Planet. Sci.* **31**, 699–725 (1996).
8. Clark, B. E. *et al.* Space weathering on Eros: Constraints from albedo and spectral measurements of Psyche crater. *Meteorit. Planet. Sci.* **36**, 1617–1637 (2001).
9. Ivezić, Ž., Jurić, M., Lupton, R. H., Tabachnik, S. & Quinn, T. in *Survey and Other Telescope Technologies and Discoveries* (eds Tyson, J. A. & Wolff, S.) Vol. 4836, 98–103 *Proc. SPIE* (2002).
10. Hapke, B. Space weathering from Mercury to the asteroid belt. *J. Geophys. Res.* **106**, 10039–10074 (2001).
11. Michel, P., Benz, W., Tanga, P. & Richardson, D. C. Collisions and gravitational reaccumulation: Forming asteroid families and satellites. *Science* **294**, 1696–1700 (2001).
12. Milani, A. & Knežević, Z. Asteroid proper elements and the dynamical structure of the asteroid main belt. *Icarus* **107**, 219–254 (1994).
13. Gaffey, M. J. *et al.* Mineralogical variations within the S-type asteroid class. *Icarus* **106**, 573–602 (1993).
14. Doressoundiram, A., Barucci, M. A., Fulchignoni, M. & Florczak, M. EOS family: A spectroscopic study. *Icarus* **131**, 15–31 (1998).
15. Deeming, T. J. Stellar spectral classification. *I. Mon. Not. R. Astron. Soc.* **127**, 493–516 (1964).
16. Ivezić, Ž. *et al.* Color confirmation of asteroid families. *Astron. J.* **124**, 2943–2948 (2002).
17. Tedesco, E. F., Noah, P. V., Noah, M. & Price, S. D. The supplemental IRAS minor planet survey. *Astron. J.* **123**, 1056–1085 (2002).
18. Sykes, M. V. *et al.* The 2MASS asteroid and comet survey. *Icarus* **146**, 161–175 (2000).
19. Bus, S. J. & Binzel, R. P. Phase II of the small main-belt asteroid spectroscopic survey. *Icarus* **158**, 106–145 (2002).
20. Migliorini, F. *et al.* Surface properties of (6) Hebe: A possible parent body of ordinary chondrites. *Icarus* **128**, 104–113 (1997).
21. Morbidelli, A. & Vokrouhlický, D. The Yarkovsky-driven origin of near-Earth asteroids. *Icarus* **163**, 120–134 (2003).
22. Marti, K. & Graf, T. Cosmic-ray exposure history of ordinary chondrites. *Annu. Rev. Earth Planet. Sci.* **20**, 221–243 (1992).
23. Binzel, R. P., Bus, S. J., Burbine, T. H. & Sunshine, J. M. Spectral properties of near-Earth asteroids: evidence for sources of ordinary chondrite meteorites. *Science* **273**, 946–948 (1996).
24. Rabinowitz, D. L. Size and orbit dependent trends in the reflectance colours of earth-approaching asteroids. *Icarus* **134**, 342–346 (1998).
25. di Martino, M., Manara, A. & Migliorini, F. 1993 VW: an ordinary chondrite-like near-Earth asteroid. *Astron. Astrophys.* **302**, 609–612 (1995).
26. Lazzarin, M., di Martino, M., Barucci, M. A., Doressoundiram, A. & Florczak, M. Compositional properties of near-Earth asteroids: spectroscopic comparison with ordinary chondrite meteorites. *Astron. Astrophys.* **327**, 388–391 (1997).
27. Gaffey, M. J. Spectral reflectance characteristics of the meteorite classes. *J. Geophys. Res.* **81**, 905–920 (1976).

Supplementary Information accompanies the paper on www.nature.com/nature.

Acknowledgements We thank C. Chapman and J. Taylor for providing background on the S-complex conundrum and B. Clark for useful discussions and further studies. D.N. thanks NASA PG&G and the SwRI Quicklook programmes for providing support. Funding for the creation and distribution of the SDSS Archive has been provided by the Alfred P. Sloan Foundation, the Participating Institutions, the National Aeronautics and Space Administration, the National Science Foundation, the US Department of Energy, the Japanese Monbukagakusho, and the Max Planck Society. The SDSS website is <http://www.sdss.org/>.

Competing interests statement The authors declare that they have no competing financial interests.

Correspondence and requests for materials should be addressed to R.J. (jedicke@ifa.hawaii.edu).

Tonks–Girardeau gas of ultracold atoms in an optical lattice

Belén Paredes¹, Artur Widera^{1,2,3}, Valentin Murg¹, Olaf Mandel^{1,2,3}, Simon Fölling^{1,2,3}, Ignacio Cirac¹, Gora V. Shlyapnikov⁴, Theodor W. Hänsch^{1,2} & Immanuel Bloch^{1,2,3}

¹Max-Planck-Institut für Quantenoptik, D-85748 Garching, Germany

²Sektion Physik, Ludwig-Maximilians-Universität, Schellingstrasse 4/III, D-80799 Munich, Germany

³Institut für Physik, Johannes Gutenberg-Universität, D-55099 Mainz, Germany

⁴Laboratoire Physique Théorique et Modèles Statistique, Université Paris Sud, Bâtiment 100, 91405 Orsay Cedex, France, and Van der Waals-Zeeman Institute, University of Amsterdam, 1018 XE Amsterdam, The Netherlands

Strongly correlated quantum systems are among the most intriguing and fundamental systems in physics. One such example is the Tonks–Girardeau gas^{1,2}, proposed about 40 years ago, but until now lacking experimental realization; in such a gas, the repulsive interactions between bosonic particles confined to one dimension dominate the physics of the system. In order to minimize their mutual repulsion, the bosons are prevented from occupying the same position in space. This mimics the Pauli exclusion principle for fermions, causing the bosonic particles to exhibit fermionic properties^{1,2}. However, such bosons do not exhibit completely ideal fermionic (or bosonic) quantum behaviour; for example, this is reflected in their characteristic momentum distribution³. Here we report the preparation of a Tonks–Girardeau gas of ultracold rubidium atoms held in a two-dimensional optical lattice formed by two orthogonal standing waves. The addition of a third, shallower lattice potential along the long axis of the quantum gases allows us to enter the Tonks–Girardeau regime by increasing the atoms' effective mass and thereby enhancing the role of interactions. We make a theoretical prediction of the momentum distribution based on an approach in which trapped bosons acquire fermionic properties, finding that it agrees closely with the measured distribution.

The physics of ultracold one-dimensional (1D) Bose systems is very different from that of ordinary three-dimensional (3D) cold gases^{1,2,4,5}. For example, by decreasing the particle density n , a usual 3D quantum many-body system becomes more ideal, whereas in a 1D Bose gas the role of interactions becomes more important. The reason is that at temperatures $T \rightarrow 0$, the kinetic energy of a particle at the mean interparticle separation is $K \propto n^2$ and it decreases with decreasing density n faster than the interaction energy per particle, $I \propto n$. The ratio of the interaction to kinetic energy, $\gamma = I/K$, characterizes the different physical regimes of the 1D quantum gas. For a large value of γ , the gas enters the Tonks–Girardeau (TG) regime, where the repulsion between particles strongly decreases the wavefunction at short interparticle distances.

Achieving such a TG regime and observing 'fermionization' of

the 1D Bose system is a great challenge, and it is complementary to the current experiments in which bosonic properties are observed in fermionic quantum gases^{6–9}. The 1D regime is obtained by tightly confining the particle motion in two directions to zero point oscillations^{4,5,10}. It was first demonstrated in experiments with weakly interacting Bose-condensed trapped gases, where $\gamma \ll 1$ (see refs 11, 12). In ref. 13, a tight radial confinement was realized by using two-dimensional (2D) optical lattice potentials to create an array of 1D quantum gases. In later experiments with optical lattices^{14,15} it has become possible to reach a 1D regime with $\gamma \approx 1$, that is, in between a weakly interacting 1D Bose condensed gas and a fermionized TG gas. So far, however, it has not been possible to bridge the last one or two orders of magnitude in γ that could bring the bosonic quantum gas fully into the TG regime. Larger values of γ could either be reached by decreasing the density of the quantum gas or by increasing the effective interaction strength between the particles^{4,5}.

In this work, we propose and demonstrate a novel way to achieve the TG regime. The main point is to include an additional optical lattice along the 1D gas, which results in an increase of γ . For a homogeneous gas, γ can be expressed as $\gamma = mg/\hbar^2 n$, where g is the 1D interaction strength, m the mass of a single atom, and \hbar denotes Planck's constant divided by 2π . The addition of a periodic potential along the third axis increases the effective mass, and thus leads to an increase of γ . In fact, in the limit in which only the first Bloch band is occupied, we have $I = U\nu$ and $K = J\nu$, where ν is the filling factor, U the on-site interaction energy and J the tunnelling amplitude, and thus $\gamma = U/J$. Additionally, in order to achieve a pure TG regime in a lattice, the filling factor ν should be smaller than unity: otherwise, doubly occupied sites would be present, and the direct correspondence to the TG gas would be lost (as in a recent experiment, see ref. 16). Following these ideas, we have been able to enter the TG regime with $\gamma \approx 5$ –200. In this regime, the bosons can be theoretically described using a 'fermionization' approach^{17,18}.

For $\gamma \rightarrow \infty$, the ground state of N bosons at zero temperature is

described by the many-body wavefunction:

$$\Psi_0(x_1, x_2, \dots, x_N) \propto |\det[\varphi_i(x_j)]|, \quad i, j = 1, 2, \dots, N \quad (1)$$

where \det denotes the Slater determinant, and $\varphi_i(x)$ is the i th eigenfunction of the single-particle hamiltonian. The presence of the Slater determinant guarantees that the wavefunction vanishes whenever two particles occupy the same position in space. However, the absolute value of the determinant ensures that the wavefunction for the bosons remains completely symmetric. This wavefunction reflects the fundamental similarities between strongly interacting bosons and non-interacting fermions in one dimension, with properties such as the spatial density distribution, the density–density correlation function, or the entropy of the gas being the same as in the case of non-interacting fermions. More interestingly though, several properties are strongly modified by the presence of the absolute value of the determinant, leading to a unique behaviour of, for example, the momentum distribution of the TG gas³. This can be understood qualitatively in the following way: the bosonic particles in a TG gas are not allowed to occupy the same position in space. Owing to this restriction, they are distributed over a more extended region in momentum space than in the case of an ideal or weakly interacting Bose gas. On the other hand, in order to keep themselves apart from each other, they do not need to be in different momentum states, as would be the case for fermions.

We first describe the experimental realization together with the measured data, and then provide a detailed theoretical analysis of the system. In order to reach the regime of low filling factor, we start with a rather small Bose–Einstein condensate (BEC) of approximately $(3\text{--}4) \times 10^4$ ⁸⁷Rb atoms in a magnetic trap. Then the BEC is loaded into a 2D optical lattice potential (along the y - and z -axes), such that an array of 1D quantum gases confined to narrow potential tubes is created (Fig. 1a). The lattice potential is formed by superimposing two orthogonal standing waves with a wavelength of 823 nm on top of the BEC. In order to transfer the atoms into the optical potential, the potential depth of the optical lattice is first gradually increased to a mean final value of $27 E_r$ (Fig. 1b). Here E_r is the recoil energy $\hbar^2 k^2/2m$, with k describing the wave vector of the lattice laser light. During this ramp up of the lattice potentials, the tunnel coupling between the different 1D quantum gases decreases exponentially. This results in a decoupling of the quantum gases, such that particle exchange between different tubes is suppressed. For the maximum lattice depth, the gaussian shape of the laser beams (160 μm waist) leads to an axial harmonic confinement of the 1D gases with a trapping frequency of $\omega_{ax} \approx 2\pi \times 60$ Hz. This has been verified by exciting a 'sloshing' motion of the thermal cloud and by parametric heating measurements, which both agree with the calculated value. Furthermore, the depths of all standing-wave potentials have been measured by vibrational band spectroscopy¹⁹. For such 1D quantum gases, without a lattice in the axial direction, we have $\gamma \approx 0.5$ near the lattice centre.

After a further hold time of 10 ms, we add an optical standing wave along the axial direction (x axis) in order to increase γ . The intensity of the laser forming this lattice potential (operated at a wavelength of 854 nm) is ramped up to a final depth V_{ax} of up to $18.5 E_r$. The axial momentum distribution of the quantum gases is subsequently probed by suddenly removing all optical and magnetic trapping potentials, and by imaging the atom clouds after a time-of-flight period of 16 ms. In order to prevent a strong expansion of the atom cloud along the propagation axis of the imaging laser beam (z axis), which would make the experiment more sensitive to misalignments in the imaging axis, we reduce the confinement along this axis by lowering the z -lattice potential to $6 E_r$ within a time of 100 μs before initiating the ballistic expansion sequence. Also, along the x axis we use a ramp down, which is not fully non-adiabatic and leads to a narrowing of the gaussian envelope in the observed momentum distribution by $\sim 20\%$. This enhances the number of atoms in the central momentum peak. From the

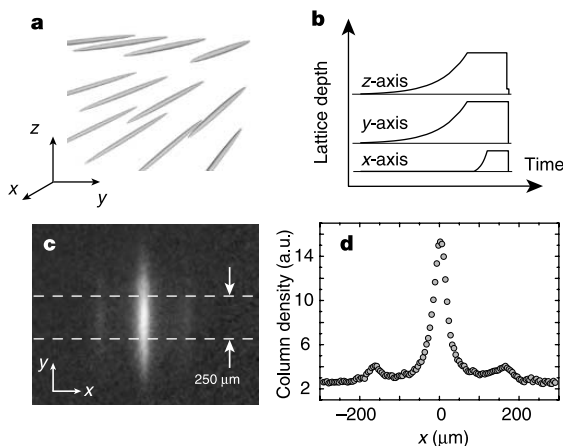


Figure 1 Experimental sequence and momentum profiles. **a**, Using a 2D optical lattice potential, we realize an array of 1D quantum gases. **b**, These quantum gases are created by first increasing the optical lattice depths along the y and z axes in an exponential ramp over a time of 160 ms (time constant $t = 40$ ms) to a mean final value of $27 E_r$. After a further hold time of 10 ms at this final lattice depth, we increase the optical lattice potential along the x axis within a time of 20 ms (time constant $t = 10$ ms) to a variable lattice depth V_{ax} . The quantum gases are then allowed to equilibrate for another 30 ms before we probe the momentum distribution as described in the text. **c**, Typical time-of-flight images after a ballistic expansion of the atom clouds over a time of 16 ms for an axial optical lattice depth $V_{ax} = 6.5 E_r$. The white dashed lines denote the area from which averaged momentum profiles along the x axis are extracted (**d**).

absorption images, we extract profiles of the axial momentum distribution by averaging horizontal profiles through the centre of the atom cloud (Fig. 1c).

In Fig. 2, we show six experimentally measured momentum profiles (see Supplementary Information for all 12 momentum profiles), corresponding to different values of the axial optical lattice depth ($V_{\text{ax}}/E_r = 0-18.5$). In Fig. 2a there is no lattice present along the x axis, and thus no first-order diffraction peak appears. Here, the value of γ is ~ 0.5 at the trap centre. For the rest of the figures (Fig. 2b–f) we can use the relation $\gamma \approx U/J$ obtaining $\gamma \approx 5-200$, which indicates that the TG regime is entered rather

rapidly when increasing the axial lattice depth. In Fig. 2b–f we also plot our theoretical predictions based on fermionization at finite temperature averaged over the different 1D tubes (see Methods). Apart from a normalizing factor for each experimental curve, only the atom number in the central tube is used as an overall adjustable parameter in this model. This atom number is, however, kept constant between different momentum profiles. The initial temperature for the lowest axial lattice depth $V_{\text{ax}} = 4.6 E_r$ has been obtained through a finite temperature fit to the corresponding momentum profiles using our fermionization approach. From this initial temperature, the temperatures of the quantum gases at

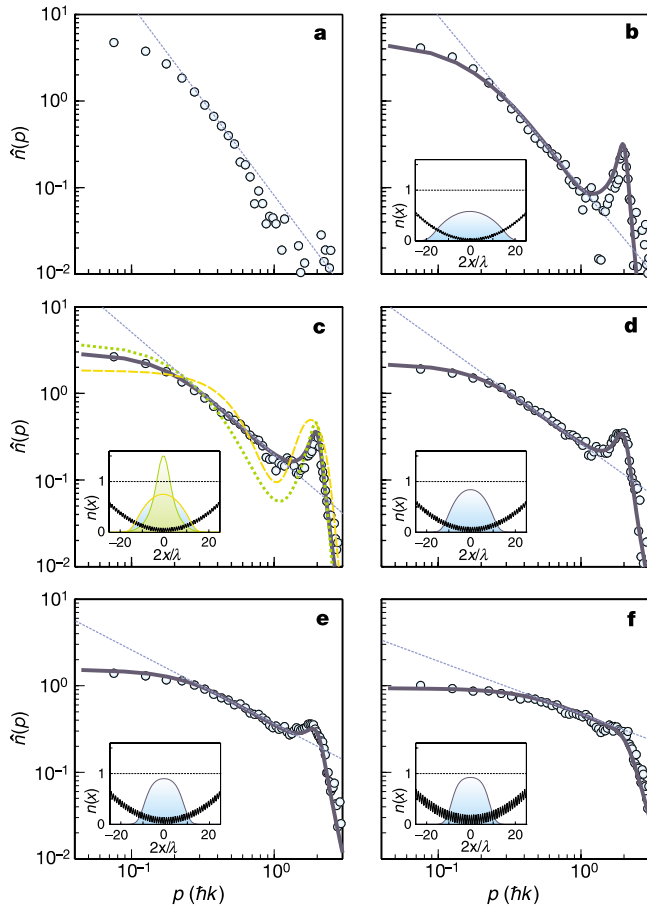


Figure 2 Momentum profiles of the 1D quantum gases for different axial lattice depths. In **b–f**, the experimental data (blue circles) are displayed together with our theoretical predictions (black line) based on fermionization at finite temperatures, averaged over the different 1D tubes. In order to emphasize the linear part of the momentum profiles, an auxiliary straight line with the corresponding slope is shown in each plot. In **c**, the momentum profiles for the ideal Bose gas (green dotted lines) and the ideal Fermi gas (yellow dashed lines) are also displayed for comparison. For all plots, an atomic distribution characterized by an atom number $N_{0,0} = 18$ in the central tube is used, for which we have found the best agreement with the experimental data (see Methods). In the insets of **b–f**, the density profile of a single 1D tube with $N = 15$ particles at the corresponding temperature and lattice depth is shown for the fermionized gas (black lines in plots **b–f**), for the ideal Fermi gas (yellow line in **c**), and for the ideal Bose gas (green line in **c**). The values of the axial lattice depths V_{ax} , the average temperatures, the slopes α of the linear part of the momentum profiles, and the values of $\gamma = U/J$ are: **b**, $4.6 E_r$ and $k_B T/J = 0.5$ (Tonks), $\alpha = 1.90$, $\gamma = 5.5$; **c**, $7.4 E_r$ and $k_B T/J = 0.7$ (Tonks), $k_B T/J = 1.6$ (ideal Bose gas), $k_B T/J = 0.7$ (ideal Fermi gas), $\alpha = 1.4$, $\gamma = 13.7$; **d**, $9.3 E_r$ and $k_B T/J = 0.9$ (Tonks), $\alpha = 1.2$, $\gamma = 23.6$; **e**, $12 E_r$ and $k_B T/J = 1.3$ (Tonks), $\alpha = 0.8$, $\gamma = 47.6$; and **f**, $18.5 E_r$ and $k_B T/J = 3.9$ (Tonks), $\alpha = 0.6$, $\gamma = 204.5$. For the momentum profile without the axial lattice (**a**), we find $\alpha = 2.2$ and $\gamma = 0.5$ at the centre of the trap.

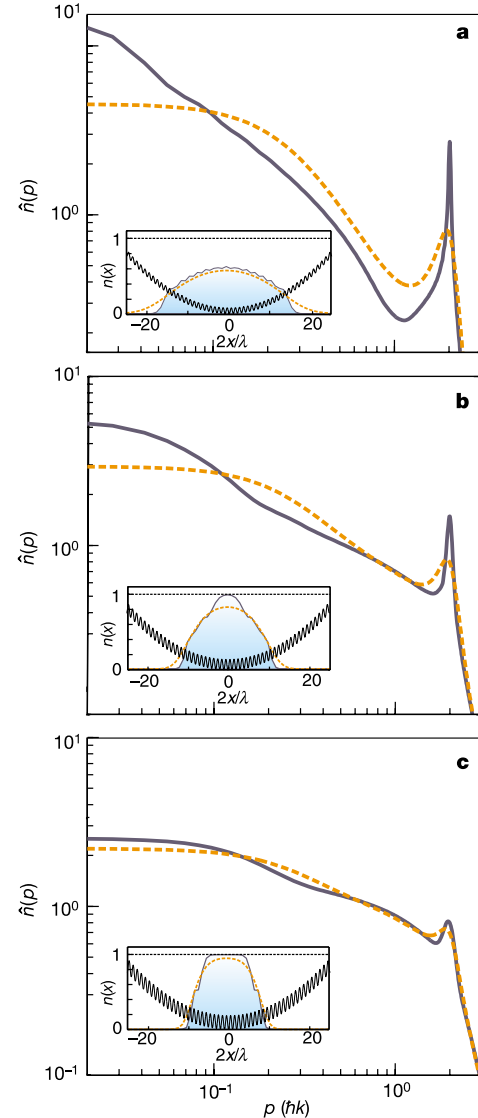


Figure 3 Momentum profiles of a single 1D tube obtained from our fermionization-based theory for different lattice depths. The plots are shown for axial lattice depths V_{ax} of $5.0 E_r$ (**a**), $9.5 E_r$ (**b**), and $12.0 E_r$ (**c**). For all plots, the number of particles is $N = 15$, and $b = 8 \times 10^{-4} E_r$ (this value of b corresponds to the trapping frequency of the experiment; see Methods). In each plot, the log-log momentum profile at $k_B T/J = 0$ (black line) is displayed together with that at $k_B T/J = 1.0$ (orange dashed line). The density profiles at $k_B T/J = 0$ and $k_B T/J = 1.0$, together with the corresponding lattice-harmonic potential, are shown in the inset of each plot. Note that at $k_B T/J = 0$, finite size effects make the slope at low momenta deviate from the ideal $1/2$. The slope α is larger than $1/2$ for small filling factors ($\alpha = 0.79$ in **a**), it approaches $1/2$ as a Mott phase is developed at the centre of the trap ($\alpha = 0.49$ in **b**), and it decreases to zero deep in the Mott phase ($\alpha = 0.29$ in **c**).

increasing lattice depth V_{ax} have been modelled by assuming conservation of entropy during the ramp up of the axial lattice. For all 12 experimentally measured momentum profiles (see Supplementary Information), we find excellent agreement with the theory based on fermionization. For reference, we have plotted the results obtained assuming an ideal Bose or Fermi gas, also averaged over all the 1D tubes and at finite temperatures (see for example, Fig. 2c).

The observed momentum distributions allow us to conclude that we are dealing with a finite, non-uniform, TG gas in a lattice. Our results show pronounced deviations²⁰ from the generic behaviour of the uniform TG gas at zero temperature, where one has a $1/p^{1/2}$ low momentum distribution³ giving a slope of 1/2 in the log-log plot. In our experiment we observe: (1) a rather flat momentum distribution at small momenta p , and (2) a linear region at larger p , with a slope decreasing with an increase in the lattice depth. This behaviour is in excellent agreement with the predictions of our fermionization-based theory for such a TG gas with a finite number of particles (about 20 per tube) in a lattice, in the presence of a harmonic trap, and at finite temperatures (see Fig. 3). Note that already for our lowest axial lattice depths we find $\gamma \gg 1$, and a further increase in the lattice depth mainly changes the average filling factor in our system and allows us to study the behaviour of a TG gas at different densities.

Most of the relevant physics concerning the momentum distribution for our case can be qualitatively understood by considering a uniform lattice system at the same temperature and with a filling factor equal to the average filling factor of the trapped system. We can then restrict the discussion to the case $\nu \leq 1/2$, because for $\nu > 1/2$ the system can be viewed as a system of holes at filling factor $1 - \nu$. The filling factor determines a characteristic momentum $p_\nu = \hbar \times 2\pi\nu/\lambda$ related to the mean interparticle separation, where λ is the wavelength of the lattice laser light. At zero temperature, for $p \ll p_\nu$, the momentum distribution should exhibit a linear 1/2 behaviour, whereas for larger momenta short-range correlations²¹ tend to increase the slope. An increase in the filling factor, and therefore a decrease in the average separation between particles, modifies p_ν and can therefore lead to a change of the observed slope. Note that for the case of $\nu = 1/2$, the momentum p_ν is the closest to the lattice momentum $\hbar \times 2\pi/\lambda$, and the momentum distribution is the least affected by short-range correlations. At finite temperatures a new momentum scale sets in^{18,22}, below which the slope has a tendency to decrease. This is the momentum $p_T = \hbar \times \pi/L_T$, where $L_T \approx \lambda/k_B T \sin \pi\nu$ is a characteristic length of thermal fluctuations. For a small filling factor, this length coincides with the gas phase result $L_T \approx \hbar^2 n/m^* k_B T$, in which the particle mass is replaced by the effective mass $m^* = 2\hbar^2/J\lambda^2$. In our experiment we have $p_T \approx p_\nu$. Therefore, finite-temperature effects overlap with effects of short-range correlations and we observe a rather flat momentum distribution at small p , and a linear region with slope larger than 1/2 for larger p .

The presence of the harmonic trapping potential introduces important changes in the observed momentum profiles. First, in contrast to the uniform case, an adiabatic increase of the lattice depth increases the ratio $k_B T/J$. This increases the momentum p_T and the flat region extends to larger momenta. Second, the slope of the linear part decreases with the lattice depth, and the generic 1/2 value is recovered on approach to the Mott insulator transition^{16,23–26}. This is a fundamental feature that is present irrespective of the number of particles and trap frequency. It is related to the fact that in the trapped case the characteristic average filling factor of the system increases with the lattice depth, because the tunnelling amplitude J decreases and particles try to accumulate near the trap centre. At the Mott insulator crossover, where the filling factor at the trap centre is equal to unity, the average filling factor is close to $\nu = 1/2$ (see Methods). This is the value for which the effects of short-range correlations are strongly suppressed in the homo-

geneous lattice system, and one comes closest to the generic behaviour with slope 1/2. Last, we note that in the weakly interacting regime for a trapped quasicondensate, one should have a lorentzian momentum distribution²⁷, which would give a slope close to 2 for $p \gg \hbar \times \pi/L_T$. Already, for low axial lattice depths V_{ax} we observe a smaller slope, which emphasizes a strong difference of our system from previously studied 1D quasicondensates.

In summary, we have prepared a TG gas in an optical lattice. Here the bosonic atoms exhibit a pronounced fermionic behaviour, and show a momentum distribution that is in excellent agreement with a theory of fermionized trapped Bose gases. In a next step, it will be intriguing to use photoassociation in optical lattices to probe the reduced two-body correlations, which are expected in a TG gas²⁸. Furthermore, by using two bosonic atomic species and tuning the sign and strength of the atomic interactions, it should be possible to observe a behaviour similar to strongly correlated fermions. For example, the bosonic atoms can undergo a BCS transition and form Cooper pairs in the same way as electrons do in a superconductor²⁹. \square

Methods

Description of the 1D quantum gases using fermionization

Here we develop the theoretical treatment based on fermionization that we have used above to model the experiment. We consider N bosonic atoms moving in the lowest band of a 1D lattice and experiencing an additional harmonic potential. This situation is described by the Bose–Hubbard hamiltonian $H = H_B + V$, where

$$H_B = -J \sum_{\ell=-\infty}^{\infty} (a_{\ell}^{\dagger} a_{\ell+1} + a_{\ell+1}^{\dagger} a_{\ell}) + b \sum_{\ell=-\infty}^{\infty} \ell^2 a_{\ell}^{\dagger} a_{\ell}$$

$$V = U \sum_{\ell=-\infty}^{\infty} a_{\ell}^{\dagger 2} a_{\ell}^2$$

The term H_B describes the motion of the atoms in the combined lattice-harmonic potential, and the term V accounts for on-site interactions. The bosonic operators a_{ℓ} annihilate one boson at the ℓ th site, and fulfil canonical commutation relations $[a_{\ell}, a_{\ell'}^{\dagger}] = \delta_{\ell, \ell'}$. The parameter b is related to the frequency ω of the harmonic potential by $b = 1/8 m \omega^2 \lambda^2$.

We are interested in the strongly interacting or Tonks regime, in which two atoms cannot occupy the same lattice site. Within this regime, the bosonic operators a_{ℓ} can be re-expressed using the Jordan–Wigner transformation³⁰ (JWT) in terms of fermionic ones c_{ℓ} fulfilling $[c_{\ell}, c_{\ell'}^{\dagger}]_{\pm} = \delta_{\ell, \ell'}$. Under the JWT, the interacting Bose hamiltonian H_B is transformed into a non-interacting fermionic hamiltonian H_F through the replacement $a_{\ell} \rightarrow c_{\ell}$. In order to predict the behaviour of the different bosonic observables, one has to transform them into fermionic ones via the JWT, and then evaluate the corresponding expectation values for the fermionic ground state. At $T = 0$, the fermionic ground state is given by the Slater determinant of equation (1). At a finite temperature T , the wavefunction is a mixture of different Slater determinants characterized by the many-body density matrix $\rho \propto \exp(-H_F/k_B T)$, where k_B is Boltzmann's constant.

Density and momentum distributions of fermionized Bose gases

The particle density $n(x)$ coincides with that of non-interacting fermions, as the JWT maps the corresponding bosonic observable onto the same fermionic one (that is $a_{\ell}^{\dagger} a_{\ell} \rightarrow c_{\ell}^{\dagger} c_{\ell}$). Under the Thomas–Fermi approximation we have:

$$n(x) = \frac{1}{\pi} \arccos \left(\max \left[\frac{\mu - bx^2}{-2J}, -1 \right] \right)$$

if $\mu - bx^2 > -2J$ and zero otherwise. The size L of the cloud is $L = \lambda \sqrt{(2J + \mu)/4b}$, and μ is determined by imposing the condition that the total number of particles is N . When $\mu \geq 2J$ a Mott phase is produced at the centre of the trap, and $n(x=0)$ is equal to 1. At this point the average filling factor of the system $\bar{\nu} = \lambda N/2L \approx 3/\sqrt{2}\pi$, a value which is close to 1/2.

The momentum distribution $\hat{n}(p)$ is related to the one-particle correlation function $\langle a_{\ell}^{\dagger} a_{\ell'} \rangle$ through:

$$\hat{n}(p) = |\Phi(p)|^2 \sum_{\ell, \ell'=-\infty}^{\infty} e^{-ip(\ell-\ell')} \langle a_{\ell}^{\dagger} a_{\ell'} \rangle$$

where $\Phi(p)$ is the Fourier transform of the Wannier function, and p denotes momentum in units of $\hbar k$. Using the JWT, the bosonic one-particle correlation function can be re-expressed as:

$$\langle a_{\ell}^{\dagger} a_{\ell'} \rangle = \langle c_{\ell}^{\dagger} (-1)^{\sum_{m=\ell'-1}^{\ell-1} c_m^{\dagger} c_m} c_{\ell'} \rangle, \ell > \ell'$$

Making extensive use of Wick's theorem, one can re-express this quantity as a Töplitz determinant $\langle a_{\ell}^{\dagger} a_{\ell'} \rangle = \det[G_{\ell, \ell'}]$, where $G_{\ell, \ell'}$ is a $\ell - \ell' - 1$ matrix with elements $(G_{\ell, \ell'})_{x, y} = \langle c_{\ell'+y-1}^{\dagger} c_{\ell+x} \rangle - \delta_{x, y-1}/2$.

Therefore, in order to evaluate the momentum distribution at a finite temperature T one has to determine the one-particle correlation functions for a non-interacting Fermi

system at that temperature. We have used the grand canonical Fermi–Dirac distribution and the exact eigenstates $\varphi_i(x)$ of the single-particle hamiltonian to determine the momentum distribution in this way.

Averaging over the array of 1D quantum gases

In order to give a quantitative prediction for the experimental situation, we have averaged the momentum distribution for different tubes. To determine the atomic distribution, we have assumed that during the ramp up of the 2D optical lattice potential, tunnelling becomes negligible, and we have an array of independent 1D gases. For each tube, we have assumed a Thomas–Fermi density profile. Minimizing the total energy of the array with respect to the number of atoms in each of the tubes, we obtain $N_{ij} = N_{0,0} \left(1 - \frac{5N}{2\pi N_{0,0}} (i^2 + j^2)\right)^{3/2}$, where N_{ij} is the number of atoms in a tube located at position (i, j) in the 2D optical lattice, N is the total number of particles in the array, and $N_{0,0}$ is the number of particles in the central tube. It follows that the probability of having a tube with M particles is:

$$P(M) = \frac{2}{3} \frac{1}{N_{0,0}^{2/3} M^{1/3}}, \quad M \leq N_{0,0}.$$

Remarkably, this distribution only depends on one parameter, namely, the number of particles in the central tube, which is the only adjustable parameter in our model.

The temperature of each 1D quantum gas has been calculated assuming adiabatic evolution of the system during the ramp up of the axial lattice. Owing to the presence of the harmonic confinement, the ratio $k_B T/J$ is not conserved in the adiabatic evolution. Given the temperature at $V_{ax} = 4.6 E_T$ (see Supplementary Information), the conservation of entropy allows us to determine the temperature at the final lattice depth V_{ax} . The entropy of the TG gas coincides with that of the non-interacting Fermi gas, as both have the same spectrum and density of states. This results in the same temperatures for a TG gas and an ideal Fermi gas, but a different temperature for the ideal Bose gas when the axial lattice depth is increased. Note that tubes with different number of particles also have different temperatures at the same lattice depth.

Received 21 February; accepted 1 April 2004; doi:10.1038/nature02530.

- Girardeau, M. Relationship between systems of impenetrable bosons and fermions in one dimension. *J. Math. Phys.* **1**, 516–523 (1960).
- Lieb, E. H. & Liniger, W. Exact analysis of an interacting Bose gas. The general solution and the ground state. *Phys. Rev.* **130**, 1605–1616 (1963).
- Lenard, A. Momentum distribution in the ground state of the one-dimensional system of impenetrable bosons. *J. Math. Phys.* **5**, 930–943 (1964).
- Petrov, D. S., Shlyapnikov, G. V. & Walraven, J. T. M. Regimes of quantum degeneracy in trapped 1D gases. *Phys. Rev. Lett.* **85**, 3745–3749 (2000).
- Dunjko, V., Lorent, V. & Olshanii, M. Bosons in cigar-shaped traps: Thomas-Fermi regime, Tonks-Girardeau regime, and in between. *Phys. Rev. Lett.* **86**, 5413–5416 (2001).
- Jochim, S. *et al.* Bose-Einstein condensation of molecules. *Science* **302**, 2101–2103 (2003).
- Greiner, M., Regal, C. & Jin, D. S. Emergence of a molecular Bose-Einstein condensate from a Fermi gas. *Nature* **426**, 537–540 (2003).
- Zwierlein, M. W. *et al.* Observation of Bose-Einstein condensation of molecules. *Phys. Rev. Lett.* **91**, 250401 (2003).
- Regal, C., Greiner, M. & Jin, D. S. Observation of resonance condensation of fermionic atom pairs. *Phys. Rev. Lett.* **92**, 040403 (2004).
- Olshanii, M. Atomic scattering in the presence of an external confinement. *Phys. Rev. Lett.* **81**, 938–941 (1998).
- Goerlitz, A. *et al.* Realization of Bose-Einstein condensates in lower dimensions. *Phys. Rev. Lett.* **87**, 130402 (2001).
- Schreck, F. *et al.* A quasipure Bose-Einstein condensate immersed in a Fermi sea. *Phys. Rev. Lett.* **87**, 080403 (2001).
- Greiner, M., Bloch, I., Mandel, O., Hänsch, T. W. & Esslinger, T. Exploring phase coherence in a 2D lattice of Bose-Einstein condensates. *Phys. Rev. Lett.* **87**, 160405 (2001).
- Moritz, H., Stöferle, T., Köhl, M. & Esslinger, T. Exciting collective oscillations in a trapped 1D gas. *Phys. Rev. Lett.* **91**, 250402 (2003).
- Laburthe Tolra, B. *et al.* Observation of reduced three-body recombination in a fermionized 1D Bose gas. Preprint at (<http://xxx.lanl.gov/cond-mat/0312003>) (2003).
- Stöferle, T., Moritz, H., Schori, C., Köhl, M. & Esslinger, T. Transition from a strongly interacting 1D superfluid to a Mott insulator. *Phys. Rev. Lett.* **92**, 130403 (2004).
- Eftov, K. B. & Larkin, A. I. Correlation functions in one-dimensional systems with strong interactions. *Sov. Phys. JETP* **42**, 390–396 (1976).
- Korepin, V. E., Bogoliubov, N. M. & Izergin, A. G. *Quantum Inverse Scattering Method and Correlation Functions* (Cambridge Univ. Press, Cambridge, 1993).
- Ovchinnikov, Y. B. *et al.* Diffraction of a released Bose-Einstein condensate by a pulsed standing light wave. *Phys. Rev. Lett.* **83**, 284–287 (1999).
- Astrakharchik, G. E. & Giorgini, S. Correlation functions and momentum distributions of one-dimensional Bose systems. *Phys. Rev. A* **68**, 031602 (2003).
- Olshanii, M. & Dunjko, V. Short-distance correlation properties of the Lieb-Liniger system and momentum distributions of trapped one-dimensional atomic gases. *Phys. Rev. Lett.* **91**, 090401 (2003).
- Cazalilla, M. A. Bosonizing one-dimensional cold atomic gases. *J. Phys. B* **37**, S1–S47 (2004).
- Fisher, M. P. A., Weichman, P. B., Grinstein, G. & Fisher, D. S. Boson localization and the superfluid-insulator transition. *Phys. Rev. B* **40**, 546–570 (1989).
- Jaksch, D., Bruder, C., Cirac, J. I., Gardiner, C. W. & Zoller, P. Cold bosonic atoms in optical lattices. *Phys. Rev. Lett.* **81**, 3108–3111 (1998).
- Greiner, M., Mandel, O., Esslinger, T., Hänsch, T. W. & Bloch, I. Quantum phase transition from a superfluid to a Mott insulator in a gas of ultracold atoms. *Nature* **415**, 39–44 (2002).
- Kollath, C., Schollwöck, U., von Delft, J. & Zwerger, W. Spatial correlations of trapped one-dimensional bosons in an optical lattice. *Phys. Rev. A* **69**, 031601 (2004).
- Richard, S. *et al.* Momentum spectroscopy of 1D phase fluctuations in Bose-Einstein condensates. *Phys. Rev. Lett.* **91**, 010405 (2003).

- Gangardt, D. M. & Shlyapnikov, G. V. Stability and phase coherence of trapped 1D Bose gases. *Phys. Rev. Lett.* **90**, 010401 (2003).
- Paredes, B. & Cirac, J. I. From Cooper pairs to Luttinger liquids with bosonic atoms in optical lattices. *Phys. Rev. Lett.* **90**, 150402 (2003).
- Sachdev, S. *Quantum Phase Transitions* (Cambridge Univ. Press, Cambridge, 1999).

Supplementary Information accompanies the paper on www.nature.com/nature.

Acknowledgements We thank F. Gerbier, D. Gangardt and M. Olshanii for discussions, and M. Greiner for help in setting up the experiment. I.B. also acknowledges support from AFOSR.

Competing interests statement The authors declare that they have no competing financial interests.

Correspondence and requests for materials should be addressed to I.B. (bloch@uni-mainz.de).

Synthesis and characterization of chiral mesoporous silica

Shunai Che¹, Zheng Liu^{2,3}, Tetsu Ohsuna³, Kazutami Sakamoto⁴, Osamu Terasaki³ & Takashi Tatsumi⁵

¹Department of Chemistry, School of Chemistry and Chemical Technology, Shanghai Jiao Tong University, 800 Dongchuan Road, Shanghai, 200240, China

²Bussan Nanotech Research Institute, 2-1 Koyadai, Tsukuba, Ibaraki 305-0074, Japan

³Structural Chemistry, Arrhenius Laboratory, Stockholm University, S-10691 Stockholm, Sweden

⁴AminoScience Laboratory, Ajinomoto Co., Inc., 1-1 Suzuki-cho, Kawasaki 210-8681, Japan

⁵CREST, JST, Division of Materials Science and Chemical Engineering, Faculty of Engineering, Yokohama National University, 79-5 Tokiwadai, Yokohama 240-8501, Japan

Chirality is widely expressed in organic materials, perhaps most notably in biological molecules such as DNA, and in proteins, owing to the homochirality of their components (D-sugars and L-amino acids). But the occurrence of large-scale chiral pores in inorganic materials is rare¹. Although some progress has been made in strategies to synthesize helical and chiral zeolite-like materials^{1–3}, the synthesis of enantiomerically pure mesoporous materials is a challenge that remains unsolved⁴. Here we report the surfactant-templated synthesis of ordered chiral mesoporous silica, together with a general approach for the structural analysis of chiral mesoporous crystals by electron microscopy. The material that we have synthesized has a twisted hexagonal rod-like morphology, with diameter 130–180 nm and length 1–6 μm . Transmission electron microscopy combined with computer simulations confirm the presence of hexagonally ordered chiral channels of 2.2 nm diameter winding around the central axis of the rods. Our findings could lead to new uses for mesoporous silica and other chiral pore materials in, for example, catalysis and separation media, where both shape selectivity and enantioselectivity⁵ can be applied to the manufacturing of enantiomerically pure chemicals and pharmaceuticals.

We recently discovered a templating route for preparing well-ordered mesoporous silicas based on the self-assembly of chiral anionic surfactants and inorganic precursors by using aminosilane or quaternized aminosilane as a co-structure-directing agent (CSDA)⁶, which provided a potential method to synthesize mesoporous materials with inherent chirality. Among the anionic surfactants tested in our previous work, N-acyl-L-alanine is a chiral organic molecule that can form a chiral nematic phase in the presence of small amounts of decanol^{7,8}. This phenomenon has

State Selective Production of Molecules in Optical Lattices

Tim Rom,^{1,2,3} Thorsten Best,^{1,2,3} Olaf Mandel,^{1,2,3} Artur Widera,^{1,2,3} Markus Greiner,^{1,2,4}
Theodor W. Hänsch,^{1,2} and Immanuel Bloch^{1,2,3}

¹*Ludwig-Maximilians-Universität, Schellingstrasse 4/III, 80799 Munich, Germany*

²*Max-Planck-Institut für Quantenoptik, 85748 Garching, Germany*

³*Johannes Gutenberg-Universität, 55099 Mainz, Germany*

⁴*JILA, University of Colorado, Boulder, Colorado 80309-0440, USA*

(Received 17 March 2004; published 10 August 2004)

We demonstrate quantum control over both internal and external quantum degrees of freedom in a high number of identical “chemical reactions,” carried out in an array of microtraps in a 3D optical lattice. Starting from a Mott insulating phase of an ultracold atomic quantum gas, we use two-photon Raman transitions to create molecules on lattice sites occupied by two atoms. In the atom-molecule conversion process, we can control both the internal rovibronic and external center of mass quantum state of the molecules. The lattice isolates the microscopic chemical reactions from each other, thereby allowing photoassociation spectra without collisional broadening even at high densities of up to $2 \times 10^{15} \text{ cm}^{-3}$.

DOI: 10.1103/PhysRevLett.93.073002

PACS numbers: 32.80.Qk, 33.80.-b, 34.50.Rk

The formation of ultracold molecules is currently one of the most actively pursued topics in atomic and molecular physics. Recently, spectacular progress in this field has been achieved by using adiabatic sweeps over Feshbach resonances to produce quantum gases of a variety of alkali dimers [1–6] culminating in the observation of Bose-Einstein condensation of molecules [7–9] and resonance superfluidity [10,11]. A complementary approach to the creation of molecules is based upon photoassociation (PA) [12–19]. Here a two-photon Raman process can access molecular states beyond the scope of magnetic Feshbach resonances. It has been pointed out that the combination of photoassociation with 3D optical lattices can considerably enhance the efficiency of the molecule formation process [20] due to the tight confinement of the atoms at lattice sites. Here we report on the production of $^{87}\text{Rb}_2$ molecules in a 3D optical lattice via one- and two-photon photoassociation. We show that, in addition to the internal quantum state of the molecule, the quantum state of the external center of mass (c.m.) motion can be controlled. Moreover, we demonstrate that two-body loss processes induced by photoassociation can be a sensitive tool in determining the number of atoms on the lattice sites.

Starting from an atomic Bose-Einstein condensate (BEC) in the optical lattice, a Mott insulator state with a central region with two atoms per site can be formed [21]. Thereby, a high number of identical microscopic two-particle systems is created. Through a coherent Raman process, one can then couple exactly two atoms on a single lattice site to a bound molecule in a well-defined rovibronic quantum state via an intermediate excited molecular state, while avoiding perturbing mean field shifts during the photoassociation process. Furthermore, if both atoms initially occupy the lowest internal atomic energy state, the density of the atoms can

be raised to values not achievable in the homogeneous case, due to the absence of any two- and three-body loss processes.

Similar to our previous experiments, we start with the production of an almost pure BEC of approximately 3×10^5 ^{87}Rb atoms in the $|F = 1, m_F = -1\rangle$ state. This condensate can then be transferred into a 3D optical lattice by superimposing far detuned optical standing waves along three orthogonal axes. These standing waves are formed by laser light with a wavelength of $\lambda = 840 \text{ nm}$ and beam waists ($1/e^2$) of $w = 150 \text{ }\mu\text{m}$ at the position of the BEC. We convert the BEC into a Mott insulator by gradually increasing the potential depth of the 3D lattice to a value of up to $27E_r$ over a time of 80 ms. Here $E_r = \hbar^2 k^2 / 2m$ denotes the recoil energy, m the mass of a rubidium atom, and $k = 2\pi/\lambda$ is the wave vector of the lattice laser light. This results in trapping frequencies at a lattice site of up to $\omega = 2\pi \times 35 \text{ kHz}$, with peak densities as high as $2 \times 10^{15} \text{ cm}^{-3}$ for doubly occupied sites. While for our experimental parameters the outer regions of the Mott insulator should mainly consist of singly occupied sites, the core should be mainly composed of doubly occupied sites.

In order to obtain an accurate detuning relative to the intermediate excited molecular state, we have first performed one-photon photoassociation. This process occurs in an ultracold atomic gas when two colliding atoms absorb a laser photon of energy $\hbar\omega_a$ corresponding to the energy difference between the asymptotic free atom state and a bound excited molecular level. The coupling strength on this transition Ω_a is determined by the electronic Rabi frequency, multiplied by an overlap integral between the free collisional and bound molecular wave function according to the Franck-Condon principle. A deep 3D optical lattice will lead not only to a quasiharmonic confinement for the c.m. motion of the atom pair,

but will also significantly affect the long-range part of the interatomic potential [see Fig. 1(a)]. As a result, the initial collisional wave function is localized in space and thereby the Franck-Condon factor of the photoassociation transition can be considerably enhanced. In fact, the confinement of atoms on lattice sites turns the free-bound transition into a bound-bound transition.

In our experiment, molecule formation is detected by monitoring atom losses. This is done by measuring the remaining atom number with standard absorption imaging after the atoms have been illuminated for a fixed period of time with a PA laser beam. From the reduction in atom number, we can deduce the number of created molecules, under the assumption that secondary loss processes can be neglected. In order to stabilize the frequency of the photoassociation laser, the laser is offset locked relative to the $D1$ line of atomic rubidium. It is tuned with an accuracy of 1 MHz to the vicinity of a particular excited molecular level of the 0_g^- potential, approximately 0.69 THz below the atomic resonance frequency [18]. This laser beam exhibits a total power of 3 mW and is focused to a $(1/e^2)$ beam waist of 200 μm at the position of the quantum gas in the optical lattice. After locating the position of the one-photon molecular resonance, we have measured the time dependence of the molecule formation process by placing the PA laser on resonance with the molecular transition and recording the atom losses vs time. Assuming only two-body losses, the atomic loss rates can be described by

$$\frac{dN}{dt} = -K_2 \int n^2(\vec{r}) d^3r, \quad (1)$$

where N is the total atom number after a time t , $n(\vec{r})$ is the atomic density, and K_2 is a characteristic loss constant.

This equation displays an interesting dimensionality effect. For a 1D optical lattice, most lattice sites contain $N \gg 2$ atoms. Therefore, many molecules can suc-

cessively be formed on one site. As more and more atoms are converted into molecules, the remaining atom number decreases, causing a change in the atomic density $n(\vec{r})$. This leads to a nonexponential decay in the atom number, which we observe in the experiment (see Fig. 2). If we impose a deep 3D optical lattice, such that we reach the Mott insulator regime, the lattice sites are occupied by single atoms or atom pairs for our experimental parameters. As the lattice isolates atoms on different sites from each other, only atoms on doubly occupied lattice sites can be converted into molecules. Figure 2 shows a decay of the remaining atom number asymptotically tending to a constant offset. The decay is related to photoassociation on doubly occupied lattice sites and its form is purely exponential since the rate is independent of the total atom number. The remaining atom number decreases as

$$N(t) = N_1 + 2N_2 \exp(-t/\tau), \quad (2)$$

where $N_{1,2}$ is the initial number of lattice sites occupied by one or two atoms, respectively. From N_1 and $N(0)$ we can conclude that for our lattice parameters the ratio of single to doubly occupied lattice sites is 1.6(1), which is consistent with a shell structure of Mott insulator regions with single and double occupancy.

Having determined the resonance frequency corresponding to the excited molecular level, we can now drive a resonantly enhanced two-photon Raman transition (see Fig. 1). In this process, two colliding atoms absorb one photon from the first laser field ω_a and emit another photon into an additional stimulating laser field ω_b . The second laser is phase locked with respect to the first in order to enable the coherent two-photon transition. Under the action of the two-photon coupling, both atoms will be transferred to a molecule in a specific molecular state. The rovibronic state is selected by choosing a Raman-laser difference frequency $\delta = \omega_a - \omega_b$, which

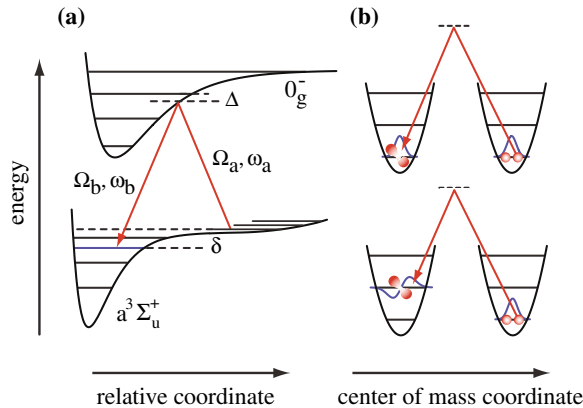


FIG. 1 (color online). Two-color photoassociation process of two atoms being placed in the external ground state at a single site of an optical lattice potential. Both the rovibrational quantum state in the relative motion of the two atoms forming the molecule (a) and the c.m. motional quantum state of the molecule (b) can be controlled.

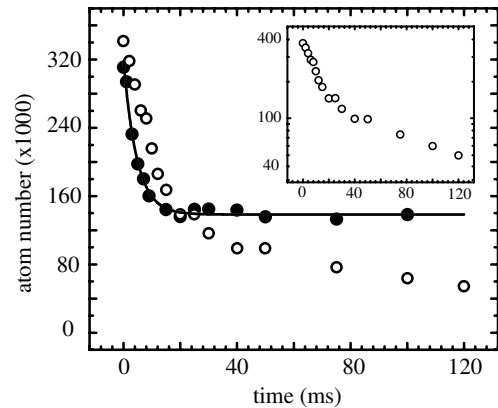


FIG. 2. Time-resolved one-color photoassociation; in 1D (empty circles) and 3D lattice (filled circles) configurations. The photoassociation laser is tuned to resonance with an intensity of $I = 5 \text{ W/cm}^2$ and illuminates the sample for a varying time, after which the total atom number is measured. The inset shows the 1D lattice loss data in a log-linear plot.

matches the binding energy of the molecular state. In our case, a parallel polarization ensures $\Delta J = 0$ transitions, where J is the rotational quantum number. As the molecules are formed in s -wave collisions, we can therefore selectively produce molecules in the rotational ground state. The final level is chosen to lie in the $a^3\Sigma_u^+$ electronic state potential. If the virtual intermediate level of energy $\hbar\omega_a$ is relatively close to a real molecular level, as in the case of our experiment, the effective two-photon Rabi frequency of the process is given by $\Omega_{\text{eff}} = \Omega_a\Omega_b/(2\Delta)$, where $\Omega_{a,b}$ are the respective one-photon Rabi frequencies and Δ is the detuning from the intermediate level. The one-photon Rabi frequencies include the Franck-Condon factors for the corresponding transitions. Therefore, the external confinement by the optical lattice also increases the efficiency of the Raman process through Ω_a .

A major obstacle lies in the possibility of spontaneous Raman scattering. A molecule that has just been formed can absorb a single photon from either laser beam and be excited to an intermediate molecular state, from where it can decay via spontaneous emission to other bound or unbound states, leading to trap losses. In order to ameliorate these problems, we choose a rather large detuning $|\Delta|$, which decreases the spontaneous scattering rate. Thus far, however, we have not been able to enter a regime, where the coherent coupling exceeds the damping rate, such that, e.g., coherent Rabi oscillations between atoms and molecules could be observed [1,22].

We present measurements at difference frequencies of $\delta \approx 2\pi \times 24$ MHz and $\delta \approx 2\pi \times 636$ MHz corresponding to the uppermost vibrational levels in the ground state potential [18]. Both lasers illuminate the atomic ensemble for a fixed time in a counterpropagating beam configuration parallel to one axis of the optical lattice. Thereafter, the remaining number of trapped atoms is again recorded (see Fig. 3). On all spectra, we observe a progression of resonances spaced by roughly 30 kHz. This series of resonances corresponds to a resolved quantized c.m. motion of the molecules formed at single lattice sites. In fact, when the lifetime of the molecules is longer than the c.m. oscillation period at each lattice site, it should be possible to resolve the different c.m. motional states, which is the case for our experimental parameters. The highest resonance frequency recorded denotes a transition in which a molecule in the ground state of a single lattice site has been formed. The other resonances originate from transitions to higher lying motional quantum states [see Fig. 1(b)]. The appearance of these resonances confirms that the emerging molecules are trapped on the sites of the optical lattice. The frequency separation of the resonances is directly given by the vibrational splitting of the c.m. motional quantum states. It is interesting to note that the observed trapping frequencies almost coincide with the atomic trapping frequencies. This can be understood as the polarizability of molecules formed in high

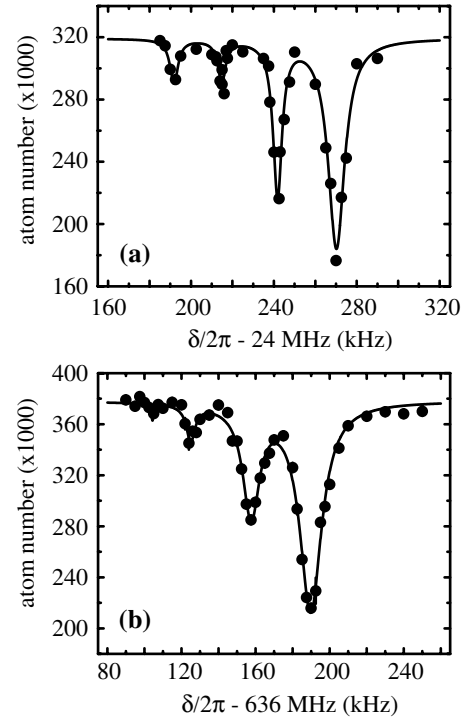


FIG. 3. Two-photon photoassociation of the uppermost vibrational level in the electronic ground state $^3\Sigma_u^+$ at $\delta/2\pi \approx 24$ MHz and at $\delta/2\pi \approx 636$ MHz, with the quantized c.m. motion resolved. The remaining atom number after a photoassociation time of about 120 ms is measured for varying difference frequencies δ at a constant detuning of (a) $\Delta = 2\pi \times 700$ MHz and laser intensities of $I_a = 12$ W/cm² and $I_b = 6$ W/cm² and (b) a detuning of $\Delta = -2\pi \times 990$ MHz and $I_a = 16$ W/cm² and $I_b = 12$ W/cm². The solid curve is a fit assuming four independent Lorentzian profiles and a constant background. The difference in the vibrational level spacings between (a) and (b) are mainly due to different lattice depths of (a) $18E_r$ and (b) $27E_r$ along the optical lattice axis of the photoassociation lasers.

lying rovibrational states should be close to twice the polarizability of a single atom [23]. Since the molecules have twice the mass of a single atom, this leads to identical trapping frequencies as in the case of free atoms. Note, however, that the external potential for the molecules is twice as deep as for the atoms and supports more bound states. Furthermore, we observe that the spacing between higher lying vibrational c.m. quantum states is slightly reduced due to the anharmonicity of the trapping potential at a lattice site.

The reduced strength of the transitions to higher lying c.m. motional quantum states is related to an additional Franck-Condon factor in the c.m. motion, which depends on the initial and final motional quantum states $|\tilde{v}\rangle$ and $|\tilde{v}'\rangle$ and is given by $\langle \tilde{v}' | \exp(2ikz) | \tilde{v} \rangle|^2$. The total transition rate to form molecules is then directly proportional to the internal rovibronic and external c.m. Franck-Condon factors. In Fig. 3, we observe a good quantitative agreement with the expected weaker transitions to higher lying motional quantum states to within 10% accuracy.

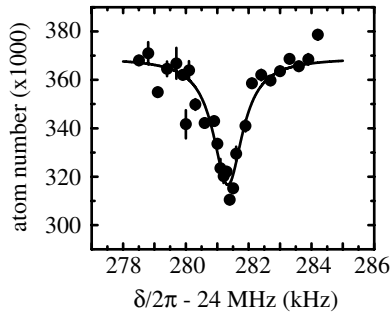


FIG. 4. High resolution two-photon photoassociation of the transition to the most weakly bound internal vibrational state in the $^3\Sigma_u^+$ potential and the ground state of the c.m. motion. The scan was taken at an intermediate detuning of $\Delta = -2\pi \times 900$ MHz. The solid line is a Lorentzian fit to the data with a width of $\gamma = 1.1(2)$ kHz.

Spontaneous Raman scattering mostly limits the observed linewidths and, by reducing the intensities of the corresponding laser, we have been able to observe narrow two-photon resonance linewidths as low as 1 kHz (see Fig. 4). Note that this high resolution spectroscopy is carried out at high atomic on-site densities of $2 \times 10^{15} \text{ cm}^{-3}$. This proves that mean field shifts are absent in our system and do not broaden the lines, as has been observed in [18] even for an order of magnitude lower densities. Limits on the linewidth observed here could be caused by a differential light shift between the atoms and the molecules, a resonant spectral background on our diode lasers, or mechanical vibrations. From the observed lowest linewidths, we can deduce the lifetime of the molecules, which should be on the order of 1 ms.

In conclusion, we have demonstrated two-photon Raman photoassociation of ^{87}Rb atoms from a Mott insulator phase in an 3D optical lattice. By choosing appropriate parameters for the photoassociation laser fields, we have achieved control over both internal and external degrees of freedom of the molecules. A combination of Feshbach techniques and two-color Raman transitions could further increase the efficiency of molecule formation while allowing one to address deeply bound molecular states in future experiments [24]. A counterintuitive photoassociation pulse sequence leading to stimulated Raman adiabatic passage (STIRAP, [25]) could result in a very fast and robust molecule production scheme. In combination with a 3D optical lattice, one would then end up with a molecular Mott insulator. The melting of this Mott insulator [20] could then be used to create a Bose-Einstein condensate of molecules in almost arbitrary internal quantum states.

We would like to thank A. Altmeyer and S. Fölling for helpful discussions and A. Scheich for assistance with the

electronics. We also acknowledge financial support from the DFG under the SPP1116 program and the AFOSR.

-
- [1] E. A. Donley, N. R. Claussen, S. T. Thompson, and C. E. Wieman, *Nature (London)* **417**, 529 (2002).
 - [2] C. A. Regal, C. Ticknor, J. L. Bohn, and D. S. Jin, *Nature (London)* **424**, 47 (2003).
 - [3] K. E. Strecker, G. B. Partridge, and R. G. Hulet, *Phys. Rev. Lett.* **91**, 080406 (2003).
 - [4] J. Herbig, T. Kraemer, M. Mark, T. Weber, C. Chin, H.-C. Nägerl, and R. Grimm, *Science* **301**, 1510 (2003).
 - [5] K. Xu *et al.*, *Phys. Rev. Lett.* **91**, 210402 (2003).
 - [6] S. Dürr, T. Volz, A. Marte, and G. Rempe, *Phys. Rev. Lett.* **92**, 020406 (2004).
 - [7] M. Greiner, C. A. Regal, and D. S. Jin, *Nature (London)* **426**, 537 (2003).
 - [8] S. Jochim, M. Bartenstein, A. Altmeyer, G. Hendl, S. Riedl, C. Chin, J. Hecker Denschlag, and R. Grimm, *Science* **302**, 2101 (2003).
 - [9] M. W. Zwierlein, C. A. Stan, C. H. Schunck, S. M. F. Raupach, S. Gupta, Z. Hadzibabic, and W. Ketterle, *Phys. Rev. Lett.* **91**, 250401 (2003).
 - [10] C. A. Regal, M. Greiner, and D. S. Jin, *Phys. Rev. Lett.* **92**, 040403 (2004).
 - [11] M. W. Zwierlein, C. A. Stan, C. H. Schunck, S. M. F. Raupach, A. J. Kerman, and W. Ketterle, *Phys. Rev. Lett.* **92**, 120403 (2004).
 - [12] P. D. Lett, K. Helmerson, W. D. Phillips, L. P. Ratliff, S. L. Rolston, and M. E. Wagshul, *Phys. Rev. Lett.* **71**, 2200 (1993).
 - [13] J. D. Miller, R. A. Cline, and D. J. Heinzen, *Phys. Rev. Lett.* **71**, 2204 (1993).
 - [14] E. R. I. Abraham, W. I. McAlexander, C. A. Sackett, and R. G. Hulet, *Phys. Rev. Lett.* **74**, 1315 (1995).
 - [15] Y. Band and P. Julienne, *Phys. Rev. A* **51**, R4317 (1995).
 - [16] C. C. Tsai, R. S. Freeland, J. M. Vogels, H. M. Boesten, B. J. Verhaar, and D. J. Heinzen, *Phys. Rev. Lett.* **79**, 1245 (1997).
 - [17] A. Fioretti, D. Comparat, A. Crubellier, O. Dulieu, F. Masnou-Seeuws, and P. Pillet, *Phys. Rev. Lett.* **80**, 4402 (1998).
 - [18] R. Wynar, R. S. Freeland, D. J. Han, C. Ryu, and D. J. Heinzen, *Science* **287**, 1016 (2000).
 - [19] C. McKenzie *et al.*, *Phys. Rev. Lett.* **88**, 120403 (2002).
 - [20] D. Jaksch, V. Venturi, J. I. Cirac, C. J. Williams, and P. Zoller, *Phys. Rev. Lett.* **89**, 040402 (2002).
 - [21] M. Greiner, O. Mandel, T. Esslinger, T. W. Hänsch, and I. Bloch, *Nature (London)* **415**, 39 (2002).
 - [22] D. J. Heinzen, R. Wynar, P. D. Drummond, and K. V. Kheruntsyan, *Phys. Rev. Lett.* **84**, 5029 (2000).
 - [23] L. B. Ratcliff, J. L. Fish, and D. D. Konowalow, *J. Mol. Spectrosc.* **122**, 293 (1987).
 - [24] S. J. J. M. F. Kokkelmans, H. M. J. Vissers, and J. Verhaar, *Phys. Rev. A* **63**, 031601R (2001).
 - [25] K. Bergmann, H. Theuer, and B. W. Shore, *Rev. Mod. Phys.* **70**, 1003 (1998).

17. Solanki, S. K. *et al.* Three-dimensional magnetic field topology in a region of solar coronal heating. *Nature* **425**, 692–695 (2003).
18. Parker, E. N. Nanoflare and the solar X-ray corona. *Astrophys. J.* **330**, 474–479 (1988).
19. Galsgaard, K. & Nordlund, A. Heating and activity of the solar corona. 1. Boundary shearing of an initially homogeneous magnetic field. *J. Geophys. Res.* **101**, 13445–13460 (1996).
20. Karpen, J. T., Antiochos, S. K. & DeVore, C. R. Reconnection-driven current filamentation in solar arcades. *Astrophys. J.* **460**, L73–L76 (1996).
21. Hachisu, I., Matsuda, T., Nomoto, K. & Shigeyama, T. Nonlinear growth of Rayleigh–Taylor instabilities and mixing in SN 1987A. *Astrophys. J.* **358**, L57–L61 (1990).
22. Ugai, M. & Shimizu, T. Computer studies on the spontaneous fast reconnection mechanism in three dimensions. *Phys. Plasmas* **3**, 853–862 (1996).
23. Kitahara, T. & Kurokawa, H. High-resolution observation and detailed photometry of a great H α two-ribbon flare. *Sol. Phys.* **125**, 321–332 (1990).
24. Innes, D. E., McKenzie, D. E. & Wang, T. SUMER spectral observations of post-flare supra-arcade inflows. *Sol. Phys.* **217**, 247–265 (2003).
25. Asai, A., Yokoyama, T., Shimojo, M. & Shibata, K. Downflow motions associated with impulsive nonthermal emissions observed in the 2002 July 23 solar flare. *Astrophys. J.* **605**, L77–L80 (2004).

Acknowledgements The authors thank N. O. Weiss, A. Asai and D. H. Brooks for comments. Use of TRACE data is acknowledged. This work was supported by the Japan–UK Cooperation Science Program of the JSPS (Principal investigators K.S. and N. O. Weiss) and a Grant-in-Aid for the 21st Century COE ‘Centre for Diversity and Universality in Physics’ from MEXT, Japan. The numerical computation was performed on the Earth Simulator.

Competing interests statement The authors declare that they have no competing financial interests.

Correspondence and requests for materials should be addressed to H.I. (isobe@kwasan.kyoto-u.ac.jp).

Spatial quantum noise interferometry in expanding ultracold atom clouds

Simon Fölling, Fabrice Gerbier, Artur Widera, Olaf Mandel, Tatjana Gericke & Immanuel Bloch

Institut für Physik, Johannes Gutenberg-Universität, Staudingerweg 7, D-55099 Mainz, Germany

In a pioneering experiment¹, Hanbury Brown and Twiss (HBT) demonstrated that noise correlations could be used to probe the properties of a (bosonic) particle source through quantum statistics; the effect relies on quantum interference between possible detection paths for two indistinguishable particles. HBT correlations—together with their fermionic counterparts^{2–4}—find numerous applications, ranging from quantum optics⁵ to nuclear and elementary particle physics⁶. Spatial HBT interferometry has been suggested⁷ as a means to probe hidden order in strongly correlated phases of ultracold atoms. Here we report such a measurement on the Mott insulator^{8–10} phase of a rubidium Bose gas as it is released from an optical lattice trap. We show that strong periodic quantum correlations exist between density fluctuations in the expanding atom cloud. These spatial correlations reflect the underlying ordering in the lattice, and find a natural interpretation in terms of a multiple-wave HBT interference effect. The method should provide a useful tool for identifying complex quantum phases of ultracold bosonic and fermionic atoms^{11–15}.

Although quantum noise correlation analysis is now a basic tool in various areas of physics, applications to the field of cold atoms have been scarce. Most of these concentrate on photon correlation techniques from quantum optics^{5,16}. It was not until 1996 that bunching of cold (but non-degenerate) bosonic atom clouds could be directly measured¹⁷, followed by the observation of reduced inelastic losses due to a modification of local few-body correlations by quantum degeneracy^{18–20}.

In our experiment, we directly measure the spatial correlation function of the density fluctuations in a freely expanding atomic

cloud^{7,21–23}. We create an ultracold Bose gas in an optical lattice with several hundred thousand occupied lattice sites, and record the density distribution after sudden switch-off of the trapping potential and a fixed period of free expansion (the ‘time of flight’). Resonant absorption of a probe laser²⁴ yields the two-dimensional column density of the cloud, that is, the density profile integrated along the probe line of sight, as illustrated in Fig. 1a. It should be noted that the density after the time of flight reflects the in-trap momentum distribution rather than the in-trap density distribution. We performed the experiment with a Bose gas initially in the Mott insulator regime^{8–10}, where repulsive interactions pin the atomic density to exactly an integer number of atoms per lattice site, typically between one and three. In this Mott insulator phase, the average density distribution after expansion is simply given by the

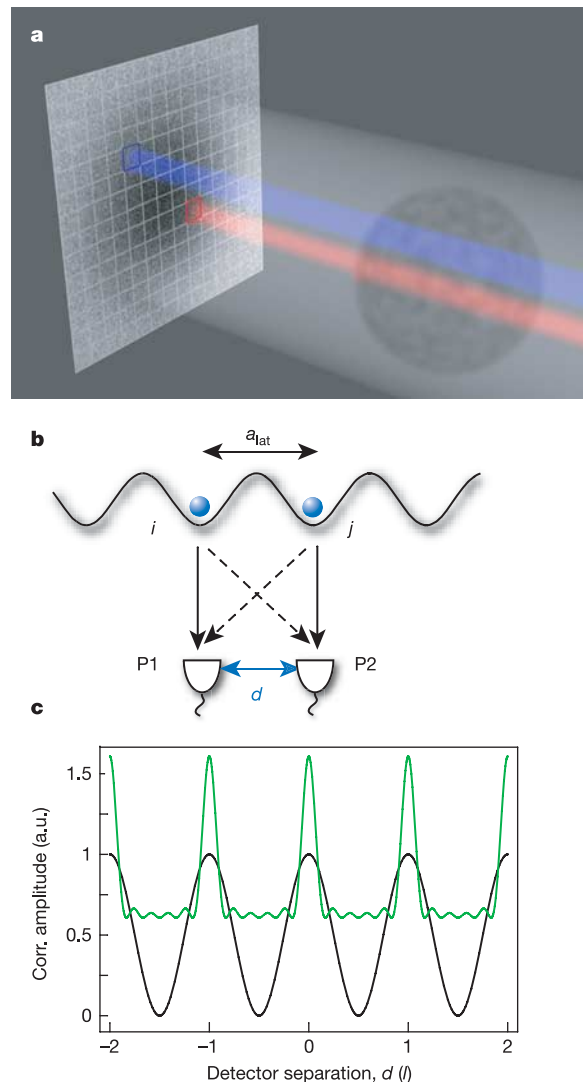


Figure 1 Illustration of the atom detection scheme and the origin of quantum correlations. **a**, The cloud of atoms is imaged to a detector plane and sampled by the pixels of a CCD camera. Two pixels P1 and P2 are highlighted, each of which registers the atoms in a column along its line of sight. Depending on their spatial separation d , their signals show correlated quantum fluctuations, as illustrated in **b**. **b**, When two atoms initially trapped at lattice sites i and j (separated by the lattice spacing a_{lat}) are released and detected independently at P1 and P2, the two indistinguishable quantum mechanical paths, illustrated as solid and dashed lines, interfere constructively for bosons (or destructively for fermions). **c**, The resulting joint detection probability (correlation amplitude) of simultaneously finding an atom at each detector is modulated sinusoidally as a function of d (black curve). The multiple wave generalization to a regular array of six sources with the same spacing is shown in green. a.u., arbitrary units.

incoherent sum of all single particle wavefunctions released from each lattice site—a featureless gaussian. However, a typical single shot absorption image as shown in Fig. 2a and b exhibits large fluctuations around this average. It is the purpose of this Letter to demonstrate that these fluctuations are related to intrinsic quantum noise and that their HBT-type correlations contain information on the spatial order in the lattice that is absent from the average density.

To analyse the fluctuations, we introduce the spatially averaged, normalized density–density correlation function:

$$C(\mathbf{d}) = \frac{\int \langle n(\mathbf{x} + \mathbf{d}/2) \cdot n(\mathbf{x} - \mathbf{d}/2) \rangle d^2\mathbf{x}}{\int \langle n(\mathbf{x} + \mathbf{d}/2) \rangle \langle n(\mathbf{x} - \mathbf{d}/2) \rangle d^2\mathbf{x}} \quad (1)$$

which denotes the conditional probability of finding two particles at two positions separated by a vector \mathbf{d} , averaged over all such positions. In equation (1), $n(\mathbf{x})$ is the column density obtained from a single absorption image and the brackets $\langle \rangle$ denote averaging over an ensemble of independently acquired images. Uncorrelated particles correspond to $C(\mathbf{d}) = 1$, whereas $C(0) > 1$ indicates a tendency of particles to bunch, typical for bosons. In Fig. 2c and d, an experimentally obtained correlation function is shown. In striking contrast to the atomic density distribution of Fig. 2a, sharp peaks emerge. They appear on positions corresponding to the reciprocal lattice vectors of the original periodic trapping potential.

We found the correlation patterns to be robust in the Mott insulating regime, and observed them over a broad range of lattice depths. For a planar lattice of several thousand one-dimensional decoupled Bose gases with random phases^{10,25}, we observed similar density correlations. The latter case is related to a recent experiment²⁶, where single shot interference patterns were observed from 30 independent Bose–Einstein condensates with random phases. Both these cases can be described through a classical field model, whereas the case of a Mott insulator presented here requires a full quantum treatment and detection of the atom number distribution at the atomic shot noise level.

In order to explain the origin of the correlations in the density fluctuations and their regularity, let us first consider the simple

model illustrated in Fig. 1b. Two bosonic atoms in a periodic potential are initially localized at two lattice sites i and j separated by n_{ij} lattice spacings. When these particles are released from the trapping potential, one can show^{7,21} that the joint detection probability by two detectors separated by a distance d is sinusoidally varying as a function of d (Fig. 1c). The spatial wavevector $2\pi n_{ij}/l$ of this modulation is determined by the separation of the sources and the characteristic length:

$$l = \frac{h}{ma_{\text{lat}}} t \quad (2)$$

where t denotes the time of flight, h is Planck’s constant, m is the atomic mass, and a_{lat} is the lattice spacing. For a large number of perfectly distributed but independent sources corresponding to the individual sites of the Mott insulator, the joint detection amplitudes for all possible pairs in the source have to be added. The wave-numbers associated with every pair formed from such a distribution are then integer multiples of $2\pi/l$, so that away from $d = 0$ the amplitudes add up constructively wherever the detector separation is a multiple of l . A lattice pattern of sharp peaks reproducing the reciprocal lattice therefore emerges as the number of particles increases, each peak width being roughly determined by l/N_s , with N_s being the number of occupied sites in the lattice in one dimension. Owing to the different quantum statistics of bosons and fermions the fundamental sine components have opposite signs, and therefore positive peaks emerge for bosons and negative peaks for fermions.

In the experiments, each detector in the above model is represented by a pixel of the CCD (charge-coupled device) camera, which detects the absorption image of the atom cloud. The array of pixels in this camera thereby samples the column density of the atomic cloud, according to $n = N_{\text{bin}}/A_{\text{px}}$. Here N_{bin} is the number of atoms detected within a column defined by the area A_{px} of each pixel and the direction of propagation of the probe light. In addition, each bin is smoothed by the point spread function of our imaging system, which we approximate by a gaussian. In our case, its root mean square (r.m.s.) radius $\sigma \approx 5.6 \mu\text{m}$ is larger than the pixel size

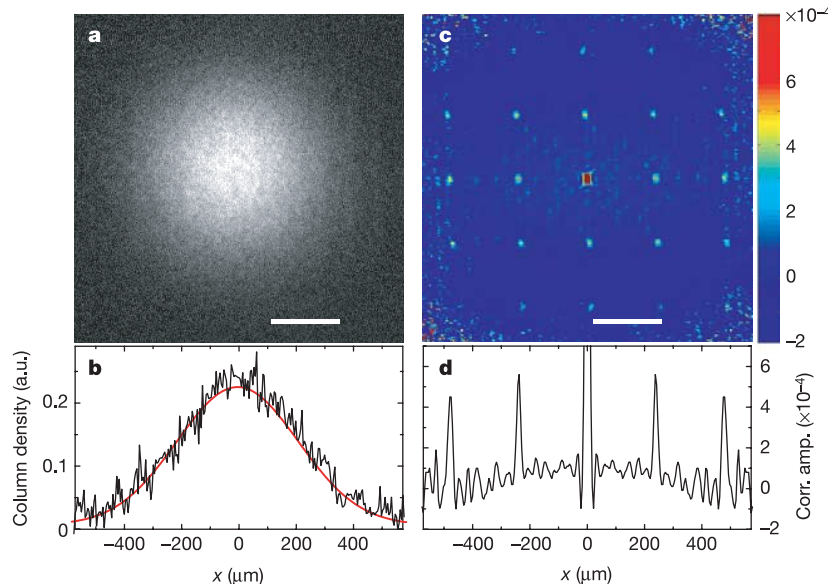


Figure 2 Single shot absorption image including quantum fluctuations and the associated spatial correlation function. **a**, Two-dimensional column density distribution of a Mott insulating atomic cloud containing 6×10^5 atoms, released from a three-dimensional optical lattice potential with a lattice depth of $50E_r$. The white bars indicate the reciprocal lattice scale l defined in equation (2). **b**, Horizontal section (black line) through the centre of the image in **a**, and gaussian fit (red line) to the average over 43 independent images,

each one similar to **a**. **c**, Spatial noise correlation function obtained by analysing the same set of images, which shows a regular pattern revealing the lattice order of the particles in the trap. **d**, Horizontal profile through the centre of the pattern, containing the peaks separated by integer multiples of l . The width of the individual peaks is determined by the optical resolution of our imaging system.

(4.4 μm) and determines an effective width for each bin.

The correlation for such a coarse-grained density can still be calculated from equation (1) by taking the integration over the probe line of sight into account and convoluting the resulting correlation signal with the resolution function described above (see also Methods section). The outcome of this calculation can be qualitatively understood from statistical considerations. One expects the amount of relative number fluctuations in a single detection bin to scale as $1/\sqrt{N_{\text{bin}}}$ for $N_{\text{bin}} \gg 1$, implying a $1/N_{\text{bin}}$ scaling for the correlation amplitude increase above the uncorrelated level $C(\mathbf{d}) = 1$ (see equation (1)). However, in our case this signal is distributed over $N_{\text{peaks}} \approx 4\pi(w/l)^2$ correlation peaks within the expanding density envelope of width w . To obtain the magnitude of the signal, we calculate the average number of atoms per bin as $N_{\text{bin}} = N_{\text{atoms}}(\sigma/w)^2$, with N_{atoms} representing the total atom number. This yields a correlation amplitude per peak:

$$C(\mathbf{d}_{\text{peak}}) - 1 \approx \frac{1}{N_{\text{peaks}}} \frac{1}{N_{\text{bin}}} \approx \frac{1}{4\pi N_{\text{atoms}}} \left(\frac{l}{\sigma}\right)^2 \quad (3)$$

The estimate in equation (3) agrees with a rigorous calculation assuming a homogeneous Mott insulator with unity filling (see Methods). For typical parameters of the experiments (5×10^5 atoms, $l/\sigma = 40$), it yields a correlation amplitude of $\sim 3 \times 10^{-4}$, in agreement with our observations.

To confirm our analysis, we plot in Fig. 3 the experimental correlation signal from the Mott insulator versus expansion time and atom number. This signal is defined by the volume under the lateral peaks, that is, the product of the peak height times its area as determined by a gaussian fit. The resulting 'correlation signal' does not require a precise determination of the resolution, and is rather insensitive to defocusing or calibration errors. According to equation (3), it depends quadratically on the time of flight and inversely on atom number for homogeneous filling. However, for a

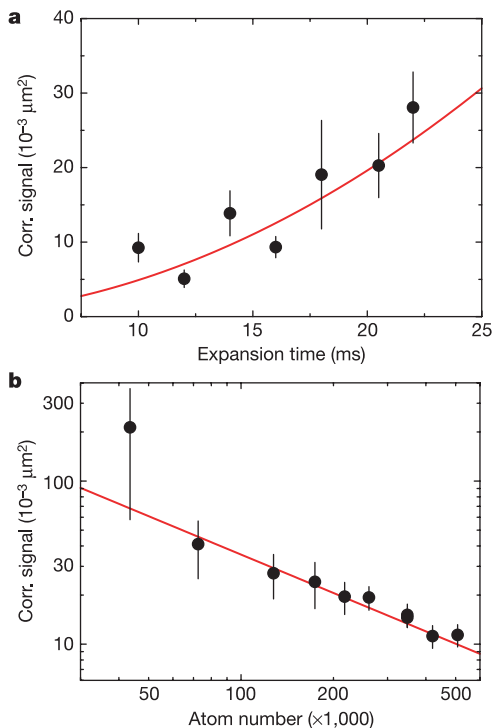


Figure 3 Correlation signal versus expansion time and atom number. **a**, **b**, Average correlation signal as a function of the time of ballistic expansion (**a**) and the number of atoms N loaded in the lattice (**b**). The solid lines denote the result of a simultaneous fit to both data sets to determine the amplitude of the signal and the power law of the decay in **b** (error bars denote root-mean-square deviations).

Mott insulator in a harmonic trap, a shell structure develops for increasing filling^{8,27}. A model of this atom number distribution (see Methods) predicts a reduction of the $(N_{\text{atoms}})^{-1}$ scaling behaviour for large atom numbers to $(N_{\text{atoms}})^{-0.64}$. Using a combined fit to both data sets in Fig. 3a and b, the measured exponent of atom number scaling is 0.78 ± 0.15 , close to the expected value. However, the amplitude of the signal is 40% lower than what would be expected from our simple theoretical model.

For a Bose–Einstein condensate in an optical lattice, a flat spatial correlation function is expected²⁸. Obtaining the correlation function in this regime, however, turned out not to be experimentally possible. In the actual experiment small fluctuations of the superfluid interference pattern between the individual images exist, owing to technical reasons such as shot-to-shot atom number variations, or excitations of the condensate by external perturbations. Such fluctuations are not cancelled by the normalization in equation (1), and the associated correlations turn out to be stronger than the quantum noise correlations observed in the Mott insulating case. We attribute the much more robust quantum noise correlation signal of a Mott insulator to the gapped excitation spectrum (with an energy gap ~ 3 kHz in our case), which protects this state from external perturbations that would otherwise degrade the correlations. We also investigated the case of a thermal cloud significantly above condensation temperature but with no observable population in the excited Bloch bands, for which we did not find a correlation signal. A possible explanation for this could be the decrease in signal (compared to the Mott insulating state) due to an increased spatial size of the system in combination with an increased noise background due to density and temperature fluctuations. We have considered the possibility that the correlation signal we observed in the Mott insulating case could be produced by shot-to-shot fluctuations of a residual fraction of atoms with long range coherence. In order to rule out this effect, we have checked that the regions that would contain the peaks of the diffraction pattern can be excluded from the analysis without significantly affecting the noise correlation pattern.

In conclusion, we have demonstrated that spatial quantum noise correlations in expanding atom clouds can be used to reveal the ordering of indistinguishable particles in optical lattices. They enable the direct and easy detection of many of the more complex and intriguing quantum phases that have been predicted for ultracold bosonic and fermionic atoms—for example, antiferromagnets or spin-waves in two-component spin mixtures loaded into the optical lattice^{12,13}. Antiferromagnetic ordering or charge density waves in Fermi gases or Bose–Fermi mixtures^{14,15}, for example, would yield additional correlation peaks at momenta given by half the reciprocal lattice vector⁷.

We note that after submission of this manuscript, we received a preprint²⁹ reporting the use of noise correlations in expanded atom clouds for identifying the fragments produced by ultracold molecule dissociation. □

Methods

Experimental sequence

Atomic Mott insulators are prepared by loading a Bose–Einstein condensate of up to 6×10^5 atoms of ^{87}Rb into an optical lattice potential. For this, three optical standing waves of wavelength $\lambda = 850$ nm are superimposed at the position of the Bose–Einstein condensate formed in a magnetic trap. This yields a lattice of simple cubic geometry with a lattice constant of $a_{\text{lat}} = \lambda/2 = 425$ nm. After a slow ramp-up of the lattice in 160 ms, the atoms are strongly confined at the lattice sites (potential depth $\sim 50E_{\text{rec}}$, with $E_{\text{rec}} = h^2/2m\lambda^2$) until they are released to free ballistic expansion by switching off all potentials.

Following a time of flight period, the two-dimensional density profile of the cloud is obtained by illuminating it with a resonant laser pulse and projecting the profile of the resulting beam onto a CCD camera. A second image is taken without the atoms in the beam, and the two resulting images are divided to determine the optical density distribution of the cloud. The number of atoms in a column corresponding to a region of the imaging plane can then be deduced from the integrated optical density in that region²⁴.

Analysis of images

In addition to the finite resolution, the camera system adds artefacts to the images owing to optical interference effects of the coherent illumination light and electronic crosstalk during readout of the CCD chip. In our case, the former results in a pattern of vertical stripes and the latter mainly creates a periodic noise with a wavelength of two pixels. As the phase and amplitude of both periodic distortions are not constant, they can not be cancelled by the normalization procedures and appear as periodic fluctuation in the noise correlation plot. Images with high amplitude of such fluctuations (visible outside the atom cloud) are removed from further analysis. The electronic noise is addressed after the determination of the correlation function, by convolving it with a horizontal three-pixel-wide gaussian mask for smoothing.

The correlation function as defined in equation (1) is obtained from a set of images as follows: from each image the autocorrelation function (ACF) is calculated by Fourier-transforming it, taking the absolute square to obtain the power spectral density and Fourier-transforming it back. Averaging the ACF of all images yields the numerator of equation (1), whereas the denominator is obtained by calculating the ACF of the average of all images.

Theoretical model

The origin of the correlation peaks can be understood as follows. Calculating the ACF determines the expectation value of the operator $\langle \hat{n}(\mathbf{x}_1, t) \hat{n}(\mathbf{x}_2, t) \rangle = \langle \hat{a}^\dagger(\mathbf{x}_1, t) \hat{a}(\mathbf{x}_1, t) \hat{a}^\dagger(\mathbf{x}_2, t) \hat{a}(\mathbf{x}_2, t) \rangle$ at time t , with $\mathbf{x}_1 = \mathbf{x} - \frac{1}{2}\mathbf{d}$, $\mathbf{x}_2 = \mathbf{x} + \frac{1}{2}\mathbf{d}$. The operators $\hat{a}(\mathbf{x}, t)$ at position \mathbf{x} and time t after release relate to the on-site operators $\hat{a}(\mathbf{r}_j)$ for the lattice sites j at positions \mathbf{r}_j as

$$\hat{a}(\mathbf{x}, t) = \sum_j w(\mathbf{x} - \mathbf{r}_j, t) e^{i(m/\hbar t)(\mathbf{x} - \mathbf{r}_j)^2} \hat{a}(\mathbf{r}_j)$$

where w is the expanding wavefunction originally localized to the Wannier function at the site. For the product of Fock states representing the Mott insulator with site occupation n_i at site i , one finds

$$\langle \hat{a}^\dagger(\mathbf{r}_k) \hat{a}^\dagger(\mathbf{r}_m) \hat{a}(\mathbf{r}_l) \hat{a}(\mathbf{r}_n) \rangle = n_k n_m \delta_{kl} \delta_{mn} + n_k n_m \delta_{kn} \delta_{lm} \quad (4)$$

where the delta-term introduced through the normal ordering of the operators has been omitted. In the correlation function C , the first term in equation (4) will create a constant offset of 1 for large atom number N , whereas the second term introduces a spatial dependence in the correlations, leading to:

$$C_{3D}(\mathbf{d}) = C(\mathbf{x}_1 - \mathbf{x}_2) = 1 + \frac{1}{N^2} \sum_{k,l} e^{i(m/\hbar t)(\mathbf{x}_1 - \mathbf{x}_2) \cdot (\mathbf{r}_k - \mathbf{r}_l)} n_k n_l \quad (5)$$

Throughout the discussion, constant offsets of order $1/N$ are neglected compared to 1. For a regular one-dimensional lattice with unity filling and spacing a_{lat} , the sum can then be simplified to $1 + \{[\sin^2(\pi Nd/l)]/[N^2 \sin^2(\pi d/l)]\}$, with $d = x_2 - x_1$ and $l = \hbar t/(ma_{\text{lat}})$, analogous to the optical interference created by a regular grating. In the limit of large N , this term corresponds to a series of peaks of height 1 and width l/N and converges to:

$$1 + \frac{1}{N} \sum_{j=-\infty}^{\infty} \delta(d/l - j)$$

For a regular three-dimensional system the structure term converges to:

$$C_{3D}(\mathbf{d}) = 1 + \frac{1}{N} \sum_j \delta((\mathbf{d} - \mathbf{p}_j) \cdot \frac{\mathbf{t}}{m})/l$$

where \mathbf{p}_j are the reciprocal three-dimensional lattice momenta. Because the imaging system registers only column densities and has a finite resolution, the operators $\hat{n}(\mathbf{x}_{1,2})$ both have to be convolved with the inverse point spread function (approximated as a gaussian of r.m.s. width σ) and integrated along the imaging axis before being evaluated. For unity filling this yields a smoothed two-dimensional correlation function:

$$C(\mathbf{d}) = 1 + \frac{1}{4\pi N} \left(\frac{l}{\sigma} \right)^2 \sum_j e^{-[|\mathbf{d} - \mathbf{p}_j|/m]^2/4\sigma^2}$$

The heights of the peaks at the reciprocal lattice momenta therefore scale as $N^{-1}l^2$ for this simple homogeneous case. As indicated in the text, the N^{-1} scaling is modified to $N^{-0.64}$ for our harmonically trapped system by the appearance of Mott domains with filling factor larger than one for higher atom numbers. The prediction for the exponent has been obtained by numerically evaluating the sum in equation (5) using a model distribution of atoms in the lattice sites confined by a global parabolic potential. This distribution is predicted assuming the system can be described in the strongly interacting limit³⁰ with a local density approximation.

Received 27 January; accepted 28 February 2005; doi:10.1038/nature03500.

- Hanbury Brown, R. & Twiss, R. Q. Correlation between photons in two coherent beams of light. *Nature* **177**, 27–29 (1956).
- Henny, M. *et al.* The fermionic Hanbury Brown and Twiss experiment. *Science* **284**, 296–298 (1999).
- Oliver, W. D., Kim, J., Liu, R. C. & Yamamoto, Y. Hanbury Brown and Twiss-type experiment with electrons. *Science* **284**, 299–301 (1999).
- Kiesel, H., Renz, A. & Hasselbach, F. Observation of Hanbury Brown-Twiss anticorrelations for free electrons. *Nature* **418**, 392–394 (2002).
- Bachor, H. A. & Ralph, T. C. *A Guide to Experiments in Quantum Optics* (Wiley-VCH, Weinheim, 2004).
- Baym, G. The physics of Hanbury Brown-Twiss intensity interferometry: From stars to nuclear collisions. *Act. Phys. Pol. B* **29**, 1839–1884 (1998).
- Altman, E., Demler, E. & Lukin, M. D. Probing many-body states of ultracold atoms via noise correlations. *Phys. Rev. A* **70**, 013603 (2004).
- Jaksch, D., Bruder, C., Cirac, J. I., Gardiner, C. W. & Zoller, P. Cold bosonic atoms in optical lattices. *Phys. Rev. Lett.* **81**, 3108–3111 (1998).

- Greiner, M., Mandel, O., Esslinger, T., Hänsch, T. W. & Bloch, I. Quantum phase transition from a superfluid to a Mott insulator in a gas of ultracold atoms. *Nature* **415**, 39–44 (2002).
- Stöferle, T., Moritz, H., Schori, C., Köhl, M. & Esslinger, T. Transition from a strongly interacting 1D superfluid to a Mott insulator. *Phys. Rev. Lett.* **92**, 130403 (2004).
- Hofstetter, W., Cirac, J. I., Zoller, P., Demler, E. & Lukin, M. D. High temperature superfluidity of fermionic atoms in optical lattices. *Phys. Rev. Lett.* **89**, 220407 (2002).
- Kuklov, A. & Svistunov, B. Counterflow superfluidity of two-species ultracold atoms in a commensurate optical lattice. *Phys. Rev. Lett.* **90**, 100401 (2003).
- Duan, L.-M., Demler, E. & Lukin, M. Controlling spin exchange interactions of ultracold atoms in an optical lattice. *Phys. Rev. Lett.* **91**, 090402 (2003).
- Lewenstein, M., Santos, L., Baranov, M. A. & Fehrmann, H. Atomic Bose-Fermi mixtures in an optical lattice. *Phys. Rev. Lett.* **92**, 050401 (2004).
- Roth, R. & Burnett, K. Quantum phases of atomic boson-fermion mixtures in optical lattices. *Phys. Rev. A* **69**, 021601(R) (2004).
- Jurczak, C. *et al.* Atomic transport in an optical lattice: An investigation through polarization-selective intensity correlations. *Phys. Rev. Lett.* **77**, 1727–1730 (1996).
- Yasuda, M. & Shimizu, F. Observation of two-atom correlation of an ultracold neon atomic beam. *Phys. Rev. Lett.* **77**, 3090–3093 (1996).
- Kagan, Y., Svistunov, B. V. & Shlyapnikov, G. V. Effect of Bose condensation on inelastic processes in gases. *Sov. Phys. JETP Lett.* **42**, 209–212 (1985).
- Burt, E. A. *et al.* Coherence, correlations, and collisions: What one learns about Bose-Einstein condensates from their decay. *Phys. Rev. Lett.* **79**, 337–340 (1997).
- Laburthe-Tolra, B. *et al.* Observation of reduced three-body recombination in a correlated 1D degenerate Bose gas. *Phys. Rev. Lett.* **92**, 190401 (2004).
- Grondalski, J., Alsing, P. M. & Deutsch, I. H. Spatial correlation diagnostics for atoms in optical lattices. *Opt. Exp.* **5**, 249–261 (1999).
- Kolovsky, A. R. Interference of cold atoms released from an optical lattice. *Europhys. Lett.* **68**, 330–336 (2004).
- Bach, R. & Rzaewski, K. Correlation functions of cold bosons in an optical lattice. *Phys. Rev. A* **70**, 063622 (2004).
- Ketterle, W., Durfee, D. S. & Stamper-Kurn, D. M. in *Proc. Int. School of Physics “Enrico Fermi”* (eds Inguscio, M., Stringari, S. & Wieman, C. E.) 67–176 (IOS Press, Amsterdam, 1999).
- Greiner, M., Bloch, I., Mandel, O., Hänsch, T. W. & Esslinger, T. Exploring phase coherence in a 2D lattice of Bose-Einstein condensates. *Phys. Rev. Lett.* **87**, 160405 (2001).
- Hadzibabic, Z., Stock, S., Battelier, B., Bretin, V. & Dalibard, J. Interference of an array of independent Bose-Einstein condensates. *Phys. Rev. Lett.* **93**, 180403 (2004).
- Batrouni, G. G. *et al.* Mott domains of bosons confined on optical lattices. *Phys. Rev. Lett.* **89**, 117203 (2003).
- Naraschewski, M. & Glauber, R. Spatial coherence and density correlations of trapped Bose gases. *Phys. Rev. A* **59**, 4595–4607 (1999).
- Greiner, M., Regal, C. A., Stewart, J. T. & Jin, D. S. Probing pair-correlated fermionic atoms through correlations in atom shot noise. Preprint at (<http://arxiv.org/cond-mat/0502411>) (2005).
- Sheshadri, K., Krishnamurthy, H. R., Pandit, R. & Ramakrishnan, T. V. Superfluid and insulating phases in an interacting-boson model: mean-field theory and the RPA. *Europhys. Lett.* **22**, 257–263 (1993).

Acknowledgements We acknowledge discussions with E. Altman and M. Greiner, as well as financial support by the DFG, AFOSR and the EU under a Marie-Curie Fellowship (E.G.) and a Marie-Curie Excellence grant.

Competing interests statement The authors declare that they have no competing financial interests.

Correspondence and requests for materials should be addressed to I.B. (bloch@uni-mainz.de).

Orbital Kondo effect in carbon nanotubes

Pablo Jarillo-Herrero, Jing Kong*, Herre S.J. van der Zant, Cees Dekker, Leo P. Kouwenhoven & Silvano De Franceschi*

Kavli Institute of Nanoscience, Delft University of Technology, PO Box 5046, 2600 GA Delft, The Netherlands

* Present addresses: Department of Electrical Engineering and Computer Science, Massachusetts Institute of Technology, Cambridge, Massachusetts 02139-4307, USA (J.K.); Laboratorio Nazionale TASC-INFN, I-34012 Trieste, Italy (S.D.F.)

Progress in the fabrication of nanometre-scale electronic devices is opening new opportunities to uncover deeper aspects of the Kondo effect¹—a characteristic phenomenon in the physics of strongly correlated electrons. Artificial single-impurity Kondo systems have been realized in various nanostructures, including semiconductor quantum dots^{2–4}, carbon nanotubes^{5,6} and individual molecules^{7,8}. The Kondo effect is usually regarded as a

Phase coherence of an atomic Mott insulator

Fabrice Gerbier, Artur Widera, Simon Fölling, Olaf Mandel, Tatjana Gericke and Immanuel Bloch
Institut für Physik, Johannes Gutenberg-Universität, 55099 Mainz, Germany.

(Dated: March 31, 2005)

We investigate the phase coherence properties of ultracold Bose gases in optical lattices, with special emphasis on the Mott insulating phase. We show that phase coherence on short length scales persists even deep in the insulating phase, preserving a finite visibility of the interference pattern observed after free expansion. This behavior can be attributed to a coherent admixture of particle/hole pairs to the perfect Mott state for small but finite tunneling. In addition, small but reproducible “kinks” are seen in the visibility, in a broad range of atom numbers. We interpret them as signatures for density redistribution in the shell structure of the trapped Mott insulator.

PACS numbers: 03.75.Lm, 03.75.Hh, 03.75.Gg

A fundamental aspect of ultracold bosonic gases is their phase coherence. The existence of long-range phase coherence, inherent to the description of a Bose-Einstein condensate in terms of a coherent matter wave, was experimentally demonstrated in interferometric [1, 2, 3] or spectroscopic [4] experiments. More recently, attention has been paid to fundamental mechanisms that may degrade or even destroy long-range coherence, for example thermal phase fluctuations in elongated condensates [5, 6, 7, 8], or the superfluid to Mott insulator (MI) transition undergone in optical lattices [9, 10, 11].

For a Bose-Einstein condensate released from an optical lattice, the density distribution after expansion shows a sharp interference pattern [10]. In a perfect Mott Insulator, where atomic interactions pin the density to precisely an integer number of atoms per site, phase coherence is completely lost and no interference pattern is expected. The transition between these two limiting cases happens continuously as the lattice depth is increased. In the superfluid phase, a partial loss of long range coherence due to an increased quantum depletion has been observed for lattice depths below the MI transition [12, 13, 14]. Conversely, in the insulating phase, numerical simulations [15, 16, 17] predict a residual interference, although *long-range* coherence and superfluidity have vanished.

In this Letter, we revisit this question of phase coherence focusing on the insulating phase. We observe that the interference pattern persists in the MI phase, and that its visibility decays rather slowly with increasing lattice depth. We explain this behavior as a manifestation of short-range coherence in the insulating phase, fundamentally due to a coherent admixture of particle/hole pairs to the ground state for large but finite lattice depths. In addition, we also observe reproducible “kinks” in the visibility at well-defined lattice depths. We interpret them as signature of density redistribution in the shell structure of a MI in an inhomogeneous potential, when regions with larger-than-unity filling form. Finally, the issue of adiabatic loading in the lattice is briefly discussed.

In our experiment, a ^{87}Rb Bose-Einstein condensate

is loaded into an optical lattice created by three orthogonal pairs of counter-propagating laser beams (see [10] for more details). The superposition of the lattice beams, derived from a common source at a wavelength $\lambda_L = 850$ nm, results in a simple cubic periodic potential with a lattice spacing $d = \lambda_L/2 = 425$ nm. The lattice depth V_0 is controlled by the laser intensities, and is measured here in units of the single-photon recoil energy, $E_R = \hbar^2/2m\lambda_L^2 \approx h \times 3.2$ kHz, where m is the atomic mass. The optical lattice is ramped up in 160 ms, using a smooth waveform that minimizes sudden changes at both ends of the ramp. After switching off the optical and magnetic potentials simultaneously and allowing for typically $t = 10 - 22$ ms of free expansion, standard absorption imaging of the atom cloud yields a two-dimensional map of the density distribution (integrated along the probe line of sight).

Four such images are shown in Fig. 1a-d, for various lattice depths. The density distribution of these expanding clouds can be expressed as [15, 16, 18]

$$n(\mathbf{r}) = \left(\frac{m}{\hbar t}\right)^3 \left|\tilde{w}(\mathbf{k} = \frac{m\mathbf{r}}{\hbar t})\right|^2 \mathcal{S}\left(\mathbf{k} = \frac{m\mathbf{r}}{\hbar t}\right). \quad (1)$$

In Eq. (1), the interference pattern is described by

$$\mathcal{S}(\mathbf{k}) = \sum_{i,j} e^{i\mathbf{k} \cdot (\mathbf{r}_i - \mathbf{r}_j)} \langle \hat{a}_i^\dagger \hat{a}_j \rangle, \quad (2)$$

where the operator \hat{a}_i^\dagger creates an atom at site i , and where \tilde{w} is the Fourier transform of the Wannier function $w(\mathbf{r}_i)$. The Fourier relation (2) shows that long-range phase coherence, *i.e.* a correlation function $\langle \hat{a}_i^\dagger \hat{a}_j \rangle$ slowly varying

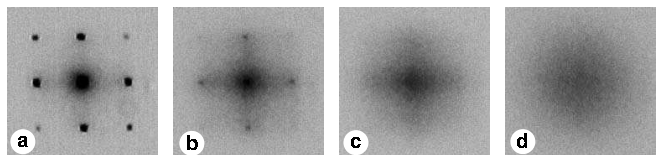


FIG. 1: Absorption images of an ultracold Bose gas released from an optical lattice, for various lattice depths: **a** $8 E_R$, **b** $14 E_R$, **c** $18 E_R$, and **d** $30 E_R$.

across the lattice, is necessary to observe a sharp diffraction pattern as in Fig. 1a. However, above the MI transition (Fig. 1b, c and d), the interference peaks evolve into a much broader, cross-like structure which weakens with increasing lattice depth. This slow modulation corresponds to short-range coherence, *i.e.* a correlation function $\langle \hat{a}_i^\dagger \hat{a}_j \rangle$ whose range extends over a few sites only.

To extract quantitative information from time-of-flight pictures as shown in Fig. 1, Eq. (1) suggests using the usual definition of the visibility of interference fringes,

$$\mathcal{V} = \frac{n_{\max} - n_{\min}}{n_{\max} + n_{\min}} = \frac{\mathcal{S}_{\max} - \mathcal{S}_{\min}}{\mathcal{S}_{\max} + \mathcal{S}_{\min}}. \quad (3)$$

In this work, we measure the maximum density n_{\max} at the first lateral peaks of the interference pattern [19], (*i.e.* at the center of the second Brillouin zone), whereas the minimum density n_{\min} is measured along a diagonal with the same distance from the central peak (see inset in Fig. 2a). In this way, the Wannier envelope is the same for each term and cancels out in the division, yielding the contrast of \mathcal{S} alone (hence the second equality in Eq. (3)). Four pairs exist for a given absorption image, and their values are averaged to yield the visibility. In previous studies of the MI transition [10, 14], the sharpness of the interference pattern was characterized by the half-width of the central peak. Such a measure is possibly sensitive to systematic effects, such as optical saturation and mean field broadening. We expect our measure of contrast to be much less sensitive to these effects, since it is calculated in regions of the image where the density is lower.

We present here measurements of the visibility as a function of lattice depth (typically in a range $6 - 30 E_R$) at a given total atom number. Each value was obtained as the visibility averaged over approximately 10 independent images. Different atom numbers (hence different filling factors) were investigated, ranging from 6×10^4 to 6×10^5 . Two illustrative sets of data are shown in Fig. 2, corresponding to approximately 5.9×10^5 atoms (black circles) and 3.6×10^5 atoms (grey circles). For lattice depths larger than $12.5 E_R$, the system is in the insulating phase [10]. Yet, the visibility remains finite well above this point. For example, at a lattice depth of $15 E_R$, the contrast is still around 30%, reducing to a few percent level only for a rather high lattice depth of $30 E_R$. We will now show that such a slow loss in visibility is expected in the ground state of the system.

As shown in [9], the physics of ultracold atoms in an optical lattice can be described by the Bose-Hubbard hamiltonian, given by the sum of a tunneling term, $\mathcal{H}_t = -t \sum_{\langle i,j \rangle} \hat{a}_i^\dagger \hat{a}_j$, plus an interaction term, $\mathcal{H}_{\text{int}} = \sum_i \frac{U}{2} \hat{n}_i (\hat{n}_i - 1)$. Here $\hat{n}_i = \hat{a}_i^\dagger \hat{a}_i$ is the on-site number operator, t is the tunneling matrix element, the notation $\langle i,j \rangle$ restricts the sum to nearest neighbors only, and U is the on-site interaction energy [11]. In the experiments, an additional, slowly varying potential $V_{\text{ext}}(\mathbf{r})$

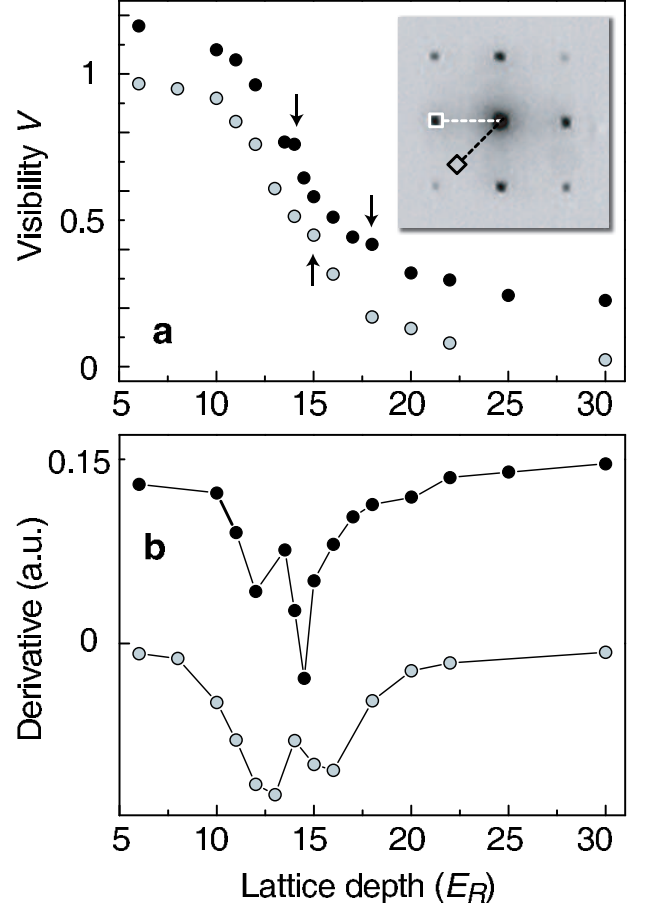


FIG. 2: (a) Visibility of the interference pattern produced by an ultracold cloud released from an optical lattice. The two sets of data shown correspond to 3.6×10^5 atoms (grey circles) and 5.9×10^5 atoms (black circles). The latter curve has been offset vertically for clarity. Arrows mark positions where “kinks” are visible. (b) Numerical derivative of the above curves.

is also present, and favors the formation of a “wedding cake” structure of alternating MI and superfluid shells [9, 15, 20], which reflects the characteristic lobes delimiting the MI phases in the phase diagram of the Bose-Hubbard model [11].

To better understand the origin of a finite visibility, we consider a homogeneous system with filling factor n_0 . In the limit of infinitely strong repulsion, $U/t \rightarrow \infty$, the ground state is what we call a “perfect” Mott insulator, *i.e.* a uniform array of Fock states, $|\Psi\rangle_{\text{MI}} = \prod_i |n_0\rangle_i$. This corresponds to a uniform $\mathcal{S} = n_0$ and zero visibility. To a good approximation, the actual ground state for a finite ratio U/t can be calculated by considering the tunneling term as a perturbation to the interaction term. To first order in t/U , this yields

$$|\Psi^{(1)}\rangle \approx |\Psi\rangle_{\text{MI}} + \frac{t}{U} \sum_{\langle i,j \rangle} \hat{a}_i^\dagger \hat{a}_j |\Psi\rangle_{\text{MI}}. \quad (4)$$

The ground state thus acquires a small admixture of

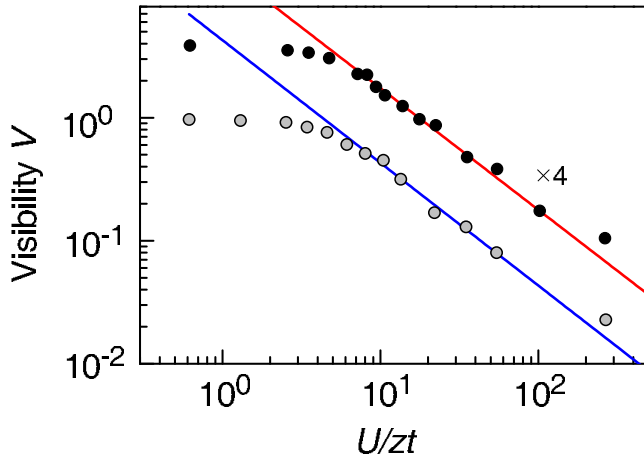


FIG. 3: Visibility of the interference pattern versus U/zt , the characteristic ratio of interaction to kinetic energy. The data are identical to those shown in Fig. 2 (5.9×10^5 , black circles, and 3.6×10^5 atoms, grey circles). The former curve has been offset vertically for clarity. The lines are fits to the data in the range $14 - 25 E_R$, assuming a power law behavior (see text).

“particle-hole” pairs (*i.e.* an additional particle at one lattice site and a missing one in a neighboring site), which restores short-range coherence and a corresponding weak modulation in the momentum distribution, $\mathcal{S}(\mathbf{k}) \propto n_0 - 2n_0(n_0+1)t(\mathbf{k})/U$, where $t(\mathbf{k}) = -2t \sum_{\nu=x,y,z} \cos(k_\nu d)$ is the tight-binding dispersion relation. The corresponding 2D visibility (integrated along one direction) is

$$\mathcal{V} \approx \frac{4}{3}(n_0 + 1) \frac{zt}{U}. \quad (5)$$

In Eq. (5), $z = 6$ is the number of nearest neighbors in a 3D cubic lattice.

To compare with the experiment, we show in Fig. 3a the visibility against U/zt in a log-log plot. For lattice depths $V_0 \geq 14 E_R$ (corresponding to $U/zt \geq 8$), the data matches the inverse law expected from Eq. (5). This has been verified by fitting the data in this range to a general power law $A(U/zt)^\alpha$ (solid lines in Fig. 3). We obtain an average exponent $\alpha = -0.98(7)$ in agreement with the prediction (see Fig. 4a). In Fig. 4b, the fitted prefactor is plotted as a function of atom number. Inspired by Eq. (5), we compare it to $4(\bar{n} + 1)/3$, where \bar{n} is the average filling factor calculated at a lattice depth of $30 E_R$ using a mean-field approximation [21, 22]. We find that this extrapolation of Eq. (5) to our trapped system indeed yields the correct order of magnitude (see Fig. 4b). We thus consider the agreement between our experimental results and the simple relations derived above as a conclusive evidence for the presence of particle-hole pairs, characteristic of the ground state of the Bose-Hubbard hamiltonian.

In addition to the smooth decay discussed above, the visibility shows small “kinks” at specific lattice depths (indicated by arrows in Fig. 2a). They are systematically observed in our data, and their positions are reproducible. In the derivative plot (Fig. 2b), they ap-

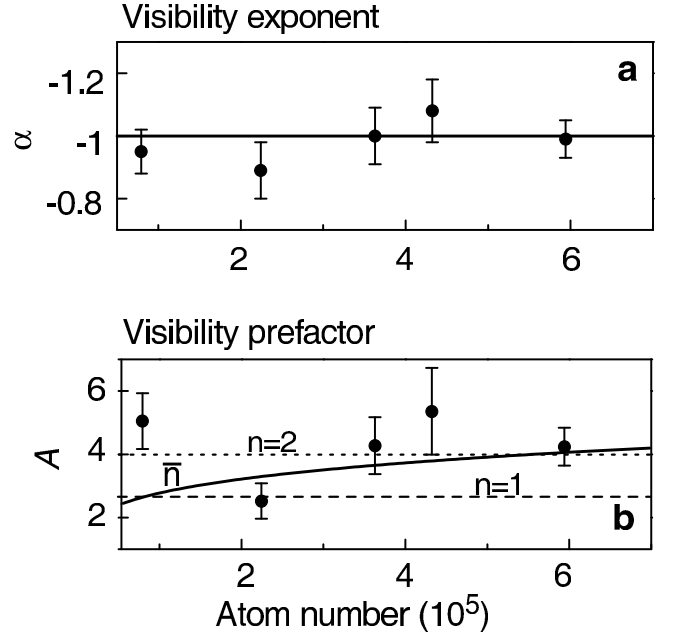


FIG. 4: Exponent α (a) and prefactor A (b) extracted from a power law fit $A(U/zt)^\alpha$ to the visibility data in Fig. 3, plotted versus total atom number. The solid line indicates the expected exponent $\alpha = -1$. In (b), we also indicate the prefactor expected for uniform MI with filling factor $n_0 = 1$ (dashed line) and $n_0 = 2$ (dotted line), as well as an extrapolation for the average filling calculated at a lattice depth of $30 E_R$ (solid line).

pear as narrow maxima on a smoother background. We obtained the kink positions by taking the middle point between two adjacent gaussian peaks with negative amplitudes fitted to the data. The most prominent kink occurs on average for a lattice depth of $14.1(8) E_R$, with a statistical error indicated between parentheses. For the largest atom numbers (4.2×10^5 and 6×10^5), a similar but much weaker kink is also visible around $16.6(9) E_R$ (see upper curves in Fig. 2). These values are close to $14.7 E_R$ and $15.9 E_R$, the lattice depths where MI regions with filling factor $n_0 = 2$ or 3 are respectively expected to form for our parameters [22]. We thus propose that the observed kinks are linked to a redistribution in the density as the superfluid shells transform into MI regions with several atoms per site. We were recently informed that similar features were reproduced numerically for one-dimensional trapped systems with a small number of particles [23].

We have considered the dependence of the visibility on the time over which the optical lattice was ramped from zero to its final value, for a specific lattice depth of $V_0 = 10 E_R$. The visibility was considerably degraded for the shortest ramp time of 20 ms, but reached a ramp-independent value for ramp times larger than $T_{ad} \sim 100$ ms (to be compared to the 160 ms time used in visibility experiments). We note that T_{ad} for this lat-

tice depth of $V_0 = 10 E_R$ is significantly longer than the microscopic time scales of the system, such as the tunneling time or the trapping periods. We note also that at the largest lattice depth we use here ($V_0 = 30 E_R$), the observed visibility is systematically above the power law fit in Fig. 3, indicating a breakdown of adiabaticity. By comparing the data to the fitted curve, we expect this to occur for $V_0 \approx 29 E_R$ ($U/zt \approx 200$), which agrees with the calculated depth of $32 E_R$ for which the ramping time 160 ms becomes smaller than the calculated tunneling time h/zt .

Although a complete study is beyond the scope of this Letter, these observations suggest that different dynamical processes are involved in the loading, depending on whether the gas is in the superfluid or in the MI phase. In the superfluid phase, the ramp time has to be slow enough not to excite long-lived collective excitations. In the MI phase, these excitations acquire an energy gap, which makes single particle tunneling the dominant dynamical process. In this case, the final tunneling time increases with final lattice depth, and eventually becomes so long that the system basically freezes out at some lattice depth, estimated here to be $29 E_R$.

In conclusion, we have studied the visibility of the interference pattern produced by an ultracold Bose gas released from a deep optical lattice. A non-vanishing visibility in the MI phase is observed and explained by the coherent admixture of particle-hole pairs to the insulating ground state, which preserves local phase coherence. This intrinsic limitation to the “quality” of a MI has important implications for various quantum information processing schemes, where the MI plays a central role [24, 25, 26]. In addition, we observe small but reproducible kinks in the visibility curve. We interpret them as the signature of density redistribution in the shell structure of the cloud as MI with several atoms per site are expected to form. Finally, a recent paper [27] suggests that in a planar array of one-dimensional Bose gases, the visibility might be further reduced when correlations build up in each tube, *i.e.* upon entering the Tonks-Girardeau regime. Experimental study of these effects seems within reach with the methods presented in this paper.

We would like to thank Dries van Oosten, Paolo Pedri and Luis Santos for useful discussions. Our work is supported by the Deutsche Forschungsgemeinschaft (SPP1116), AFOSR and the European Union under a Marie-Curie Excellence grant. FG acknowledges support from a Marie-Curie Fellowship of the European Union.

[1] M. R. Andrews, C. G. Townsend, H.-J. Miesner, D. S. Durfee, D. M. Kurn, and W. Ketterle, *Science* **275**, 637

(1997).
 [2] E. W. Hagley et al., *Phys. Rev. Lett.* **83**, 3112 (1999).
 [3] I. Bloch, T. W. Hänsch, and T. Esslinger, *Nature* **403**, 166 (2000).
 [4] J. Stenger, S. Inouye, A. P. Chikkatur, D. M. Stamper-Kurn, D. E. Pritchard, and W. Ketterle, *Phys. Rev. Lett.* **82**, 4569 (1999).
 [5] D. S. Petrov, G. V. Shlyapnikov, and J. T. M. Walraven, *Phys. Rev. Lett.* **85**, 3745 (2000).
 [6] S. Dettmer et al., *Phys. Rev. Lett.* **87**, 160406 (2001).
 [7] S. Richard, F. Gerbier, J. H. Thywissen, M. Hugbart, P. Bouyer, and A. Aspect, *Phys. Rev. Lett.* **91**, 010405 (2003).
 [8] D. Hellweg, L. Cacciapuoti, M. Kottke, T. Schulte, K. Sengstock, W. Ertmer, and J. J. Arlt, *Phys. Rev. Lett.* **91**, 010406 (2003).
 [9] D. Jaksch, C. Bruder, J. I. Cirac, C. W. Gardiner, and P. Zoller, *Phys. Rev. Lett.* **81**, 3108 (1998).
 [10] M. Greiner, O. Mandel, T. Esslinger, T. W. Hänsch, and I. Bloch, *Nature* **415**, 39 (2002).
 [11] W. Zwerger, *J. Opt. B: Quantum Semiclass. Opt.* **5**, S9 (2003).
 [12] C. Orzel, A. K. Tuchman, M. L. Fenselau, M. Yasuda, and M. K. Kasevich, *Science* **291**, 2386 (2001).
 [13] Z. Hadzibabic, S. Stock, B. Battelier, V. Bretin, and J. Dalibard, *Phys. Rev. Lett.* **93**, 180403 (2004).
 [14] C. Schori, T. Stöferle, H. Moritz, M. Köhl, and T. Esslinger, *Phys. Rev. Lett.* **93**, 240402 (2004).
 [15] V. A. Kashurnikov, N. V. Prokof'ev, and B. V. Svistunov, *Phys. Rev. A* **66**, 031601(R) (2002).
 [16] R. Roth and K. Burnett, *Phys. Rev. A* **67**, 031602(R) (2003).
 [17] C. Schroll, F. Marquardt and C. Bruder, *Phys. Rev. A* **70**, 053609 (2004).
 [18] P. Pedri, L. Pitaevskii, S. Stringari, C. Fort, S. Burger, F. S. Cataliotti, P. Maddaloni, F. Minardi, and M. Inguscio, *Phys. Rev. Lett.* **87**, 220401 (2001).
 [19] The value is obtained by averaging over 3×3 pixels around each position. We have checked that the visibility obtained this way was almost independent of the size of the integration region used to find n_{\max} and n_{\min} .
 [20] G. G. Batrouni, V. Rousseau, R. T. Scalettar, M. Rigol, A. Muramatsu, P. J. H. Denteneer, and M. Troyer, *Phys. Rev. Lett.* **89**, 117203 (2002).
 [21] K. Sheshadri, H. R. Krishnamurthy, R. Pandit, and T. V. Ramakrishnan, *Euro. Phys. Lett.* **22**, 257 (1993).
 [22] D. van Oosten, P. van der Straten, and H. T. C. Stoof, *Phys. Rev. A* **63**, 053601 (2000).
 [23] F. Schmitt, M. Hild and R. Roth, private communication.
 [24] P. Rabl, A. J. Daley, P. O. Fedichev, J. I. Cirac, and P. Zoller, *Phys. Rev. Lett.* **91**, 110403 (2003).
 [25] G. Pupillo, A. M. Rey, G. K. Brennen, C. W. Clark, and C. J. Williams, *Journal of Modern Optics* **51**, 2395 (2004).
 [26] B. DeMarco, C. Lannert, S. Vishveshwara, and T.-C. Wei, *cond-mat/0501718* (2005).
 [27] D. M. Gangardt, P. Pedri, L. Santos, and G. V. Shlyapnikov, *cond-mat/0408437* (2004).

Coherent collisional spin dynamics in optical lattices

Artur Widera,* Fabrice Gerbier, Simon Fölling, Tatjana Gericke, Olaf Mandel, and Immanuel Bloch
Johannes Gutenberg-Universität, Staudingerweg 7, 55099 Mainz, Germany
 (Dated: May 19, 2005)

We report on the observation of coherent, purely collisionally driven spin dynamics of neutral atoms in an optical lattice. For high lattice depths, atom pairs confined to the same lattice site show weakly damped Rabi-type oscillations between two-particle Zeeman states of equal magnetization, induced by spin changing collisions. This paves the way towards the efficient creation of entangled atom pairs in an optical lattice. Moreover, measurement of the oscillation frequency allows for precise determination of the coupling parameters of the collisional interaction. For smaller lattice depths, we observe an increased damping of the coherent oscillations, which we attribute to the onset of spin transport in the Mott-insulator regime.

PACS numbers: 03.75.Lm, 03.75.Gg, 03.75.Mn, 34.50.-s

The creation and manipulation of spinor Bose-Einstein condensates (BEC) in optical traps [1, 2, 3, 4, 5, 6] has opened a wide field of fascinating phenomena originating from the spin degree of freedom. Spinor systems have been proposed for the investigation of quantum magnetism phenomena [7, 8, 9, 10, 11] such as spin mixing properties [12, 13] and spin waves [14, 15], or the generation of entangled states [16, 17]. More recently, a variety of strongly correlated ground states have been predicted in optical lattices [18, 19, 20], opening the possibility for studying spin hamiltonians in a wide range of parameters not accessible in solid state physics [21]. The fundamental mechanism responsible for many of these spin phenomena is a coherent collisional process in which the spin of each colliding particle is changed while the total magnetization is preserved.

In this Letter, we investigate this microscopic collision process in an ensemble of isolated atom pairs localized to lattice sites of a deep optical lattice. We observe coherent oscillations between two-particle Zeeman states, coupled by the spin-changing interaction. We show that for a broad range of parameters this dynamics can be described by a Rabi-type model. Our system allows for a precise measurement of the coupling parameters for spin changing collisions. Furthermore, for decreasing lattice depths, but still in the Mott-insulator, we observe an increase in the damping of the coherent oscillations, which we attribute to the onset of spin transport in the system.

Let us consider a pair of ^{87}Rb atoms, localized in the vibrational ground state of a deep trapping potential, as shown in Fig. 1a. The trapping frequency ω is assumed to be much larger than the typical interaction energy, so that excitations into higher vibrational levels are suppressed. The atom pair can then be solely described by a spin wavefunction $|f_1, m_1; f_2, m_2\rangle$, where f_i, m_i are the total angular momentum and its projection onto the z -axis, and $i = 1, 2$ labels the first and second atom, respectively. In the following, we assume that both atoms are in the upper hyperfine ground state with $f_1 = f_2 = 2$, and abbreviate the non-symmetrized two particle states as $|m_1, m_2\rangle$. In the absence of an external radio-frequency (rf) field, interatomic collisions drive the spin evolution of this system. In a collision be-

tween two alkali atoms, the projection of the total angular momentum on the quantization axis is conserved, even in a finite magnetic field [1, 2, 3, 7, 8, 12, 13]. The interaction thus couples an initial state $|\phi_i\rangle \equiv |m_1, m_2\rangle$ to a final state $|\phi_f\rangle \equiv |m_3, m_4\rangle$, provided the total magnetization is conserved, i. e. $m_1 + m_2 = m_3 + m_4$. Furthermore, s -wave collisions between spin $f = 2$ bosons are characterized by three scattering lengths a_F for the collision channels with total angular momentum F ($F = 0, 2, 4$) [7, 9, 10]. The matrix element Ω_{if} of the interaction hamiltonian between states $|\phi_i\rangle$ and $|\phi_f\rangle$ is proportional to $4\pi\hbar a_{\text{eff}}/m$, where a_{eff} is a weighted difference of the a_F 's that depends on the specific values of the magnetic quantum numbers. For example, in the case $|\phi_i\rangle = |0, 0\rangle$ and $|\phi_f\rangle = |1, -1\rangle$, one finds $a_{\text{eff}} = (-7a_0 - 5a_2 + 12a_4)/35$. It should also be noted that since the two particles at a certain lattice site are indistinguishable, the final state is an entangled state $|\phi_f\rangle = (|1, -1\rangle + |-1, 1\rangle)/\sqrt{2}$ [16, 17].

Due to the localization in the vibrational ground state and to the constraint of a conserved magnetization, for a given initial state only a few final two-particle states participate in the spin evolution (see Fig. 1b). In the case where only one final state is available (relevant for most experiments described below), the dynamics reduces to a Rabi-like model. The atom pair then oscillates between initial and final state at the effective Rabi frequency $\Omega'_{if} = [\Omega_{if}^2 + \delta_{if}^2]^{1/2}$. We stress however that differently from "usual" single-particle Rabi oscillations driven by an external rf field, in this Letter we investigate the coherent coupling between two-particle states. The Rabi model is parameterized by a coupling strength Ω_{if} discussed above, and a detuning $\delta_{if} = \delta_0 + \delta(B^2)$ between the initial and final states, where B is the value of the static external magnetic field. As the magnetization is conserved, the initial and final states experience the same first order Zeeman shift which has no influence on the spin dynamics. However, the second order Zeeman shifts are different and introduce the B^2 -dependent detuning. The constant detuning δ_0 originates from the difference in interaction energies in the initial and final states.

In our experiment we investigate an array of localized atom pairs. We prepare a Mott-insulator in a combined optical and magnetic trap similar to previous work [22], and sub-

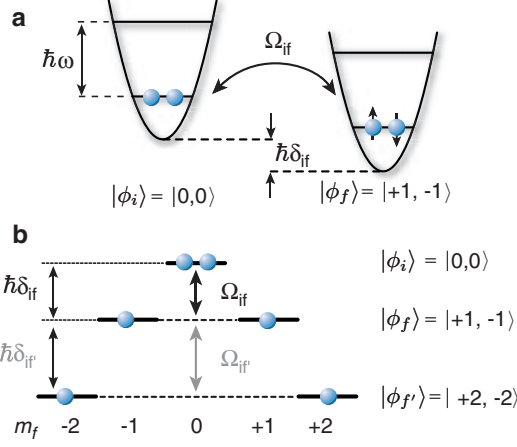


FIG. 1: (a) Two atoms localized in the vibrational ground state of a common lattice well can change their spin orientation while preserving total magnetization. The atoms remain in the lowest vibrational state at all times. (b) The process can be described as a coherent coupling between two-particle Zeeman states $|\phi_i\rangle$, $|\phi_f\rangle$ and $|\phi_{f'}\rangle$, where the coupling constant Ω_{if} depends on the choice of initial and final state, and the detuning δ_{if} can be varied by the second order Zeeman shift.

sequently load the sample of around 2×10^5 ^{87}Rb atoms in $|f=1, m_f=-1\rangle$ in a pure optical lattice [23]. In order to preserve spin polarization of the atoms, a homogeneous magnetic field of approximately 1.2 G is maintained [24]. The spin dynamics is initialized by transferring the sample into either $|f=2, m_f=0\rangle$ or $|f=2, m_f=-1\rangle$, and the magnetic field is subsequently ramped to a final value between 0.2 G and 2 G. After time evolution for a variable time t the optical trap is switched off. In order to spatially separate the different magnetic substates, a magnetic gradient field is switched on during the first 3 ms of time-of-flight (TOF) [1, 2, 3, 4, 5]. The population N_{m_j} of each magnetic sublevel m_j is then detected after 7 ms TOF with standard absorption imaging.

We first consider the case where we start with both atoms in $|\phi_i\rangle = |0,0\rangle$. This state couples to $|\phi_f\rangle = |+1, -1\rangle$ and $|\phi_{f'}\rangle = |+2, -2\rangle$. The coupling constant for $|\phi_i\rangle \leftrightarrow |\phi_{f'}\rangle$ is calculated to be two orders of magnitude smaller than for $|\phi_i\rangle \leftrightarrow |\phi_f\rangle$, and can be neglected. However, a two-step coupling channel $|\phi_i\rangle \leftrightarrow |\phi_f\rangle \leftrightarrow |\phi_{f'}\rangle$ is also possible, with a coupling constant comparable to the $|\phi_i\rangle \leftrightarrow |\phi_f\rangle$ process. Although present at low magnetic field [3, 5], this two-step process is increasingly suppressed as the magnetic field is increased due to the large detuning. For $B > 0.6$ G, the system mostly oscillates between $|0,0\rangle$ and $|+1, -1\rangle$. This is shown in Fig. 2 for the case of $B = 0.8$ G and a lattice depth of $40 E_r$. Here $E_r = \hbar^2/2m\lambda^2$ is the single photon recoil energy, m the atomic mass and $\lambda = 840$ nm the lattice laser wavelength. The relative populations in Fig. 2 have been calculated as N_0/N_{tot} for $|0,0\rangle$ and $(N_{+1} + N_{-1})/N_{\text{tot}}$ for $|+1, -1\rangle$, where N_{tot} is the total atom number. For the other initial state $|\phi_i\rangle = |-1, -1\rangle$, however, no third level exists to which the final state $|0, -2\rangle$ could couple while

preserving magnetization, and the dynamics can be described by a two level system even for low magnetic fields.

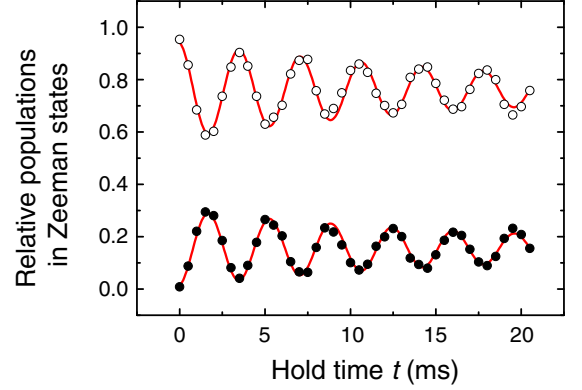


FIG. 2: Spin dynamics of atom pairs localized in an optical lattice at a magnetic field of $B = 0.8$ G. The atoms are initially prepared in $|\phi_i\rangle = |0,0\rangle$ and can evolve into $|\phi_f\rangle = |+1, -1\rangle$. Shown are the populations in $m_f = 0$ (\circ) and $m_f = \pm 1$ (\bullet) together with a fit to a damped sine. The extracted oscillation frequency is $2\pi \times 278(3)$ Hz.

In order to describe the oscillations we use a Rabi-like model, where the transition probability to the final state is [25]

$$P_f = \frac{\Omega_{if}^2}{\Omega_{if}'^2} \frac{1}{2} \left(1 - \cos(\Omega_{if}' t) e^{-\gamma_{if} t} \right), \quad (1)$$

with γ_{if} being the damping rate. The measured population in $m_f = \pm 1$ can be written as

$$\frac{N_{+1} + N_{-1}}{N_{\text{tot}}} = n P_f, \quad (2)$$

where n is the fraction of atoms localized in doubly occupied lattice sites. In order to check the validity of the Rabi model, spin oscillations have been observed for various magnetic fields up to 2 G, corresponding to different detunings, and for the two initial two-particle states $|0,0\rangle$ and $|-1, -1\rangle$. The measured oscillation frequency is plotted versus magnetic field B in Fig. 3. The measured frequencies are fitted to the expected behaviour of the effective Rabi frequency $\Omega'(B)$ with varying detuning (solid lines in Fig. 3), with which we observe an excellent agreement. As explained above, for small magnetic fields $B \leq 0.6$ G, the process $|+1, -1\rangle \leftrightarrow |+2, -2\rangle$ starts to play a role. A Fourier transform of the measured spin oscillations allows for the extraction of the effective Rabi frequency of the second process $|+1, -1\rangle \leftrightarrow |+2, -2\rangle$. The coupling parameters for the different processes determined by the fits are summarized in Table I. We find a general agreement between the measured oscillation frequencies and the frequencies calculated from two recently available sets of scattering lengths [10, 23, 26].

The visibility of the oscillation shown in Fig. 2 is smaller than expected from the Rabi model (1) alone for this detuning.

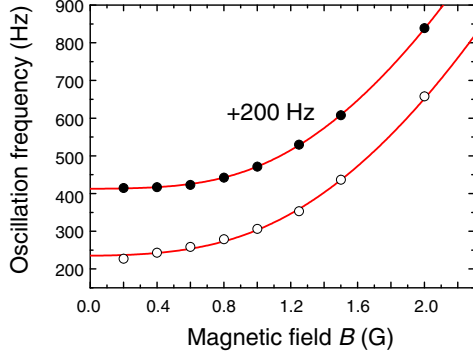


FIG. 3: Oscillation frequency of spin dynamics versus magnetic field for the case $|0, 0\rangle \leftrightarrow |+1, -1\rangle$ (\circ) and $|-1, -1\rangle \leftrightarrow |0, -2\rangle$ (\bullet). The solid lines are fits to the expected behaviour of the effective Rabi frequency (1). The upper curve has been offset by 200 Hz for clarity. The error bars are typically on the order of a few percent.

Process	$\Omega_{if}/2\pi$	$\delta_{if}/2\pi$	$\Omega'_{if}(B=0)/2\pi$
$ 0, 0\rangle \leftrightarrow +1, -1\rangle$	233(4) Hz	62(7) Hz	241(8) Hz
$ -1, -1\rangle \leftrightarrow 0, -2\rangle$	211(1) Hz	27(3) Hz	213(3) Hz
$ +1, -1\rangle \leftrightarrow +2, -2\rangle$	—	—	340(40) Hz

TABLE I: Summary of measured coupling parameters at $40 E_r$ lattice depth.

This fact can be explained by the atom number distribution in the lattice. The overall harmonic confinement of the system leads to the creation of Mott-shells with different filling factors [27]. Only those atoms that are in lattice wells with a filling of two or more contribute to the spin dynamics, which is accounted for by Eq. (2). Since the relative populations are normalized with respect to the overall number of atoms, this leads to an artificial decrease of the visibility observed compared to the Rabi prediction. With the extracted values of Ω_{if} and δ_{if} we fit the amplitude of the spin oscillation in Eq. (2), where only the fraction of atoms n remains as a free parameter. The measured amplitudes, together with the fits, are shown in Fig. 4a for $|0, 0\rangle \leftrightarrow |+1, -1\rangle$ and $|-1, -1\rangle \leftrightarrow |0, -2\rangle$. The measured fraction resulting from the fit is $n = 0.43(3)$ for $|0, 0\rangle \leftrightarrow |+1, -1\rangle$ and $n = 0.41(3)$ for $|-1, -1\rangle \leftrightarrow |0, -2\rangle$. Using the same model for the atom number distribution as in [22] we calculate $n \approx 50\%$ for our trapping parameter, close to the measured values.

This explanation for the artificial decrease in visibility suggests that the contrast can be enhanced by selectively discarding all atoms from the measurement which are in sites with unity filling. This is accomplished by first evolving the system for one half period of spin-oscillation, at which the occupation of the $|+1, -1\rangle$ -state is maximal, whereas unpaired atoms remain in the $m_f = 0$ state. Those atoms are then transferred into the $f = 1$ hyperfine state and remain undetected while the subsequent spin dynamics is recorded. The resulting high contrast oscillations are shown in Fig. 4b for the case

of $B = 0.6$ G and $40 E_r$ lattice depth. The visibility of approximately 72(3)% for $|0, 0\rangle$ is close to the maximum expected contrast of 81% for this detuning.

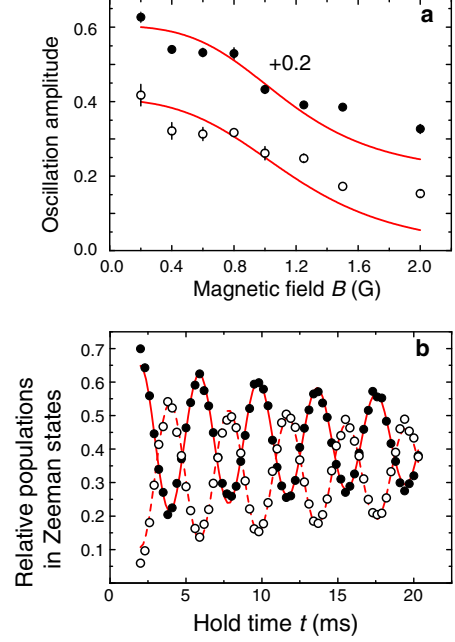


FIG. 4: (a) Oscillation amplitude vs. magnetic field for the processes $|00\rangle \leftrightarrow |+1, -1\rangle$ (\circ) and $|-1, -1\rangle \leftrightarrow |0, -2\rangle$ (\bullet). The lines are fits to (2), where only the fraction of atoms n remains as free parameter. The upper curve has been offset by 0.2. (b) High contrast spin oscillations between $|0, 0\rangle$ (\circ) and $|+1, -1\rangle$ (\bullet) at 0.6 G and $40 E_r$. Here, only atoms in sites with a filling larger than one are counted (see text).

The picture of isolated atom pairs coherently oscillating between two-particle states does not allow to understand the damping of these oscillations, clearly seen in Fig. 2. In particular, we estimate the inhomogeneous dephasing rate to be too low to account for it. To investigate the damping mechanism, we record the decay rate as a function of lattice depth at $B = 0.6$ G (see Fig. 5). Here, the depth has been changed between $20 E_r$ and $54 E_r$ in both horizontal lattice axes, whereas the vertical axis depth stayed fixed at $40 E_r$. For high lattice depths the damping rate levels at a finite value, whereas it increases for decreasing lattice depths. We interpret this increase as the enhanced probability to emit spin excitations in the lattice. In a Mott-insulator, particle exchange processes between two neighboring wells, such as $|n=1\rangle_i \otimes |n=1\rangle_j \rightarrow |n=0\rangle_i \otimes |n=2\rangle_j$, are suppressed due to a large offset in interaction energy [28]. However, spin exchange processes like from $|+1, -1\rangle_i \otimes |+1, -1\rangle_j$ to $|+1, +1\rangle_i \otimes |-1, -1\rangle_j$ can occur, because the spin-dependent interaction is much smaller than the spin independent one. This is reminiscent of usual ferro- or antiferromagnetic insulators, where density excitations are suppressed by an energy gap, whereas spin excitations are gapless [29]. From a simple Fermi's Golden rule argument, we deduce the excitation probability to be propor-

tional to the tunneling matrix element J . A fit to the damping rate of the form $\alpha J/h + \gamma_0$ returns a proportionality constant $\alpha = 9(1)$ and a constant offset $\gamma_0 = 37(3) \text{ s}^{-1}$ (see solid line in Fig. 5 for the fit and dashed line for the offset). This offset can be explained by the atom loss rate in the lattice. The inset of Fig. 5 shows a curve of atom loss in the optical lattice. For this experiment, the sample was prepared in the $|0, 0\rangle$ state in a $40 E_r$ deep lattice, and spin dynamics was suppressed by a magnetic field around 10 G. The initial loss rate $\gamma_1 = 35(5) \text{ s}^{-1}$ is attributed to two-body loss processes with a measured two-body loss coefficient $K_2 = (8.8 \pm 1.5) \times 10^{-14} \text{ cm}^3/\text{s}$. Note that the overall atom losses are strongly suppressed at longer times, where only sites with one atom per site remain [30]. For lat-

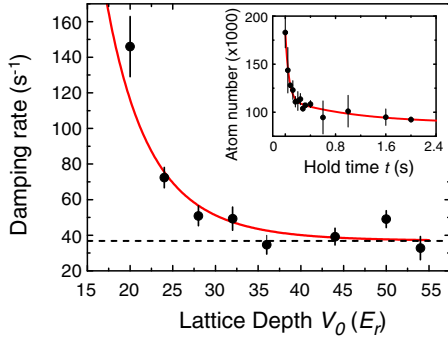


FIG. 5: Damping rate of spin oscillations vs. lattice depth for $|0, 0\rangle \leftrightarrow |1, -1\rangle$. The solid line is a fit to $\alpha J/h + \gamma_0$ with $\gamma_0 = 37(3) \text{ s}^{-1}$ (illustrated as dashed line). The inset shows atom loss vs. hold time at a 10 G magnetic field, where spin dynamics is suppressed. The fast loss rate of $\gamma_1 \approx 35(5) \text{ s}^{-1}$ coincides with the offset γ_0 of the damping rate even at high lattice depths.

tice depths smaller than $20 E_r$, but still in the Mott-insulator, the coherent oscillations could not be recorded any more.

We have also detected spin dynamics in the $f = 1$ hyperfine manifold between the two-particle states $|0, 0\rangle \leftrightarrow |-1, +1\rangle$ and find a coupling constant which is roughly one order of magnitude smaller than in $f = 2$ [23].

In summary, we have observed coherent spin dynamics between two-particle states in the upper hyperfine ground state of ^{87}Rb due to spin changing collisions. The observation of high contrast Rabi-type oscillations make this system a promising starting point for quantum information purposes. In this work we have demonstrated a method to create an array of entangled atom pairs similar to the long-lived Bell pairs produced in ion traps [31]. This is the first step towards the creation of pair-correlated atomic beams as proposed in [16, 17]. Another intriguing question is the evolution of quantum correlations upon melting the Mott-insulator. A possible outcome would be a non-local condensate of Bell-like pairs delocalized over the entire cloud. This highly entangled state could be distinguished from a coherent superposition of condensates through counting statistics.

We would like to thank Servaas Kokkelmans, Belén Pare-des and Ignacio Cirac for helpful discussions. This work was

supported by the DFG, the European Union (OLAQUI) and the AFOSR. FG acknowledges support from a Marie-Curie fellowship.

* Electronic address: Widera@Uni-Mainz.DE

- [1] D. M. Stamper-Kurn and W. Ketterle, in *Coherent matter waves*, edited by R. Kaiser, C. Westbrook, and F. David (Springer NY, 2001); arXiv:cond-mat/0005001 (2000).
- [2] M. D. Barrett, J. A. Sauer, and M. S. Chapman, Phys. Rev. Lett. **87**, 010404 (2001).
- [3] H. Schmaljohann *et al.*, Phys. Rev. Lett. **92**, 040402 (2004).
- [4] M.-S. Chang *et al.*, Phys. Rev. Lett. **92**, 140403 (2004).
- [5] T. Kuwamoto, K. Araki, T. Eno, and T. Hirano, Phys. Rev. A **69**, 063604 (2004).
- [6] J. M. Higbie *et al.*, Preprint at arXiv:cond-mat/0502517 (2005).
- [7] Tin-Lun Ho, Phys. Rev. Lett. **81**, 742 (1998).
- [8] T. Ohmi and K. Machida, J. Phys. Soc. Jpn. **67**, 1822 (1998).
- [9] C. V. Ciobanu, S.-K. Yip, and Tin-Lun Ho, Phys. Rev. A **61**, 033607 (2000).
- [10] N. Klausen, J. Bohn, and Ch. Greene, Phys. Rev. A **64**, 053602 (2001).
- [11] Masahito Ueda and Masato Koashi, Phys. Rev. A **65**, 063602 (2002).
- [12] C. K. Law, H. Pu, and N. P. Bigelow, Phys. Rev. Lett. **81**, 5257 (1998).
- [13] H. Pu, C. K. Law, S. Raghavan, J. H. Eberly, and N. P. Bigelow, Phys. Rev. A **60**, 1463 (1999).
- [14] J. M. McGuirk, H. J. Lewandowski, D. M. Harber, T. Nikuni, J. E. Williams, and E. A. Cornell, Phys. Rev. Lett. **89**, 090402 (2002).
- [15] Q. Gu, K. Bongs, and K. Sengstock, Phys. Rev. A **70**, 063609 (2004).
- [16] H. Pu and P. Meystre, Phys. Rev. Lett. **85**, 3987 (2000).
- [17] L.-M. Duan, A. Sørensen, J. I. Cirac, and P. Zoller, Phys. Rev. Lett. **85**, 3991 (2000).
- [18] E. Demler and F. Zhou, Phys. Rev. Lett. **88**, 163001 (2002).
- [19] S. K. Yip, Phys. Rev. Lett. **90**, 250402 (2003).
- [20] A. Imambekov, M. Lukin, and E. Demler, Phys. Rev. A **68**, 063602 (2003).
- [21] J. J. García-Ripoll, M. A. Martin-Delgado, and J. I. Cirac, Phys. Rev. Lett. **93**, 250405 (2004).
- [22] S. Fölling, F. Gerbier, A. Widera, O. Mandel, T. Gericke, and I. Bloch, Nature **434**, 481 (2005).
- [23] A. Widera *et al.* (in preparation).
- [24] The magnetic fields are calibrated by microwave spectroscopy. The field values have an uncertainty of approximately 10 mG.
- [25] C. Cohen-Tannoudji, B. Diu, and F. Laloë, *Quantum mechanics* (Wiley VCH, 1977).
- [26] E. G. M. van Kempen, S. J. J. M. F. Kokkelmans, D. J. Heinzen, B. J. Verhaar, Phys. Rev. Lett. **88**, 093201 (2002); S. Kokkelmans (private communication).
- [27] D. Jaksch, C. Bruder, J. I. Cirac, C. W. Gardiner, and P. Zoller, Phys. Rev. Lett. **81**, 3108 (1998).
- [28] M. Greiner, O. Mandel, T. Esslinger, T. W. Hänsch, and I. Bloch, Nature **415**, 39 (2002).
- [29] A. Auerbach, *Interacting Electrons and Quantum Magnetism* (Springer, New York, 1998).
- [30] A. Widera, O. Mandel, M. Greiner, S. Kreim, T. W. Hänsch, and I. Bloch, Phys. Rev. Lett. **92**, 160406 (2004).
- [31] C. F. Roos *et al.*, Phys. Rev. Lett. **92**, 220402 (2004).

Probing Number Squeezing of Ultracold Atoms across the Superfluid-Mott Insulator Transition

Fabrice Gerbier,* Simon Fölling, Artur Widera, Olaf Mandel, and Immanuel Bloch

Institut für Physik, Johannes Gutenberg-Universität, 55099 Mainz, Germany

(Received 28 October 2005; published 6 March 2006)

The evolution of on-site number fluctuations of ultracold atoms in optical lattices is experimentally investigated by monitoring the suppression of spin-changing collisions across the superfluid-Mott insulator transition. For low atom numbers, corresponding to an average filling factor close to unity, large on-site number fluctuations are necessary for spin-changing collisions to occur. The continuous suppression of spin-changing collisions is thus direct evidence for the emergence of number-squeezed states. In the Mott insulator regime, we find that spin-changing collisions are suppressed until a threshold atom number, consistent with the number where a Mott plateau with doubly occupied sites is expected to form.

DOI: [10.1103/PhysRevLett.96.090401](https://doi.org/10.1103/PhysRevLett.96.090401)

PACS numbers: 03.75.Hh

One of the most fundamental signatures of the Mott insulator (MI) transition undergone by ultracold atomic gases in optical lattices [1–13] is a drastic change in atom number statistics. In a very shallow lattice, ultracold bosons tend to form a Bose-Einstein condensate. In this case, a measurement of the probability for finding n atoms at a given lattice site would reveal a characteristic Poisson distribution with large on-site fluctuations. However, for deeper lattices, the influence of repulsive interactions, which disfavor such fluctuations, becomes increasingly dominant and results in the emergence of number-squeezed states with suppressed number fluctuations. Above a critical lattice depth, the ultracold gas enters the MI regime, where the number fluctuations almost vanish. In experiments so far, interaction-induced number-squeezed states were detected through the observation of increased phase fluctuations, the canonically conjugate variable to number fluctuations [1–3], or through an increased time scale for phase diffusion [4].

In this Letter, we directly observe the continuous suppression of number fluctuations when the ultracold sample evolves from the superfluid (SF) regime to deep in the MI regime. The idea behind our measurement is illustrated in Fig. 1. After producing an ultracold gas in an optical lattice, we suddenly increase the lattice intensity, suppressing tunneling and freezing the number distribution. A probe sensitive only to the presence of *atom pairs* at a given lattice site is finally applied. Close to unity filling, a nonzero probe signal is obtained only if initially large on-site fluctuations produce a nonzero fraction of sites with two atoms. While we observe this behavior for a gas initially in the SF regime, the probe signal is progressively suppressed when approaching the Mott transition, indicating increasingly number-squeezed states.

The specific two-particle probe used in this work are spin-changing collisions (see [14], and references therein), which convert at each lattice site pairs of spin $f = 1$ atoms in the $m = 0$ Zeeman sublevel to pairs with one atom in $m = +1$ and the other in $m = -1$. In principle, other

schemes, e.g., measuring the interaction energy [11] or monitoring atom losses due to Raman photoassociation [15,16] or Feshbach resonances [17], could be suitable for this measurement. Spin-changing collisions have advantages when used as a probe for atom pairs: they are nondestructive (see also [18]), and they can be resonantly controlled using the differential shift between Zeeman sublevels induced by an off-resonant microwave field [19–21]. We show that this technique allows one to measure selectively doubly occupied sites in the optical lattice.

Our experimental setup has been described in detail in [14]. We first load a degenerate gas of ^{87}Rb atoms in the $|F = 1, m = -1\rangle$ Zeeman sublevel into a combined magnetic trap plus optical lattice potential at an initial lattice depth V_0 . The intensities are then rapidly increased from V_0 to $V_f = 40E_r$ within $t_{\text{up}} = 1$ ms (see Fig. 2). Here $E_r = \hbar^2/2M\lambda^2$ is the single photon recoil energy, and $\lambda = 842$ nm the lattice laser wavelength. Immediately after this ramp, the magnetic potential is switched off, and the cloud is held for 60 ms in order to let the magnetic bias

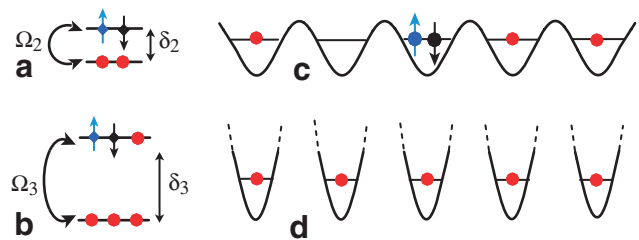


FIG. 1 (color). Illustration of the number statistics measurement. Spin-changing collisions turn atom pairs initially in the Zeeman substate $m = 0$ (no arrow) to pairs in $m = \pm 1$ states (up and down arrows). This process happens for sites with $n = 2$ (a) or $n = 3$ (b) atoms. For one atom per site on average, whether this occurs depends drastically on the many-body correlations. For a Bose-Einstein condensate (c), large on-site fluctuations create a finite number of sites with 2 or 3 atoms, where ± 1 pairs can be created. On the contrary, for a MI state (d), only isolated atoms are found and no $m = \pm 1$ pairs are created.

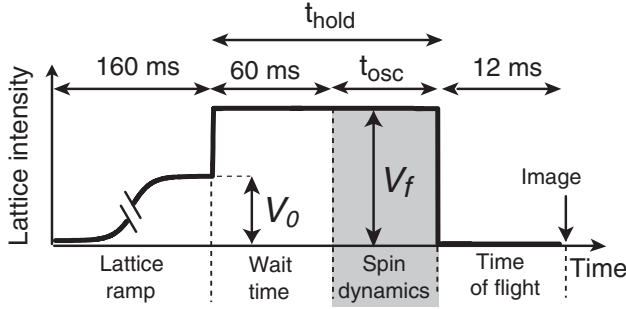


FIG. 2. Time sequence of the experiment.

field stabilize to its final value $B \approx 1.2$ G. The atoms are then prepared in the $m = 0$ state using microwave transfer pulses, and held for a variable time t_{osc} , during which a collisional spin oscillation takes place. This coherent evolution is detected experimentally as a reversible exchange between the populations in the $m = 0$ and $m = \pm 1$ Zeeman sublevels, measured by absorption imaging after 12 ms of free expansion.

Spin-changing interactions in deep optical lattices have been described in detail in [14]. We consider spin $f = 1$ atoms and assume that tunneling can be neglected, so that the lattice sites are isolated from each other. At a single lattice site, the spin-changing collisions are critically sensitive on the filling n of the well. For sites with filling $n = 0$ or 1, spin-changing collisions cannot occur. The first nontrivial case corresponds to doubly occupied wells. In this case, only two spin states (one with both atoms in $m = 0$ and the other with a single $m = \pm 1$ pair) are accessible [see Fig. 1(a)]. Therefore, the atom pair undergoes Rabi-like oscillations at the effective Rabi frequency $\sqrt{\delta_2^2 + \Omega_2^2}$. The energy mismatch (“detuning”) between the two states is $\hbar\delta_2 = \Delta\epsilon + U_s$, where $\Delta\epsilon = \epsilon_{+1} + \epsilon_{-1} - 2\epsilon_0$ corresponds to the difference in Zeeman energies ϵ_m . The spin-dependent interaction energy U_s depends on atomic and lattice parameters [14], and also determines the coupling strength as $\Omega_2 = 2\sqrt{2}U_s$. Sites with $n = 3$ atoms behave in a similar way [Fig. 1(a)], however, with an energy difference $\hbar\delta_3 = \Delta\epsilon - U_s$ and a coupling strength $\Omega_3 = 2\sqrt{6}U_s$.

In principle, site occupancies $n > 3$, whose spin dynamics involve more than one $m = \pm 1$ pair, are also possible. However, during the hold time t_{hold} indicated in Fig. 2, those sites can be emptied by three-body (3B) recombination events at an event rate $\gamma_n = \gamma_{3B}n(n-1)(n-2)$ [22], with $\gamma_{3B} \approx 0.5 \text{ s}^{-1}$ for our parameters. Therefore, sites with $n \geq 4$ are efficiently removed after the wait time.

In our experiment, we produce large ensembles of atoms in the optical lattice with spatially inhomogeneous atom number distribution. The inhomogeneity results from an additional trapping potential V_{ext} present on top of the optical lattice [23]. In the MI regime, this potential leads to the formation of flat Mott plateaus with a well-defined

atom number per site [5,7,24]. Also, the local fluctuations have an inhomogeneous distribution. Experimentally, we measure the “spin-oscillation amplitude” for the entire atomic cloud, i.e., the global population $\mathcal{A}_{\text{osc}} = (N_{+1} + N_{-1})/N$ of the $m = \pm 1$ states after an evolution time t_{osc} , normalized to the total atom number N . This amplitude is related to the probability \bar{P}_n of finding n atoms per lattice site, averaged over the cloud spatial profile.

Let us suppose that we are able to tune the single-particle detuning to $\Delta\epsilon = -U_s$, such that doubly occupied sites are exactly on resonance. Then, neglecting sites with $n \geq 4$, the oscillation amplitude is obtained by summing the contribution from sites with $n = 2$ and $n = 3$,

$$\mathcal{A}_{\text{osc}} \approx \bar{P}_2 \sin^2\left(\frac{\Omega_2 t_{\text{osc}}}{2}\right) + \frac{6}{7} \bar{P}_3 \sin^2\left(\sqrt{\frac{7}{8}} \Omega_2 t_{\text{osc}}\right). \quad (1)$$

From Eq. (1), we conclude that atom pairs and triplets oscillate essentially out of phase. By choosing $\Delta\epsilon = -U_s$ and $t_\pi = \pi/\Omega_2$, all doubly occupied sites are converted to $m = \pm 1$ pairs, whereas the conversion efficiency for triplets is around 3%. Recording the amplitude of the spin oscillations thus allow one to probe the distribution of atom pairs alone. This is reminiscent of cavity quantum electrodynamics [25,26], where Fock states of the cavity field could be discriminated due to different coupling strengths to an atomic transition. In particular, choosing $\Delta\epsilon = U_s$ would allow one to measure the fraction of triply occupied sites remaining after three-body decay.

To achieve full conversion of doubly occupied sites, it is necessary to tune the spin oscillations for doubly occupied sites into resonance, i.e., set $\Delta\epsilon = -U_s$. In a magnetic field B , the quadratic Zeeman shift contributes a *positive* amount to $\Delta\epsilon$. Hence, if $U_s > 0$ (which is the case for ^{87}Rb), the interaction energy U_s leads to a residual detuning in zero magnetic field that prevents reaching the resonance. For this reason, we introduce a different technique using the differential level shift induced on the individual Zeeman sublevels by a far off-resonant microwave field (“ac-Zeeman shift”). With a suitable choice of polarization, detuning, and power, the detuning $\Delta\epsilon$ can be tuned at will in the range of interest, and allows one to compensate the magnetic field contribution to $\Delta\epsilon$ *plus* the interaction term U_s . In this work, the microwave field is detuned by several hundred MHz to the red of any hyperfine resonance to suppress population transfer to $f = 2$. Indeed, no such transfer is observed within our experimental sensitivity.

In Fig. 3, the fraction of atoms found in $m = \pm 1$ is plotted as a function of the microwave power for a fixed $t_{\text{osc}} = 15.5 \text{ ms} \approx t_\pi$, corresponding to maximum conversion. These data were taken for constant initial lattice depth ($V_0 = V_f = 40E_r$) and atom number ($N \approx 2.6 \times 10^5$). For very low microwave powers, the spin dynamics is suppressed by the quadratic Zeeman detuning ($\Delta\epsilon \approx 2\pi \times 207 \text{ Hz}$), much larger than the spin-dependent interaction $U_s \approx 2\pi \times 10.7 \text{ Hz}$. The ac-Zeeman shift can compensate

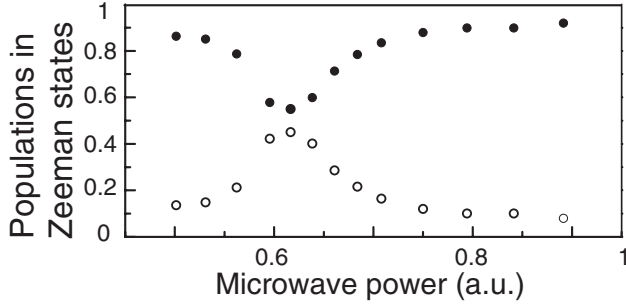


FIG. 3. Resonance curve of the spin-oscillation amplitude in the far-detuned microwave field, measured at a magnetic field $B \approx 1.2$ G and at a fixed hold time $t_{\text{hold}} = 15.5$ ms. Solid (open) circles denote the population in the Zeeman substate $m = 0$ ($m = \pm 1$).

for this detuning and for the interaction part, inducing a resonance in the number of $m = \pm 1$ pairs shown in Fig. 3. The oscillation amplitude, close to the expected $\mathcal{A}_{\text{osc}} \approx 0.5$, indicates that nearly all atom pairs are converted into ± 1 pairs, in agreement with further experiments discussed in a companion paper [21].

We now turn to the measurement of number statistics. We choose $t_{\text{osc}} \approx 15.5$ ms and a dressing field tuned to resonance, as in the previous paragraph. At a given lattice depth V_0 , we have recorded the oscillation amplitude in a broad range of atom numbers, from about 10^4 to a few 10^5 [27]. The experiment is then repeated for various lattice depths, from the SF regime ($V_0 = 4E_r$) to deep in the MI regime ($V_0 = 20E_r$ and $40E_r$). As shown in Fig. 4, at low lattice depths, the spin oscillations occur for any atom number N , with an amplitude slowly increasing with N .

For small atom number, the oscillation amplitude is increasingly suppressed with increasing lattice depth, and completely vanishes for large lattice depths. This qualitative behavior is consistent with the behavior expected from the Bose-Hubbard model [5–13]. On approaching the Mott transition, the ground state adapts to an increased interaction energy by reducing its number fluctuations, eventually producing an array of one-atom Fock states at each site where spin-changing collisions cannot occur.

Within the MI regime [Figs. 4(d)–4(f)], we observe that the suppression of spin oscillations persists up to some threshold atom number [$6.0(3) \times 10^4$ for the data in Fig. 4(f)]. This is consistent with the expected formation of Mott plateaus with increasing atom number, as the cloud expands in the trapping potential. A Mott plateau with n atoms per site forms when the cloud radius reaches the size R_n where the potential energy $V_{\text{ext}}(R_n)$ matches the on-site interaction energy $U(n-1)$. For a harmonic potential with trapping frequency ω_{ext} , this happens at a threshold number [29] $N_n \approx N_2 \sum_{k=1}^n k^{3/2}$. Above $N_2 \approx 4\pi/3(m\omega_{\text{ext}}^2 d^2/2U)^{-3/2}$, a core with two atoms per site starts to grow, thus enabling the spin oscillations. For the parameters that correspond to Fig. 4(f) ($\omega_{\text{ext}} = 2\pi \times 80$ Hz and $V_0 = 40E_r$), we calculate $N_{\text{th}} \sim 6.8 \times 10^4$, close to the measured value. For even higher atom number (corresponding to $N_3 \sim 3 \times 10^5$), a shell of triply occupied sites start to form, reducing the fraction of atoms in the $n = 2$ shell. This can be seen in Fig. 4(f), where we indeed observe a decrease of the spin amplitude above this number.

In order to compare our experimental results with the prediction of the Bose-Hubbard model [5], we solve this

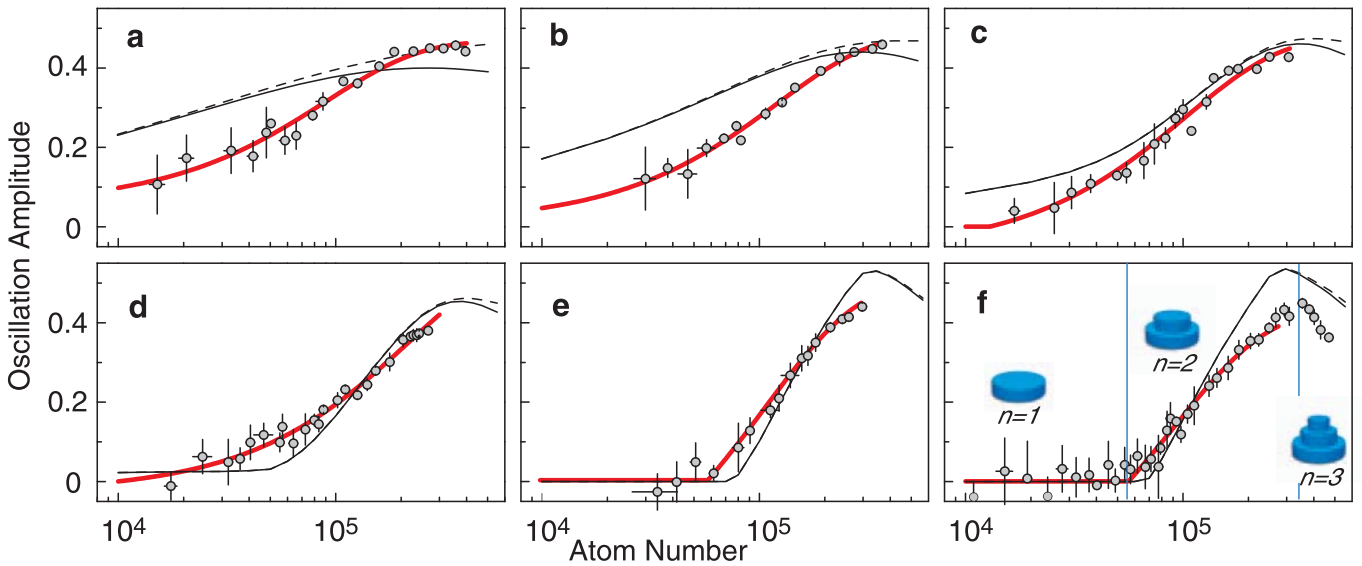


FIG. 4 (color). Amplitude of the spin oscillation vs atom number and different lattice depths: $V_0 = 4, 8, 11, 13, 20, 40E_r$ (a)–(f). The thin dashed lines show the prediction of a theoretical model, where the atom number distribution is deduced from a mean-field approach at $T = 0$ (see text). The thin solid lines show only the fraction of atom pairs calculated from the same model. The thick solid lines are guides to the eye. In (f), the vertical lines indicate where Mott plateaus with 2 and 3 atoms per site are expected to form.

model numerically within a mean-field approximation at zero temperature [30,31]. Accounting for losses during the hold time t_{hold} (wait time plus oscillation time), we obtain the distribution \bar{P}_n . For each filling n and a given t_{osc} , we calculate the conversion efficiency $\eta_{\pm 1}(n)$ to $m = \pm 1$ pairs, and obtain the total spin amplitude from $\mathcal{A}_{\text{osc}} = \sum_n n \eta_{\pm 1}(n) \bar{P}_n$. The results of this calculation, indicated by the thin dashed lines in Fig. 4, lie very close to the fraction of pairs \bar{P}_2 predicted by the same model (thin solid lines), in agreement with the arguments leading to Eq. (1). Deep in the MI regime [Figs. 4(e) and 4(f)], the calculations agree well with the measurements. For lower lattice depths, although the qualitative trend is still reproduced, we find discrepancies. Near the Mott transition [Fig. 4(d)], the mean-field calculations predict an amplitude lower than observed, a behavior consistent with the study of number correlations beyond mean-field reported in [12]. Below the transition point [Figs. 4(a)–4(c)], the model predicts an oscillation amplitude higher than observed. Deviations from the initial distribution may arise in this low lattice depth regime if excitations are generated during the preparation phase and result in an increased populations in the low-density regions of the cloud, which barely participate to the spin oscillations. Such “finite temperature” effects have possibly less influence in the MI regime, where the many-body system is protected by an interaction gap.

In conclusion, we have shown how spin oscillations can be used to probe number squeezing in optical lattices via the detection of the fraction of atom pairs. Our observations confirm the expected scenario: near-Poissonian fluctuations for shallow lattices, strongly suppressed fluctuations for deep lattices, and a smooth interpolation in between. Moreover, the observed behavior is consistent with the expected formation of Mott plateaus, a signature of the incompressibility of this system. Our results indicate that number squeezing is robust with respect to experimental manipulations, such as transfer to the purely optical trap. In this sense, they are promising to employ those number-squeezed states, e.g., in Heisenberg-limited atom interferometry [32].

We acknowledge support from the DFG, from AFOSR, and from the EU under the OLAQUI and the Marie Curie EIF (FG) programs.

*Current address: Laboratoire Kastler Brossel, Département de Physique de l'ENS, 24 rue Lhomond, 75 005 Paris, France.
Electronic address: fabrice.gerbier@lkb.ens.fr

- [1] C. Orzel, A. K. Tuchman, M. L. Fenselau, M. Yasuda, and M. K. Kasevich, *Science* **291**, 2386 (2001).
- [2] M. Greiner, O. Mandel, T. Esslinger, T. W. Hänsch, and I. Bloch, *Nature (London)* **415**, 39 (2002).
- [3] T. Stöferle, H. Moritz, C. Schori, M. Köhl, and T. Esslinger, *Phys. Rev. Lett.* **92**, 130403 (2004).
- [4] M. Greiner, O. Mandel, T. W. Hänsch, and I. Bloch, *Nature (London)* **419**, 51 (2002).
- [5] D. Jaksch, C. Bruder, J. I. Cirac, C. W. Gardiner, and P. Zoller, *Phys. Rev. Lett.* **81**, 3108 (1998).
- [6] J. Javanainen, *Phys. Rev. A* **60**, 4902 (1999).
- [7] V. A. Kashurnikov, N. V. Prokof'ev, and B. V. Svistunov, *Phys. Rev. A* **66**, 031601(R) (2002).
- [8] K. Burnett, M. Edwards, C. W. Clark, and M. Shotton, *J. Phys. B* **35**, 1671 (2002).
- [9] M. Shotton, *J. Phys. B* **35**, 3019 (2002).
- [10] R. Roth and K. Burnett, *Phys. Rev. A* **67**, 031602(R) (2003).
- [11] D. C. Roberts and K. Burnett, *Phys. Rev. Lett.* **90**, 150401 (2003).
- [12] J. J. Garcia-Ripoll *et al.*, *Opt. Express* **12**, 42 (2004).
- [13] L. I. Plimak, M. K. Olsen, and M. Fleischhauer, *Phys. Rev. A* **70**, 013611 (2004).
- [14] A. Widera *et al.*, *Phys. Rev. Lett.* **95**, 190405 (2005).
- [15] T. Rom *et al.*, *Phys. Rev. Lett.* **93**, 073002 (2004).
- [16] C. Ryu *et al.*, *cond-mat/0508201*.
- [17] T. Stöferle, H. Moritz, K. Günther, M. Köhl, and T. Esslinger, *Phys. Rev. Lett.* **96**, 030401 (2006).
- [18] A. Widera *et al.*, *Phys. Rev. Lett.* **92**, 160406 (2004).
- [19] H. Pu and P. Meystre, *Phys. Rev. Lett.* **85**, 3987 (2000).
- [20] A. Sorensen, L.-M. Duan, J. I. Cirac, and P. Zoller, *Nature (London)* **409**, 63 (2001).
- [21] F. Gerbier, A. Widera, S. Fölling, O. Mandel, and I. Bloch, *cond-mat/0601151*.
- [22] M. W. Jack and M. Yamashita, *Phys. Rev. A* **67**, 033605 (2003).
- [23] The potential V_{ext} is nearly harmonic, with a trapping frequency $\omega_{\text{ext}} \approx \sqrt{\omega_m^2 + 8V_0/mw^2}$, where $\omega_m = 2\pi \times 16$ Hz is the oscillation frequency in the magnetic trap and where $w \approx 136$ μm is the laser beam size.
- [24] G. G. Batrouni *et al.*, *Phys. Rev. Lett.* **89**, 117203 (2002).
- [25] M. Brune *et al.*, *Phys. Rev. Lett.* **76**, 1800 (1996).
- [26] B. T. H. Varcoe, S. Brattke, M. Weidinger, and H. Walther, *Nature (London)* **403**, 743 (2000).
- [27] The atom number has been calibrated by measuring the condensation temperature $T_c \propto N^{1/3}$ in the magnetic trap, using the same method as in [28]. This calibration has been checked against measurements of the absorption cross section for various probe polarizations. Both measurements agree within their uncertainty, around 15%.
- [28] F. Gerbier *et al.*, *Phys. Rev. Lett.* **92**, 030405 (2004).
- [29] B. DeMarco, C. Lannert, S. Vishveshwara, and T.-C. Wei, *Phys. Rev. A* **71**, 063601 (2005).
- [30] K. Sheshadri *et al.*, *Europhys. Lett.* **22**, 257 (1993).
- [31] D. van Oosten, P. van der Straten, and H. T. C. Stoof, *Phys. Rev. A* **63**, 053601 (2001).
- [32] J. A. Dunningham and K. Burnett, *Phys. Rev. A* **70**, 033601 (2004).